Mechanistic differences in mouse models of heart failure with preserved ejection fraction

Dissertation

for the award of the degree

“Doctor of Philosophy”

of the Georg-August-Universität Göttingen

within the doctoral program Cardiovascular Science

of the Georg-August University School of Science (GAUSS)

submitted by

Surabhi Swarnkar

born in New Delhi, India

Göttingen, December 2022

Thesis Committee Members

Prof. Dr. med. Dörthe M. Katschinski (Supervisor and first member of the Thesis Committee)

Department of Cardiovascular Physiology; University Medical Center, Georg-August-Universität, Humboldtallee 23, 37073 Göttingen, Germany.

PD. Dr. med. Dr. Moritz Schnelle (Supervisor)

University Medical Center Göttingen Institute of Clinical Chemistry; Georg-August-Universität, Robert-Koch-Straße 40, 37075 Göttingen, Germany.

Prof. Dr. rer. nat. Sven Thoms (Second member of the Thesis Committee)

Department of Biochemistry and Molecular Medicine; Bielefeld University, Universitätsstraße 25, 33615 Bielefeld, Germany.

Prof. Dr. mult. Thomas Meyer (Third member of the Thesis Committee)

Department of Psychosomatic Medicine and Laboratory of Molecular Psychocardiology; University Medical Center, Georg-August-Universität, Waldweg 33, 37073 Göttingen, Germany.

Members of the Examination Board

Prof. Dr. Susanne Lutz

Institute of Pharmacology and Toxicology; Georg-August-Universität, Robert-Koch-Straße 40, 37075 Göttingen, Germany.

Prof. Dr. Katrin Streckfuß-Bömeke

Institute of Pharmacology and Toxicology; University of Würzburg, Versbacher Straße 9, 97078 Würzburg

PD. Dr. rer. nat. Laura Zelarayán-Behrend

Institute of Pharmacology and Toxicology; Georg-August-Universität, Robert-Koch-Straße 40, 37075 Göttingen, Germany.

Date of Disputation: 22.2.2023

Affidavit

I hereby declare that I have written the dissertation **"Mechanistic differences in mouse models of heart failure with preserved ejection fraction"** independently with no other aids or sources than quoted.

_____

Surabhi Swarnkar, Göttingen, December 2022 (Revision, February 2024).

List of Abbreviations

AGE/RAGE : Receptors of/and advanced glycation end products

Akt: Protein kinase B

ANOVA: Analysis of variance

ANP: Atrial natriuretic peptide

ARVC: Arrhythmogenic right ventricular cardiomyopathy

BNP: Brain natriuretic peptide

BPM: Beats per minute

Ca2+ : Calcium

CAM: Cell adhesion molecule

CaMKII: Calcium/calmodulin-dependent protein kinase type II

CD: Cluster of differentiation

cGMP: Cyclic guanosine monophosphate

c-JNK: C-JUN N-terminal kinase

CO: Cardiac output

Col: Collagen

CSA: Cross-sectional area

cTnI: Cardiac troponin I

DAPI: 4',6-diamidino-2-phenylindole

DD: Diastolic dysfunction

DEGs: Differentially expressed genes

dNTP: Deoxynucleotide triphosphates

DTT: Dithiothreitol

Ea: Arterial elastance

ECM: Extra cellular matrix

ED: Endothelial dysfunction

EDP: End diastolic pressure

EDPVR: End diastolic pressure volume relationship

EDV: End-diastolic volume

Ee: End-systolic elastance

EF: Ejection fraction

EndoMT: Endothelial to mesenchymal transition

ERK: Extra-cellular signal regulated kinase

ESPVR: End systolic pressure volume relationship

ESV: end systolic volume

ET: Endothelin

FDR: False discovery rate

FN: Fibronectin

FS: Fractional shortening

GO: Gene ontology

HF: Heart failure

HFD: High fat diet

HFmrEF: Heart failure with mid-range ejection fraction

HFpEF: Heart failure with preserved ejection fraction

HFrEF: Heart failure with reduced ejection fraction

HR: Heart rate

HTN: Hypertension

IFN: Interferon

IL: Interleukin

IP3: Inositol triphosphate

IVCO: Inferior vena cava occlusion

IVS: Intraventricular septum

KEGG: Kyoto encyclopedia of genes and genomes

LA: Left atrium

LV: Left ventricle

LVEDD: Left ventricular end-diastolic dimension

LVPWd: Left ventricular posterior wall dimension

MAPKs: Mitogen-activated protein kinases

Mhc: Myosin heavy chain

MMPs: Matrix metalloproteinases

mTORC: Mammalian target of Rapamycin

n.s.: not significant

NCX: Sodium calcium exchanger

ND: Normal diet

NFAT: Nuclear factor of activated T-cells

NO: Nitric oxide

NOS: Nitric oxide synthase

NOX: NADPH oxidase

Nppa: Natriuretic peptide type A (gene encoding ANP)

Nppb: Natriuretic peptide type B (gene encoding BNP)

ORA: Overrepresentation analysis

ORO: Oil red O

PBS: Phosphate-buffered saline

PCA: Principle component analysis

PFA: Paraformaldehyde

PK: Protein kinase

PKA: Protein kinase A

PLN: Phospholamban

PO: Pressure overload

PRSW: Pre-load recruitable stroke work

PV loop: Pressure-volume loop

rLSR: Reverse longitudinal strain rate

ROS: Reactive oxygen species

RWT: Relative wall thickness

RyR2: Ryanodine receptor 2

SEM: Standard error of the mean

Ser: Serine

SERCA-2α: Sarcoplasmic/endoplasmic reticulum calcium ATPase-2α

Sham: Placebo surgery

SR: Sarcoplasmic reticulum

SV: Stroke volume

T2DM: Type 2 Diabetes Mellitus

TAC: Transverse aortic constriction

TGF: Transforming growth factor

Thr: Threonine

TIMPs: Tissue inhibitors of matrix metalloproteinases

TL: Tibia length

TNF: Tumor necrosis factor

TUNEL: TdT-mediated dUTP-biotin nick end labelling

Tyr: Tyrosine

vs: Versus

WGA: Wheat germ agglutinin

β-AR: β-adrenergic receptor

Table of contents

List of figures

List of tables

Abstract

Heart failure (HF) is the most potent epidemic of the 21st century. Based on ejection fraction (EF), HF has been classified into two distinct entities; heart failure with reduced EF (HFrEF) and heart failure with preserved EF (HFpEF). At present, HFpEF accounts for about half of all HF cases worldwide but owing to the rising incidence of comorbid diseases and an aging population, its prevalence is expected to rise in the coming years. While the medical community has a good arsenal of therapeutics to deal with HFrEF, there exists no dedicated treatment for HFpEF as of now. An important limitation in this context is the lack of animal models to capture the multifactorial and multi-organ pathological profile of HFpEF. This dearth of reliable animal models often translates into a lack of our collective understanding of the disease. This dissertation aims to create tailor-made models of ''HFpEF like'' states based on different comorbid etiologies and seeks to stratify them based on clinically relevant end-points to gather insights about their pathomechanisms. To this end, two models were created using the most common factors associated with HFpEF. The first model was made by combining dyslipidemia induced by high fat diet (HFD) and low grade pressure overload (PO) using transverse aortic constriction (TAC) to realistically reflect the metabolic syndrome in HFpEF. The other model was based on natural aging and looked at the advanced age of 18-20 months in mice in terms of HF.

After 10 weeks of HFD and 2 weeks post TAC the models were assessed. For the first model we observed that the combination of HFD+PO resulted in a selective shift in EF towards a preserved state (≥50%) while control mice on normal diet (ND) + PO presented with a reduction in EF (≤40%) which reflects HFrEF. This prompted us to hypothesize that metabolic deregulation led by HFD induced dyslipidemia in presence of low grade PO was important in the differential presentation of HF. An in-depth structural characterization of the myocardium revealed a hypertrophic, apoptotic and a highly fibrotic phenotype which presented with evidence of atrial remodeling. There was significant accumulation of neutral lipid deposits in the myocardial tissue indicating global dyslipidemic effects. The model showed an overall preserved systolic function in HFD- TAC (in contrast to ND-TAC controls) as evidenced by unchanged echocardiographic parameters like EF and reverse longitudinal strain rate (r-LSR) and pressure volume (PV) loop parameters like ESPVR, dp/dt_{max} and PRSW when compared to HFD-Sham group. Moreover, an impairment in diastolic function was confirmed by significant changes in EDPVR, EDP and Tau. On the aspect of remodeling, the dyslipidemic HFpEF state presented with concentric hypertrophy as evidenced by higher relative wall thickness (RWT) as compared to dyslipidemic shams. Fetal gene reprogramming was highly active in both dietary groups but differed in terms of Serca-2α downregulation seen only in the HFrEF group. Perivascular fibrosis was uniquely enhanced in HFpEF state. The inflammatory cytokine profile within the two states also revealed a differential signature with more upregulation in the dyslipidemic group. VCAM-1 and PECAM-1 also presented with enhanced expression only in HFpEF group suggestive of distinct dynamics of endothelial dysfunction(ED). IL-1 showed enhanced expression in HFpEF only, while IL-6 showed no change in either groups. Endothelin-1 was exclusively upregulated in HFpEF state. Nox2 was upregulated in both HF states. In terms of cardiac kinases and calcium handling, phosphorylation levels of HDAC-4, Akt, Erk, RyR(2814) and Plb(Thr17) were only exclusively enhanced in HFpEF and cardiac troponin phosphorylation was preserved to basal levels in the HFpEF group indicating yet another differential aspect. Transcriptomic analysis of the two HF states identified several key genes involved mainly in actin-myosin structural and functional dynamics. Pathway analysis revealed an enrichment of gene-set involved in adrenergic signaling indicating that adrenergic deficits play a differentiating role between the two HF states.

The second model of cardiac aging was characterized on similar levels. In contrast to dyslipidemic HFpEF, it presented with an overall non-hypertrophic, non-remodeled, highly fibrotic, highly apoptotic

and non-steatotic phenotype. There was no evidence for LA remodeling and concentric hypertrophy of the LV. Systolic parameters discussed above were preserved and all studied diastolic parameters were significantly perturbed. Fetal gene reprogramming was evident but, Acta-1 showed no change in contrast to dyslipidemic HFpEF. BNP was upregulated in both HFpEF states but ANP was preserved in aging. Perivascular fibrosis as the previous HFpEF group was remarkably enhanced. Inflammatory cytokine analysis showed no changes in IFN-γ levels which was in contrast to dyslipidemic HFpEF. PECAM-1 upregulation was not observed here as well (just like dyslipidemic HFpEF) suggesting an exclusive role. IL-6 expression unlike the previous HFpEF group, was upregulated here. Endothelin-1 expression was again upregulated in this HFpEF state too. Notably, higher accumulation of $CD45^{+}$ cells was seen in LV myocardium of the aging HFpEF state only. Nox2 expression was not enhanced here unlike the previous dyslipidemia induced HFpEF cohort and HFrEF. Akt phosphorylation was not upregulated while Erk, p-38 and Jnk were. The latter two are in contrast with dyslipidemic HFpEF. In terms of calcium handling, phosphorylation of CAMKII, RyR(2814) , RyR(2808), Plb (Thr17) and Plb (Ser 16) were all enhanced showing a more potent deregulation than the dyslipidemic HFpEF group. Only HDAC-4 phosphorylation which was present in the previous group, could not be seen here. Assessment of the coding transcriptome of the two HFpEF states revealed an over representation of genes involved in response to chemokine and extracellular matrix (ECM) organization and the resulting KEGG pathway showed an enrichment in ECM-receptor pathway interaction genes. It suggests that these two HFpEF states differ strongly in the context of ECM based signaling.

PCA plot revealed a clustering of both HFpEF groups together despite their divergent etiologies. This further stresses on the multifactorial nature of HFpEF. The differences and similarities between the two ‘’HFpEF like’’ states and between HFpEF vs HFrEF reveal a distinct mechanistic profile. This study provides first such cross-comparative insight which ultimately may contribute to our collective understanding of different HFpEF pheno-groups and help in identifying mechanistically intuitive therapeutic targets for this elusive entity.

Introduction

1. Heart failure and its definition

Heart failure (HF) is a global pandemic of the present age. Most recent statistics emerging from 2017 indicate that about 64.3 million people are currently affected with the disease (Murray et al., 2018). HF is seen as a collection of different pathophysiologies and aetiology instead of one specific disease. The non-consensus on its definition immediately makes sense in this light. Traditional definitions of HF were restricted to the incapability of the heart structurally and functionally, to ensure optimal cardiac output in concert with neurohormonal processes and elevated left ventricular (LV) filling pressures (Savarese et al., 2023). In 2021, two major additions were made to the universal definition namely, elevated natriuretic peptides and systemic or pulmonary congestion (Bozkurt et al., 2021) as shown as the schematic in **figure 1**.

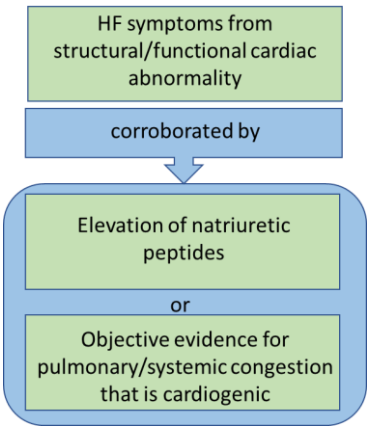

Fig. 1 Universal definition and classification of heart failure as revised in 2021 (modified according to Bozkurt et al., 2021).

To diagnose HF, the presence of cardiac dysfunction is important to demonstrate which may present as myocardial abnormality in structure and function leading to systolic or diastolic dysfunction. HF can also be a consequence of other conditions like valve abnormalities as in stenosis and regurgitation; rhythmogenic defects and pericardial or endocardial problems. This wide spectrum of causation necessitates that therapeutic decisions be made only after proper identification of the pathophysiology being presented.

2. Current classifications of heart failure

To address the spectrum of pathophysiology of HF, several grades of classification have been laid down to specify distinct subtypes as tabulated below.

Table 1. Classification schemes of Heart failure (modified according to Lam et al., 2021)

Scheme	Characteristics
New York Heart association (NYHA) class	I, II, III, IV based on severity of symptoms
Ejection Fraction (EF)	HFr(reduced)EF, HFmr(mid-range)EF, HFp(preserved)EF
Aetiology	Ischaemic/non-ischaemic, valvular, hypertensive, infiltrative cardiomyopathy, viral myocarditis, peripartum cardiomyopathy, chemotherapy-related cardiomyopathy
Disease progression (American Heart association)	Stages A,B,C,D based on HF symptoms and structural changes to cardiac tissue
MOGES	Morpho-functional phenotype (M), organs involvement (O), genetic inheritance (G), aetiological annotation (E), functional status (S)
INTERMACS profile for advanced HF	Levels 1-7 based on symptoms, functional capacity, hemodynamic stability in patients considered for advanced HF strategies

2.1. HF classifications based on Ejection fraction (EF)

A key measure of LV systolic function and a cornerstone of HF diagnosis is ejection fraction or EF. LVEF is defined as the ratio of LV chamber blood volume ejected at the end of systole with respect to the initial amount present at the end of diastole. It is basically a fraction of stroke volume (SV) v/s end diastolic volume (EDV) and characterizes ventricular ejection.

Stroke volume can be calculated as a difference of EDV and end systolic volume (ESV)

Thus, LVEF: (SV/EDV) X 100

Table 2. Grades of HF classification as per EF according to Lam et al., 2021

Gender	Normal	Mildly abnormal	Moderately abnormal	Severely abnormal
Male	52%-72%	41%-51%	30%-40%	Below 30%
Female	54%-74%	41%-53%	30%-40%	Below 30%

Clinical trial inclusion criteria have often classified HF subtypes based on EF by conforming to the universal nomenclature defined namely under HFrEF: HF with reduced EF ≤40% ; HFmrEF: HF with mid-range EF ≤50% and HFpEF; HF with preserved EF ≥50%. HFpEF has recently further been divided into two subcategories; ''borderline'' corresponding to EF of 41–49% and ''improved'' with an EF of >40%.

However, definitions of HFpEF have differed across several clinical trials:

1. CHARM-Preserved, EMPEROR-Preserved, DELIVER, SPIRIT-HF and SPIRRIT-HFpEF trials >40% or ≥40 (Yusuf et al., 2003; Abraham et al., 2021; Lund et al., 2017).
2. TOPCAT, I-PRESERVE and PARAGON-HF ≥45% (Solomon et al., 2016).
3. SOLOIST-WHF trial ≥50% (Bhatt et al., 2021).

The inclusion of HFmrEF is thus a necessary step to counter the inconsistent process of including patients within EF range of 40-49%. It is also widely accepted now that LVEF on its own fails to adequately characterize all HF patients and a more holistic approach is needed. Cardiac output (CO) and LV filling pressures should also be evaluated to improve characterization and diagnosis (Mele et al., 2018).

3. Pathophysiology of HF

In broad terms, HF can be classified as diastolic HF of diastolic dysfunction (DD) where there is impaired relaxation leading to sub-optimal ventricular filling at end-diastole. In this form, left ventricle is mainly affected. On the other hand, systolic HF hampers the ability of the heart to eject blood properly. A failing heart in advanced stages is usually a combination of both components. A failing heart undergoes abnormal changes in shape and structure due to maladaptive cardiac remodeling and neurohormonal activation resulting into LV systolic dysfunction. There are many factors that can cause such alterations namely, afterload, preload, exacerbated wall tension, stretch, reactive oxygen/nitrogen species, collagen deposits etc. Even though primarily cardiomyocyte function can be hampered but changes in the extracellular matrix can also be a dominant presentation. Abnormalities in heart rhythm, increased metabolic demands and structural defects of the heart as in valve disorders and congenital defects can also lead to HF. Fundamentally, HF can be viewed as a progressive disorder starting from any of these factors or ''index events'' onwards. (Bristow et al., 2016). Such an index event whether it is sudden onset like a myocardial infarction or a chronically developing condition, can lead to an impairment in cardiac compliance which then forces the heart to activate adaptive compensatory mechanisms. These in addition to secondary damages can then lead to the clinical manifestations of HF. In both systolic and diastolic HF, the patients may remain asymptomatic or minimally symptomatic for years until the maladaptive phase of compensation takes over and they start exhibiting symptoms with a concomitant increase in morbidity and mortality.

Viewing the heart as a neurohormonal model posits that HF progression is a cascade effect of active biological molecules that cause deleterious effects on the cardiovascular system (Stephen et al., 1966). These molecules may include hormonal modulators like norepinephrine, peptide growth factors or cytokines like tumor necrosis factor (TNF), endothelin, angiotensin II and Natriuretic peptides. The neurohormonal mechanism lead by these similar biologics successfully explains why despite different etiologies, patients exhibit remarkably consistent phenotypes and why HF develops chronically after an acute event such as MI. Furthermore, loss of cardioprotective effects of endogenous vasodilators like kinins, nitric oxide (NO) and prostaglandins can also fail to counteract the compensatory mechanisms and lead to endothelial dysfunction. Another important compensation is adrenergic activation which can lead to a variety of effects like cardiomyocyte hypertrophy, positive ionotropic

effects, increase in contractility, increase in chronotropy and enhanced end diastolic volume (Eichhorn E.J. et al., 1996).

4. HFpEF

HFpEF is a complex constellation of cardiovascular symptoms and it often presents with dysmetabolic and pro-inflammatory comorbidities along with the hallmark of preserved EF at ≥ 50% (Borlaug et al., 2011). Several characteristics of this entity include diastolic impairment, cardiomyocyte hypertrophy, fibrosis and activation of pro-inflammatory mechanisms. In its contract, HFrEF presents with cardiomyocyte loss, systolic impairment and defects in contraction. A main finding from the clinic is that some form of chronic comorbidity often precedes HFpEF like, renal dysfunction, diabetes (type 2), hypertension or obesity (Clemenza et al., 2022). On the other hand, HFrEF is preceded by loss of cardiomyocytes due to ischemia, valve disorders, genetics etc. Mechanisms pertaining to HFrEF have been quite well understood and the neurohormonal activation theory has provided a trove of therapeutic targets which in the last few decades have led to a steady decline in its prevalence. Clinically proven and efficacious drugs for HFpEF still remain elusive and that has caused its prevalence to rise continuously. At present more than 50% of HF cases are HFpEF and it is expected to rise further (Tsao et al., 2018). HFpEF shares the same grim prognosis as HFrEF with a 75% five-year mortality rate (Shah et al., 2017).

When we couple this with the current aging demograph, better life expectancy and increased incidence of HFpEF-comorbid conditions, we are looking at a pandemic of epic proportions that the current medical community is ill-equipped to handle. Despite the shared risk factors, certain comorbidities between the two HFs differ. Aging is a common factor as HFpEF is the prevalent type of HF seen in older patients (Ho et al., 2013), incidence rate is two-fold higher in women (Lee et al., 2009) and the spectrum of non-cardiac comorbidities like hypertension, T2DM, stroke, anemia, lung/liver disease, sleep apnea, gout, and cancer is quite different from those in HFrEF. The major point of concern is that regardless of these differences, the morbidity and mortality rates of HFpEF and HFrEF are similar and importantly, the incidence of hospitalizations related to comorbid complications are higher in HFpEF (Streng et al., 2018).

Subtle contractile dysfunction may also be present in HFpEF and can be detected using advanced imaging methods (Van Aelst et al., 2018). As compared to HFrEF, there is similar increase in end-diastolic pressure (EDP) and congestion. The major factors that lead to this EDP elevation in HFpEF are diastolic dysfunction, reduced atrial compliance and myocardial stiffness so essentially the whole heart is involved (Borlaug et al., 2014). From a patients perspective, HF symptoms in HFpEF tend to be more subtle and often manifest on physical exertion which is the main cause of delayed diagnosis.

4.1. Subtypes of HFpEF

The heterogeneity in HFpEF is due to the wide array of comorbidities that lead to a multi-organ and systemic involvement. Different methods aimed at disease classification have been proposed to guide decisions for therapies and designing clinical trials. These stratifying parameters include clinical (etiological or HFpEF symptoms driven by the primary comorbidity), pathophysiological (driven by a primary pathomechanism in the patient), type of presentation at clinic, myocardial and data-driven. Machine learning approaches on OMICS data have recently identified several pheno-groups in which HFpEF patients can be broadly categorized (Sanders-van Wijk et al., 2020).

Table 3. Classification of HF into distinct pheno-groups based on the main factor driving pathogenesis according to Sanders-van Wijk et al., 2020

Pheno-group	Driving factor	Presentation
1	Natriuretic peptide deficiency	Obesity, insulin resistance, BNP reduction, increased Aldosterone
2	Cardio-metabolism	Obesity, Type 2 Diabetes Mellitus, Inflammation, endothelial dysfunction, LV hypertrophy, fibrosis, increased myocardial and vascular stiffness, muscular impairment
3	Extra-cardiac comorbidity	Kidney failure, Pulmonary artery hypertension, skeletal myopathy
4	Right heart failure	RV failure, dilatation
5	Left atrial (LA) myopathy	Arterial hypertension, LA dilatation/dysfunction, Atrial fibrillation, secondary atrial mitral regurgitaion
6	Aging	Cardiac aging manifestations

From a purely clinical vantage point, these subclassifications can be quite bothersome because the categories and hallmarks of clinical presentation are not mutually exclusive. There are huge and varying degrees of overlap so, categorization of patients into one specific pheno-group is challenging. Unlike HFrEF, the underlying phenotypic heterogeneity in HFpEF could be an important factor for the failure or inconclusiveness of several clinical trials in the past but these trial histories have helped in advancing our understanding of the heterogeneity and have led to better classification systems.

Table 4. HFpEF categorization (Adapted from Shah et al., 2014)

Classification scheme	Categories of HFpEF	Description
Clinical classification	"Garden-variety" HFpEF	HTN, diabetes, obesity, and/or chronic kidney disease
	CAD-HFpEF	Typically, multivessel CAD with prior coronary revascularization
	Right heart failure-HFpEF	Predominant right-sided HF with or without pulmonary HTN
	Atrial fibrillation-predominant HFpEF	Atrial arrhythmias dominate the clinical presentation
	HCM-like HFpEF	These patients do not have genetic forms of HCM, but their clinical course and echocardiographic features are typical of HCM
	High-output HFpEF	Typically, due to liver disease, severe anemia
	Valvular HFpEF	Multiple moderate valvular lesions
	Rare causes of HFpEF	For example, infiltrative cardiomyopathies, cardiotoxicities, genetic cardiomyopathies
Presentation phenotypes	Exercise-induced increase in LA pressure	These patients typically are very breathless with exertion but do not have overt signs of volume overload and typically do not have a history of HF hospitalization
	Volume overload	Signs and symptoms of volume overload; typically have a history of HF hospitalization
	RV failure + pulmonary HTN	Right heart failure predominates the clinical picture; often pulmonary HTN is present and systemic blood pressure is reduced
Myocardial phenotypes	Type 1: HCM	Typical genetic forms of HCM
	Type 2: Infiltrative	Cardiac amyloidosis and other forms of infiltrative or restrictive cardiomyopathies
	Type 3: Non-HTN, non-LVH	No history of HTN and LV wall thickness < 1.2 cm
	Type 4: HTN	Typical, "garden-variety" form of HFpEF with history of HTN
Latent class analysis	A: Younger males with CAD, lower LVEF	Based on latent class analysis of the I-PRESERVE AND CHARM-Preserved trials. The authors used latent class analysis of 11 clinical features (age, gender, BMI, atrial fibrillation, CAD, diabetes, hyperlipidemia, valvular disease, alcohol use, eGFR, and hematocrit) to find 6 distinct groups of HFpEF in I-PRESERVE and validated these findings in CHARM-Preserved
	B: Younger females with lowest NT-proBNP	
	C: Obesity, hyperlipidemia, diabetes mellitus, anemia, and renal insufficiency	
	D: Obese females	
	E: Older males with CAD, lowest LVEF	
	F: female predominance, advanced age, lower BMI, atrial fibrillation, CKD, highest NT-proBNP	
Pheno-mapping	Pheno-group 1: BNP deficiency syndrome	Model-based clustering of 67 continuous variables (phenotypes): physical characteristics, vital signs, ECG data, laboratory data, and echocardiographic parameters
	Pheno-group 2: Cardiometabolic phenotype	
	Pheno-group 3: RV failure + cardiorenal phenotype	

CAD coronary artery disease, ***HCM*** hypertrophic cardiomyopathy, ***HF*** heart failure, ***RV*** right ventricular, ***HTN*** hypertension, ***LVH*** left ventricular hypertrophy, ***LVEF*** left ventricular ejection fraction, ***BMI*** body mass index, ***CKD*** chronic kidney disease, ***NT-proBNP*** N-terminal pro-B-type natriuretic peptide

5. Structural and functional alterations in HFpEF

5.1. Diastolic dysfunction (DD) and ventricular stiffness

DD is an important precursor of symptomatic HFpEF and patients exhibit alterations in both the active and passive phases of relaxation (Zile et al., 2015). Active relaxation is when LV goes from end contraction to relaxation stage, it is energy consuming while the second phase is energetically passive and LV relaxation occurs as a consequence of natural filling. One important mechanism is the hypo-phosphorylation of protein kinase A and G (PKA, PKG) on cardiac Titin protein. (Borbély et al., 2005). Apart from changes in levels of phosphorylation, titin stiffness is also modulated by isoform shifts caused by alternate splicing. (LeWinter et al., 2013). There are two isoforms of Titin N2B and N2BA, where N2B is the smaller and stiffer version. In a normal post-natal heart, the N2BA: N2B ratio is about 40-60%. In HFpEF, an isoform shift occurs which increases the amount of more compliant N2BA

isoform. The overall effect of increased N2BA isoform and hypo-phosphorylation on PKA/PKG sites is an elevation in resting tension in HFpEF cardiomyocytes. (Borbély et al., 2005). Hamdani et al., in 2013 showed that components of metabolic syndrome aside from hypertension are enough to cause changes in passive stiffness due to reduced titin phosphorylation. Moreover, oxidative stress can induce disulfide bridges in titin leading to increased passive stiffness (Grützner et al., 2009). However, there could be other causes of ventricular stiffness in HFpEF aside from titin phosphorylation. For example, perturbation in extracellular matrix (ECM) collagen where the collagen volume fraction i.e. relative abundance of collagen 1 and cross linking are increased (Kasner et al., 2011). Another important contributor can be several mechanisms that restore systolic $[Ca^{2+}]_{in}$ to systolic levels (Selby et al., 2011). Cross-bridge dissociation dynamics are energy dependent and thus, slowed LV relaxation can be due to energy deficit in the myocardium as evidenced by low creatine phosphate: ATP ratio (Phan et al., 2009, Donaldson et al., 2012). These mechanisms are summarized in **figure 2**.

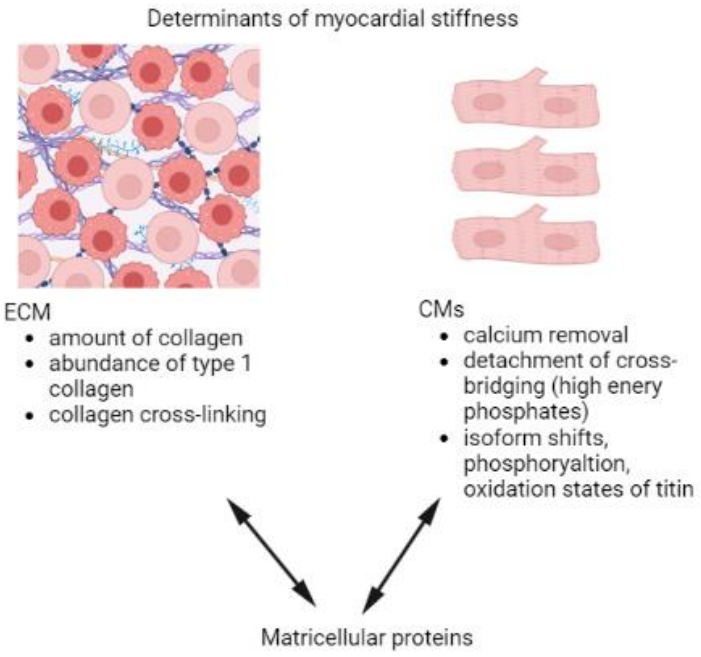

Fig. 2 Mechanisms leading to myocardial stiffness in HFpEF.
Extra cellular matrix (ECM) and cardiomyocyte (CM) milieu collaborate with distinct driving factors (created using BioRender).

5.2. Reduced cardiac reserve and chronotropic incompetence

At rest HFpEF patients may appear asymptomatic but on exertion they often start to complain which points to affected cardiac reserve subsequent to exercise stress (Ennezat et al., 2008; Brubaker et al., 2006). In a healthy heart, peripheral vasodilation, heart rate, venous return and contractility act in a concerted manner to increase cardiac output during exertion. HFpEF patients are often unable to achieve this and may present with a defect in any of these mechanisms. Ideally when a normal heart

faces exercise exertion, it is able to increase ventricular filling volume at preload in a short time without imbalancing filling pressure. Diastolic reserve is reduced in a HFpEF heart and thus the increase in preload volume at exertion is reduced and filling pressure is increased. Proposed determinants are likely increased stiffness of ventricular chamber (Westermann et al., 2008), delayed relaxation (Wachter et al., 2009) and restraint from the pericardial tissue (Dauterman et al., 1995). Minute and subtle defects in systolic function are also sometimes unmasked with exercise stress (Tan et al., 2009).

Exercise induced increase in heart rate is also lower i.e. chronotropic incompetence is observed in HFpEF even on comparison with older, age matched controls (Borlaug et al., 2010). Defects in downstream pathways of β-adrenergic stimulation are an important mediator of this. "Baroreflex sensitivity" has been shown to be reduced in HFpEF patients so there may be some autonomic deficits as well along with reduced arterial elastance (Borlaug et al., 2006). Many of these deficits are found in a naturally aging heart but in HFpEF they are more pronounced. Overall, diastolic, systolic, chronotropic and vascular function defects may together contribute to the cardiovascular reserve dysfunction.

5.3. Ventricular-arterial coupling and vascular dysfunction

Along with ventricles, blood vessel abnormalities also have an important role in HFpEF pathophysiology. Stiffness of the large arteries like aorta is evident in patients with comorbid certain conditions like diabetes, hypertension and ageing (Owan et al., 2006) and strongly correlate with exercise intolerance (Hundley et al., 2001). A healthy heart is able to provide optimal blood flow at physiological pressures when the body demands for it. Ventricular-arterial compliance allows the pulse and peak pressures to be buffered so that massive fluctuations in blood pressure are circumvented and prevent damage to the end-organs. Arterial elastance (Ea) and End-systolic elastance (Ee) are both increased in HFpEF and lead to ''labile blood pressure changes'' in response to changing preload and afterload. (Gandhi et al., 2001;Borlaug et al., 2008).

Moreover, systemic vasodilatory mechanisms are also impaired in HFpEF resulting in reduced delivery of blood to skeletal muscles during increased oxygen demands. Endothelial dysfunction and Nitric oxide (NO) bioavailability are important mediators here engaged in a complex crosstalk. (Borlaug et al., 2010). It has been shown that patients without defects in vasodilation have a better prognosis than those with impaired vasodilation (Akiyama et al., 2012).

5.4. Endothelial dysfunction (ED), role of oxidative-nitrosative stress and the pro-inflammatory hypothesis of HFpEF

The endothelial layer is highly interactive and dynamic in nature and plays a pivotal role in homeostasis and vascular regulation through the release of vasoactive substances like NO, Endothelin1 and Apelin. The main effector of endothelium is the gaseous molecule, NO which works through the cyclic guanosine monophosphate (cGMP) pathway to prevent shear pressures induced vascular injury (Segers et al., 2018). However, in the setting of HFpEF and many of its associated comorbidities, endothelial homeostasis is greatly disturbed and driven towards vasoconstriction, inflammation and thrombosis.

Paulus and Tschöpe in their seminal work from 2013 showed that ED plays an important role in HFpEF development though coronary microvascular defects caused by the comorbidities. Secondary to ED, circulating pro-inflammatory cytokines and ROS activate and inflame the global endothelium. NO bioavailability is reduced which decreases PKG activity in cardiomyocytes leading to fundamental hallmark characteristics of HFpEF like concentric remodeling, cardiac hypertrophy and titin hypo-phosphorylation. Cardiomyocyte stiffness and collagen deposition are also concurrent. A more direct effect is seen through eNOS expression (Yoshizumi et al., 1993). This state of systemic inflammation has been highly correlated with incidences of HFpEF and not HFrEF, indicating an important driving force to shift the HF spectrum (Kalogeropoulos et al., 2010). These mechanisms are summarized in **figure 3.**

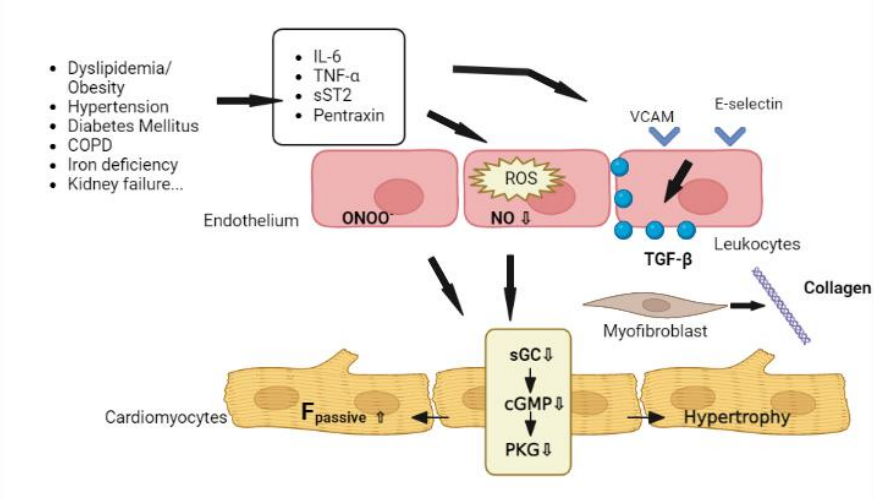

Fig. 3. Several HFpEF linked comorbidities lead to a systemic state of chronic-low grade inflammation. This meta-inflammation then imparts direct effects on the endothelium and cardiomyocytes (created in BioRender and modified from Segers et al., 2018; Yoshizumi et al., 1993).

Nitrosative-oxidative stress arising from NADPH oxidases NOX2 and NOX4 (Santos et al., 2016), xanthine oxidase, monoamine oxidase (Kaludercic et al., 2010), inducible nitric oxide synthase (iNOS) and uncoupled nitric oxide synthase (eNOS) (Schiattarella et al., 2019) are important in conferring downstream endothelial injury.

5.5. Cardiomyocyte remodeling

As previously highlighted, LV hypertrophy is a prominent feature of HFpEF and it directly leads to elevated filling pressures and diastolic dysfunction at normal EF. However, clinical trials have established that 30-60% patients show LV hypertrophy so, it is not an absolute requirement for HFpEF and reinforces the heterogeneity of the condition (Armstrong et al., 2014). Nakamura and Sadoshima in their work from 2018 report that the major determinants of pathological cardiomyocyte hypertrophy are impairment in calcium handling, oxidative stress, apoptosis, suboptimal angiogenesis, metabolic dysfunction, fetal gene reprogramming, cell growth and hypertrophic protein synthesis. Most hypertrophic effects are exerted through G-protein-coupled receptors (GPCRs) and their ligands. These ligands are of four major classes.

1. Hormonal: angiotensin II, endothelin 1, α-adrenergic receptors and β- adrenergic receptor substrates
2. Signaling Kinases: ERK1/2, Janus kinase (JNK), Ca2+/calmodulin-dependent protein kinase II (CAMKII), Protein kinase C, A, G (PKC/PKA/PKG), p38 , mechanistic target of rapamycin 1 (mTORC1) and AMPK.

3. Epigenetic modifiers: myocyte enhancer factor 2 (MEF2), nuclear factor of activated T cells (NFAT), GATA4, class II Histone deacetylases (HDACs) and Hippo.
4. Mechanosensory membrane channels: Transient receptor potential channel (TRPC) and TRPV.

In contrast with HFrEF, activation of the Renin Angiotensin Aldosterone System (RAAS) and sustained catecholamine hyperstimulation play "no primary role in HFpEF hypertrophy". (Wintrich et al., 2020; Yamamoto et al., 2014).

5.6. Fibrosis and ECM remodeling

Interstitial fibrosis stimulated by LV hypertrophy and hypertension have been known to cause passive stiffness and reduced ventricular compliance in HFpEF (Doi et al., 2000). Advanced glycation end products from diabetes are also known to cause matrix protein alterations and lead to fibrosis (van Heerebeek et al., 2008). Since, diabetes is a common comorbidity in HFpEF, this driving factor is an important one. Obesity is also linked to enhanced hepatic and myocardial fibrosis (Panchal et al., 2011). But the question here is, when is fibrosis in HFpEF pathophysiologically relevant? It seems that not the amount of fibrosis per se but the type of fibrosis and its location seems to be more relevant in HFpEF context as well as the quality of collagen cross-linking (Ravassa et al., 2018). There are multiple types of complex fibroblast cells which are derived from different lineages and they lead to the variation found in scar-tissue after injury. The main pro-fibrotic signaling mechanisms are insulin resistance, RAAS, TGF-β, Endothelin 1, dynamics of matricellular proteins, RHO-Kinase and Leptin mediated signaling (Cavalera et al., 2014). The ECM is made up of collagens, proteoglycans, glycoproteins and glycosaminoglycans. The amount of collagen is intricately balanced by synthesis, modifications, post-translational modification and degradation. Interstitial fibrosis is an important occurrence in most HFpEF subtypes although the severity varies (Hahn et al., 2020). Mainly, the crosstalk between inflammatory cells and the resident fibroblast happens via paracrine signaling. Continued myofibroblast activation then produces pro-fibrotic ECM and matricellular proteins. Matrix-crosslinking enzymes like Lysyl oxidase (Lox) prevent collagen degradation leading to its deposition causing enhanced collagen content and stiffness. Matrix metalloproteinases (MMPs), which can degrade ECM proteins and tissue inhibitors of matrix metalloproteinases (TIMPs) play an important role in ECM remodeling consequently, MMP1/TIMP1 ratio is an important plasma biomarker of fibrosis. The schematic in **figure 4** attempts to elaborate on the fibrotic-inflammatory pathways in HFpEF.

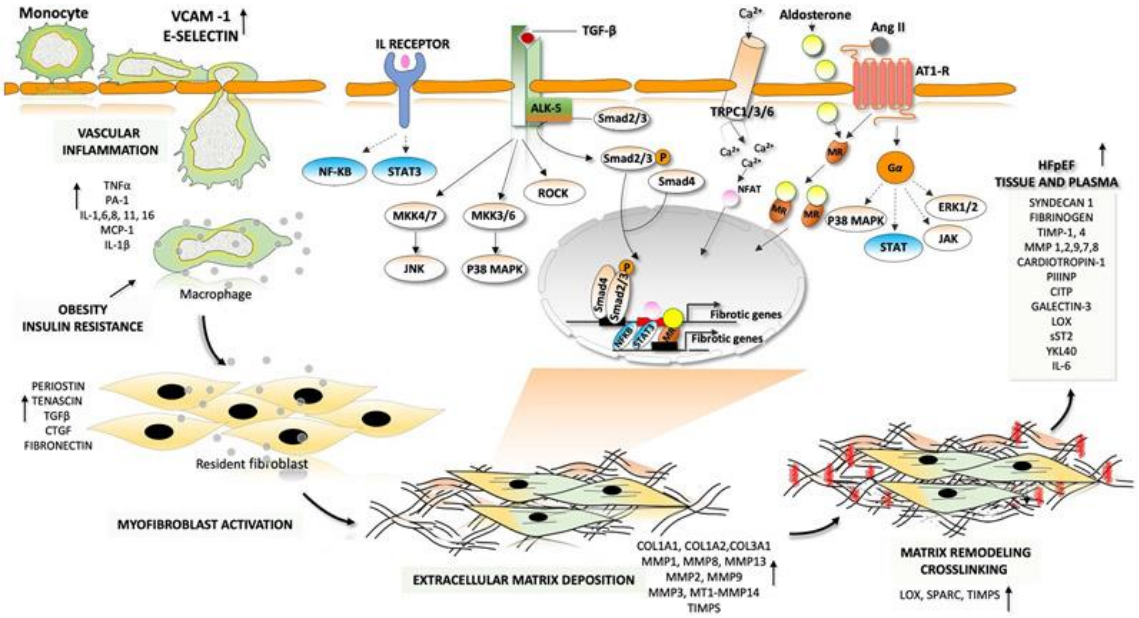

Fig. 4. Crosstalk between pro-fibrotic inflammatory pathways in HFpEF
IL-1, IL-6 and IL-8, Interleukins; G-CSF, granulocyte-colony stimulating factor; M-CSF ,macrophage colony-stimulating factor; GM-CSF, granulocyte-macrophage colony-stimulating factor; CCL2, C-C motif chemokine 2; TNF , tumor necrosis factor, VCAM1, vascular cell adhesion protein 1; LOX, lysyl oxidase; TGFβ, transforming growth factor-β; SMAD2–SMAD3, mothers against decapentaplegic homologue 2,3; ROCK ,Rho-associated protein kinase; ERK , extracellular-signal-regulated kinase; JAK, Janus kinase; STAT, signal transducer and activator of transcription; NFAT ,calcineurin–nuclear factor of activated T cells; TRPCs , transient receptor potential channels; AngII, angiotensin II; AT1R, angiotensin II receptor type 1; CITP, carboxy-terminal pro-peptide of procollagen type I; COL, collagen; CTGF, connective tissue growth factor; JNK, JUN N-terminal kinase; MAPK, mitogen-activated protein kinase; MMP, matrix metalloproteinase; MEK, MAPK/ERK kinase; NF-κB, nuclear factor-κB; P, phosphate; PIIINP, amino-terminal pro-peptide of procollagen type III; sST2, soluble protein ST2; TGFBR1, transforming growth factor-β receptor type 1; TIMP, metalloproteinase inhibitor; YKL40, chitinase-3-like protein 1. (Adapted from Mishra et al., 2021).

5.7. Calcium handling

HFpEF is mainly a ventricular relaxation defect and a part of it is energy-dependent where intracellular Ca^{2+} homeostasis play an important role (Barry et al., 1993). Electrophysiological studies on animal models have shown that it is mainly a cascade effect of increased Sarcoplasmic reticulum (SR) Ca^{2+} leak current and a decreased Ca^{2+} release from ryanodine receptors (RyR) (Zile et al., 2011, Borbély et al., 2005). The regulatory protein, phospholamban (PLN) is also relevant here in addition to downstream CaMKII (Bridge et al., 1990). At the level of cardiomyocytes, efficient relaxation is directly linked to efficient removal of Ca^{2+} from SR cytosol. The main mechanisms that facilitate Ca^{2+} removal are recycling back to SR by SR Ca^{2+} ATPase 2a (SERCA2a), Ca^{2+} outflow mediated by Na^{+}/ Ca^{2+} exchanger (NCX) and through mitochondrial Ca^{2+} Uniporter. The type of impairment is variable across different subtypes of HFpEF populations (Louch et al., 2012). In contrast, in HFrEF Ca^{2+} release is affected which leads to slower and smaller contractions which may be because of reduced SERCA2a activity, increased RyR leak, T-tubule disruption leading to orphaned RyRs and lastly, increased NCX activity. These

mechanisms are not completely absent in HFpEF however, their presentation varies vastly. In addition, HFrEF patients have impaired myocardial Na^+ gradient but in HFpEF it is not the case (Pieske et al., 2017). Mitochondria also plays pivotal role in calcium dynamics and in HFpEF rat models it has been shown that due to differential cytosolic and mitochondrial calcium processing, free mitochondrial [Ca^{2+}] was higher (Miranda-Silva et al., 2020).

5.8. Mitochondrial and metabolic alterations

Recent reviews indicate that abnormal mitochondrial function and metabolism may be highly implicated in HFpEF (Noordali et al., 2018; Karwi et al., 2018). Exercise stress tests on HFpEF patients often show a reduction in exercise duration, peak power output, CO and peak exercise oxygen consumption (Haykowsky et al., 2011). These alterations suggest that there is an imbalance in oxygen delivery and utilization systems. Predominantly, factors like mitochondrial dysfunction in skeletal muscle or cardiomyocyte seemed to be important here. On the other hand, in HFrEF the same effects appear to be mediated through cardiac pump performance (Pugliese et al., 2019). The main mechanisms of skeletal and cardiomyocyte mitochondrial dysfunction can be due to reduced Electron Transport chain (ETC) activity (Garnier et al., 2003), assembly defects in the ETC complexes (Rosca et al., 2008), increase in ROS (Sheeran et al., 2006), alteration in mitochondrial inner membrane or mitochondrial uncoupling (Murray et al., 2008), quality control defects in mitochondrial fission and fusion (Song et al., 2015).

Alterations in a wide variety of metabolic pathways can alter ATP production in mitochondria and substrate utilization which then leads to reduced myocardial energy stores and work efficiency. Here also, the spectrum of comorbidities can lead to differential presentation. For example in obesity, there is an oversupply of systemic fatty acid through adipose tissues which are then directed to peripheral organs like the heart. There is essentially an imbalance between uptake of fatty acids and fatty acid oxidation leading to accumulation of metabolites like diglycerides and ceramides in the myocardium (Dávila-Román et al., 2002). Hypoxic states can shift the metabolism towards glycolysis thus impairing pyruvate dehydrogenase. Compensatory mechanisms divert metabolism towards anaplerosis through hexosamine biosynthetic pathway and the pentose phosphate pathway (Lauzier et al., 2013). Elevated levels of myocardial triglycerides are reported in HFpEF (Mahmod et al., 2018) and the extent of steatosis directly relates to impaired diastolic strain rates and exercise intolerance (Wei et al., 2016). Moreover, a higher risk in HFpEF is associated with increased plasma levels of fatty acids (Djoussé et al., 2014). In addition, ketone bodies are reported to increase in HFpEF as a compensatory mechanism to energy deficit (Zordoky et al., 2015). A major ketone body is β-Hydroxybutyrate which is known to inhibit HDACs (Newman et al., 2014) so ketone body supplementation may exert beneficial effects

that go beyond metabolism (Jeong et al., 2018). Cardioprotective effects of empagliflozin are known to act through increasing ketone levels in the plasma (Ferrannini et al., 2016). Deng et al., in 2021 also showed that increasing utilization of mitochondrial ketone can help in certain HFpEF subtypes by reducing the acetyl-CoA pool and increase activity of citric synthase which then breaks the harmful cycle of mitochondrial dysfunction.

6. Risk factors involved in HFpEF

As per the above review of literature, it is evident that HFpEF is a constellation of comorbidities that induce a systemic pro-inflammatory state. The risk factors involved in the disease are a reflection of this vast collection of comorbid illnesses. Cardiac factors like hypertrophic/infiltrative cardiomyopathy, systemic HTN and CAD are some risk factors central to the heart. Apart from these, extra cardiac factors like obesity, metabolic syndrome, diabetes, insulin resistance, kidney disorders, chronic obstructive pulmonary disease (COPD), sleep apnea, muscular deconditioning and iron deficiency are highly relevant. Some social and demographic factors include aging, female gender, menopause and sedentary lifestyle (Juillière et al., 2018).

Some risk factors that are especially relevant to this dissertation are discussed in detail in the following section.

6.1. Metabolic syndrome

Metabolic syndrome is defined as a collection of conditions that simultaneously increase the risk of heart disease, stroke and other serious illnesses. These conditions include abdominal obesity, hypertension, high blood sugar, high triglycerides and low levels of high density lipoprotein (HDL). Patients with HFpEF and metabolic syndrome exhibit more cardiovascular abnormalities, deteriorated renal function and overall worse quality of life (Zhou et al., 2021). The incidence rate of metabolic syndrome is usually high in HF but it becomes seemingly more important in the context of HFpEF. Ferrari et al., in 2015 demonstrated that 85% of patients present with a form of metabolic syndrome. Glucose intolerance and dysglycemia are characteristic end-points triggered by central obesity (Mottillo et al., 2010). Hyperinsulinemic states afforded by metabolic syndrome can result in peripheral vasoconstriction and sodium retention (Perrone-Filardi et al., 2015). Echocardiographic findings also show worse diastolic function in HFpEF patients with metabolic syndrome than without (Zhou et al., 2021). Increased occurrence of dyslipidemic states can lead to increased free fatty-acid utilization by cardiomyocytes leading to mitochondrial dysfunction and ultimately production of ROS and toxic lipid intermediates (McHugh et al., 2019). Adipocytes also secrete cytokines involved in inflammation and AGEs which can enhance microvascular and endothelial damage. The clinical consensus is that increased neurohumoral activation due to dyslipidemic states precede the vascular

congestion and cardio-renal symptoms in HFpEF leading to increased hospitalizations (Chirinos et al., 2019). It is no surprise that the obesity epidemic has been parallel to the HFpEF epidemic in recent times.

6.2. Aging

Aging in HFpEF has been seen in the light of a ''geriatric syndrome'' as multiple age related changes in cardiovascular function and structure are involved in HFpEF. More than 50% of HF patients over the age of 65 and almost all patients above the age of 90 years exhibit HFpEF (Upadhya et al., 2020). Age related changes to arterial/myocardial stiffness, diastolic relaxation, LV mass, contractility, coronary flow reserve and β-adrenergic stimulation; all follow a pattern that is commonly seen in HFpEF patients (Rich et al., 2000). Aging also affects endothelial vasodilation in a negative manner and is associated with poor vascular compliance. Geriatric comorbidities associated with aging can initiate or aggravate chronic systemic inflammation that can lead to a deleterious signaling cascade leading to the belief that older patients with HFpEF may exhibit a form of presbycardia. Interesting experiments involving parabiosis have shown that young animals develop HFpEF like features when exposed to the blood of of animals supporting the idea of a ''systemic trigger'' (Loffredo et al., 2013). Studies have also shown that senescent mice have low incidence of common HFpEF risk factors like hypertension indicating that aging helps enhance the condition independent of these conventional risk factors (Roh et al., 2020).

6.3. Female gender

Female gender is independently associated with increased incidence of diastolic dysfunction (Lau et al., 2020). Female HFpEF patients outnumber men by a ratio of 2:1 at any given age (Dunlay et al., 2017). Several studies have shown that female patients show worse forms of exercise induced hemodynamic parameters like impaired diastolic reserve and lower systemic-pulmonary compliance at stress (Beale et al., 2019). These findings hint that gender-specific pathways to HFpEF might exist. Sex-differences can affect calcium handling, myocyte stiffness and cardio-metabolism (Parks et al., 2014; Peterson et al., 2008). Low estrogen states in men have been correlated with an activated RAAS (Zhao et al., 2014) and drop in PKA and NO with menopause in older female patients may also be a differentiating factor (Kravtsov et al., 2007). Other causal risk factors like anemia and iron deficiency are more prevalent in women (Scantlebury et al., 2011) who also show that in response to arterial HTN, women show increased concentric left ventricular remodeling and reduced ventricular dilatation. A hypothesis supports that females have a higher predisposition towards HFpEF due to a similar cardiac output compared to men despite the reduced ventricular size and stroke volume

(Acropinto et al., 2022). Cardioprotective effects of estrogen are well studied and the decline in its levels post-menopause could be the trigger of enhanced microvascular endothelial damage in older female patients. Women are also predisposed to greater levels of pro-inflammatory cytokines and higher involvement of T cell mediated immunity which may enhance the chronic low-grade systemic inflammation, an important sect of HFpEF pathophysiology (Klein et al., 2016). The association of obesity is also stronger in women (Eaton et al., 2016).

6.4. Pressure overload (PO)

PO secondary to aortic valve stenosis is a well characterized process leading to syndromes reminiscent of HFpEF. From a pathological standpoint, it is one of the most important risk factors for LV-DD and HFpEF, about 60-80% patients with HFpEF present with HTN induced PO (McMurray et al., 2008). Pathophysiologies subsequent to PO cause a concentric type compensatory cardiac remodeling leading to increased filling pressures commonly seen in HFpEF (Gao et al., 2021). Molecular mechanisms relating to PO culminate in cardiomyocyte hypertrophy and activation of pro-fibrotic pathways (van den Borne et al., 2010). PO also culminates in other molecular and cellular mechanisms involved in promoting LVDD like structural changes to ECM, structural and functional perturbations in cardiomyocytes, posttranslational changes to sarcomeric titin, enhanced oxidative-nitrosative stress, reduced NO bioavailability and reduced cGMP/PKG signaling (van Heerebeek et al., 2012). This can also alter the hemodynamics of the heart in terms of impairment in contractility, relaxation delay, increased myocardial stiffness and reduction in compliance. The schematic in **figure 5** attempts to summarize the global effects of PO leading to HFpEF symptoms.

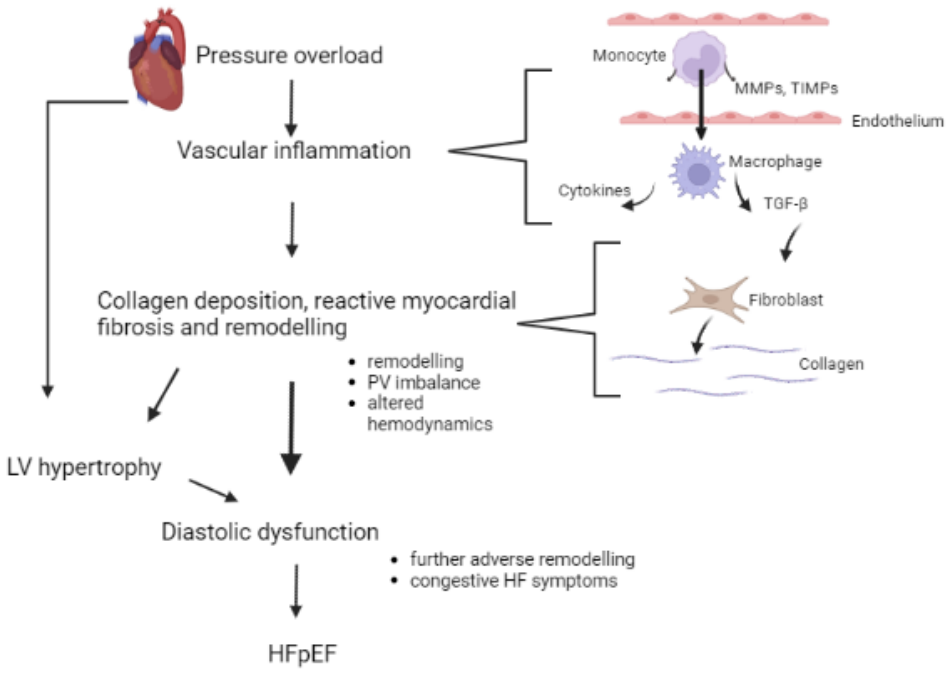

Fig. 5. Pressure overload and the cascade leading to HFpEF. Endothelial injury activates a cytokine cascade leading to vascular inflammation.
The cytokine driven inflammatory state also affects collagen dynamics due to fibroblast activation which in turn leads to reactive myocardial fibrosis and subsequent remodeling. This along with hypertrophic and diastolic defects lead to further adverse remodeling and the typical symptoms of HFpEF. (created using BioRender, modified from Gao et al., 2021; Van-Hereebeek et al., 2012)

7. Modeling HFpEF in the lab

Since the recognition of HFpEF as a distinct and separate entity, development of its specific therapeutics have remained largely elusive. Therapeutics borrowed from HFrEF like angiotensin converting enzyme (ACE) inhibitors, mineralocorticoid receptor antagonists and angiotensin receptor blockade have failed to convincingly decrease the morbidity and mortality in HFpEF (Khan et al., 2017; Pitt et al., 2014). Moreover, clinical trials that aimed to increase NO bioavailability and stimulate cGMP also proved non-significant, inconsistent or inconclusive (Pieske et al., 2017; Borlaug et al., 2018). Our advances in understanding HFpEF have sadly not paralleled in treating it and currently no specific therapeutic exists for the condition. Animal models exhibiting the constellation of HFpEF symptoms are a bottleneck in the drug development pipeline. This unsuccessful translation from bench-to-bedside has been made even more cumbersome by the heterogeneity of HFpEF subpopulations that are infamously difficult to categorize. A consensus needs to exist between pre-clinical animal models and clinical HFpEF but it is a difficult aim to achieve. It has been suggested that pre-clinical animal models should fit the majority of the following requirements to be sufficient, reliable and accurate (Withaar et al., 2021) as illustrated in **figure 6.**

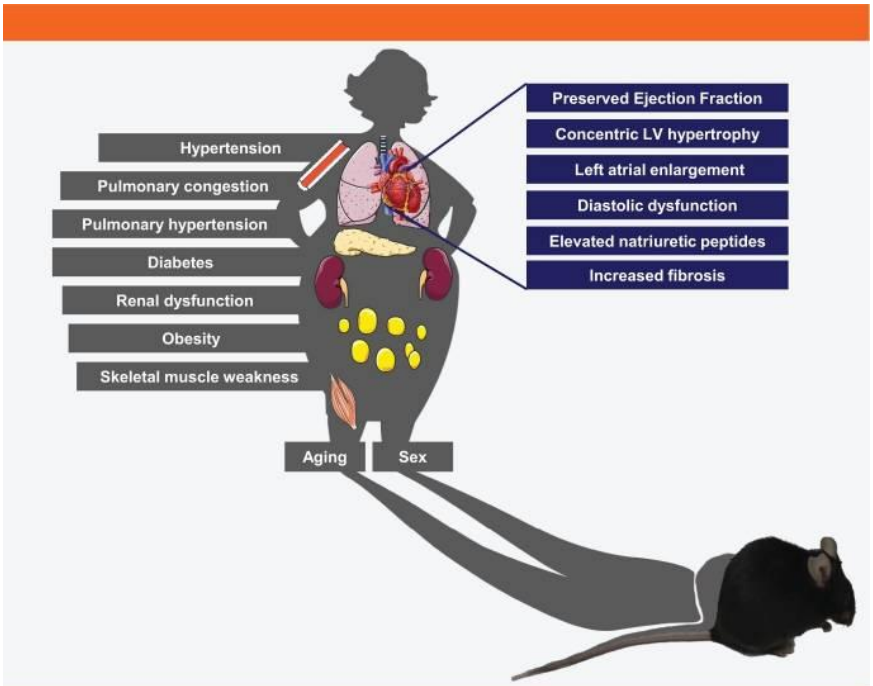

Fig. 6. Capturing the inherent complexity of HFpEF in animal models.
Factors deemed essential to develop a reliable and accurate pre-clinical HFpEF model: (1) pulmonary congestion and elevated natriuretic peptides; (2) a distinct phenotype with preserved systolic LV function with concentric hypertrophy, fibrosis, atrial remodeling and diastolic dysfunction; (3) extra-cardiac comorbidities and (4) evaluation of the effect of sex and aging. (Adapted from Withaar et al., 2021)

However, meeting this standard criteria is no easy task. Animal models have yet to achieve complete recapitulation of the complexities that exist in this truly multifactorial syndrome. Another setback in laboratory modelling is that it is a sudden HF onset while in reality, the condition develops in continuity over several years. With regards to DD, it is also worth noting that rodent models gradually progress to HFrEF like states which is different from humans (Van Ham et al., 2022).

Angiotensin II (ANGII) infusion models are reliable to induce HF with hypertrophy and remodeling even though the effects of infusion appear to be strain specific (Peng et al., 2011). DD dysfunction is clearly evident but the effects of obesity are largely not included resulting in low relevance. **Leptin receptor-deficient (db/db) models** aimed at inducing dyslipidemia develop DD, fibrosis and concentric hypertrophy on aging but do not include congestion and elevation of natriuretic peptides (Broderick et al., 2012). In contrast, the **Leptin-deficient model (ob/ob)** recapitulate lipid accumulation induced concentric hypertrophy and DD. But they lack relevance because the maladaptive effects are absolutely related to the loss of leptin-signaling and HFpEF patients with leptin deficiency are rare so they do not fully mimic the human phenotype despite being a good model to study pathomechanisms (Clément et al., 2006). **High fat diet (HFD)/western diet models** have been adapted to holistically mimic the effects of obesity. These models are able to

capture dyslipidemic effects subsequent to hyperglycemia and insulin resistance in a strain and sex specific manner (Agrawal et al., 2019; Salinero et al., 2018). Pulmonary hypertension, concentric remodeling, fibrosis and DD have been well characterized in HFD mice. Pulmonary congestion, natriuretic peptide elevation and skeletal muscle weakness has not been reported consistently throughout literature (Meng et al., 2017).

Natural aging models beyond the age of 24 months exhibit maladaptive cardiac phenotypes associated with HFpEF including DD, hypertrophy, fibrosis and reduced exercise tolerance (Aurich et al., 2013). Some studies report lung congestion and increased natriuretic peptides however, hypertension and effects of diabetes have not been reported (Roh et al., 2020). To accelerate aging, **accelerated senescence model (SAMP)** have been developed to reduce the time span of studies and report similar findings.

The last few years have seen a paradigm shift in the development in pre-clinical models of HFpEF as multifactorial models have gained more prominence. **Deoxycorticosterone acetate salt-sensitive model (DOCA)** exhibits fibrotic hypertrophy, NP elevation, DD and mild increase in blood pressure but the age and sex related differences have not yet been described. Models with **aldosterone + uni-nephrectomy** show renal dysfunction, hypertension, lung congestion, and decreased exercise capacity but effects of obesity and T2DM are largely ignored (Withaar et al., 2021). Combination models with HFD have also been a trend recently considering the growing recognition of metabolic and dyslipidemic contributions to HFpEF. **HFD + ANGII** infusion mice develop DD, concentric hypertrophy with fibrosis and high NP levels but the evidence for lung congestion and exercise impairment is missing (Piek et al., 2019). Aging has been added as a factor to increase the relevance of this model. Very recently, an elegant study by Schiattarella et al. successfully developed a two-hit pre-clinical mouse model that comes close to resembling human HFpEF. **HFD + L-NAME** (constitutive nitric oxide synthase inhibitor) was used to induce lung congestion, reduced exercise capacity and increased NP along with typical DD symptoms. More recently, gender specific effects have also been shown in this model (Tong et al., 2019). The effect of aging remains yet to be determined here.

Aims and project design

In light of the literature review, it is quite evident that animal models that reliably capture the inherent complexity of HFpEF are urgently needed. However, the heterogeneity of the condition makes achieving a 'one-size-fits-all' model highly difficult and improbable. Here, the parable of cancer can be drawn where the condition itself is so variable on a wide spectrum that a personalized approach is deemed necessary towards modeling it. It is also of note that in the clinic, patients often exhibit a constellation of symptoms that can be broadly (but not perfectly) categorized into various subtypes so, the fishing expedition for one perfect model that achieves this is impossible but also highly redundant.

Therefore, this dissertation broadly aims to:

1. Create models of HFpEF by mimicking separate pheno-groups into different mouse models that recapitulate a particular subtype of patients.
2. Characterize these models based on phenotypic stratifications reflecting clinically relevant endpoints.
3. Adopt a novel cross-comparative approach to find differences between patho-mechanisms that drive different pheno-groups of HFpEF which might further assist in identifying novel therapeutic targets for patients.

Materials and Methods

1. Animal housing, care and maintenance

All animal experiments used in this thesis were approved by the Institutional Review Board (Lower Saxony State Office for Consumer Protection and Food Safety (LAVES), including certain amendments. Care was taken so that the investigations conform to the Guide for Care and Use of Laboratory Animals published by the US National Institutes of Health (publication No. 85-23, revision 1996) and were in accordance with the ethical standards laid down in the Declaration of Helsinki 1964.

Wild type male and female C57Bl/6J and FVB/N mice were acquired from Charles River and were housed under the standard conditions of 12 hours light/dark cycling with ad-libitum access to food and water. All animals were allowed to acclimatize for 1-2 weeks before starting any experimental protocols.

2. Dyslipidemia through high fat diet

For all experiments involving HFD, female C57BL/6J mice between the age of 6-8 weeks were used. To acclimatize, these mice were fed with standard chow (10-12% kcal fat, in-house diet at the central animal facility) for two weeks. After acclimatization, the mice were divided into four groups HFD sham and TAC groups received a modified diet with 60% kcal fat obtained from ResearchDiets Inc. (diet number D12492) for 8-10 weeks. The diet composition is shown in **table 5** and it has been proven effective in inducing a dyslipidemic state consistent with metabolic syndrome through several studies (Che et al., 2018, Johnston et al., 2007). The control groups of normal diet sham and TAC were put on regular chow. Body mass was regularly measured every week for both groups.

Table 5. Composition of High fat diet D12492 (Source: Research Diets Inc. USA)

Ingredient	**Gm**	**Kcal**
Protein	26.2%	20%
Carbohydrate	26.3%	20%
Fat	34.9%	**60%**
Casein	200	800
L-Cystine	3	12

Corn starch	0	0
Maltodextrin 10	125	500
Sucrose	68.8	275.2
Cellulose	50	0
Soybean oil	25	225
Lard	245	2205
Mineral Mix, S10026	10	0
Di-Calcium Phosphate	13	0
Calcium Carbonate	5.5	0
Potassium Citrate	16.5	0
Vitamin mix, V10001	10	40
Choline Bitartrate	2	0
Blue dye	0.05	0
Total	**773.5**	**4057**

3. Aged mice

For HFpEF models based on aging, one year old female C57BL/6J mice from Charles River laboratories were purchased and kept at the central animal facility for an additional 6-8 months. It has been shown that 18-24 months of age in mice correlates with 56-69 years of human age (Flurkey, 2007). 4-6 weeks old female mice were used as controls.

4. Transverse aortic constriction (TAC)

After HFD, the animals underwent a transverse aortic constriction procedure as described by Hu et al., in 2003. TAC creates PO by limiting outflow of the LV by reducing the diameter of transverse section of aorta. Mice were briefly anesthetized by injecting 50 µl 0.9% sodium chloride solution containing Medetomidin (0.5 mg/kg), Midazolam (5 mg/kg) and Fentanyl (0.05 mg/kg) peritoneally. A 1.5 cm long suprasternal incision was made to visualize the aortic arch and a 6-0 polyviolene non-absorbable surgical suture was used to make a loose knot between the first and second aortic arch trunk. The constriction was standardized using a 26-gauge blunt needle under the loose knots before fastening as shown in **figure 7**. This corresponds to a low-grade of PO than the ones caused by a 27-gauge needle. Sham animals went through the identical process except there was no tying of the aorta.

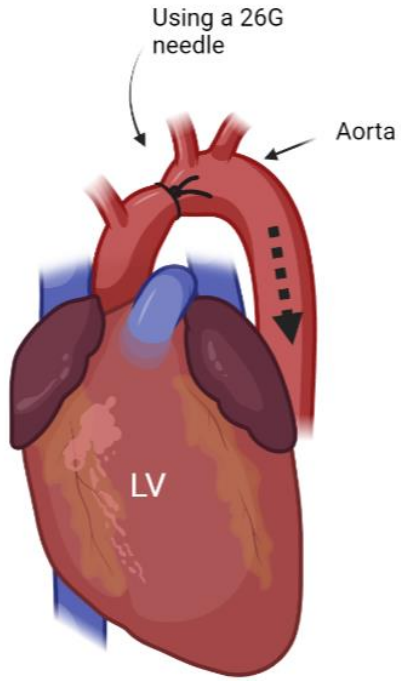

Fig. 7. Schematic representation of the transverse aortic constriction (TAC) surgery.
The location of the constriction is between the brachiocephalic and left carotid artery near the left ventricle. The direction of blood flow in aorta is shown through the dotted arrow (created using BioRender).

Subsequently, a subcutaneous injection of 50 µl 0.9% sodium chloride solution containing Atipamezol (2.5 mg/kg) and Flumazenil (0.1 mg/kg) was given to reverse the effects of anesthesia. Operated mice were then allowed to recover on a warm plate incubator. Post-Op care included injection with buprenorphine (0.1mg/kg) 3 hours later to relieve pain. On the first and second day post-Op, analgesic therapy with carprofen (0.1mg/kg) was given and for one week, 3mL/L of Metamizol was added to the drinking water. The animals were consistently monitored every week until the experiment ended. These surgeries were performed by Sabrina Koszewa (Cardiology and Pneumology, University Medical

Center Goettingen) and Sarah Zafar (Pharmacology and Toxicology, University Medical Center Goettingen) from the SFB1002 service unit.

5. Transthoracic echocardiography

Mice were anesthetized using 2-3% Isoflurane in an induction system with 0.5-1 L/min of 100% O2, then subsequently maintained with 1.5% isoflurane through an inhalation mask on a heated pad in supine position. Vital parameters were closely monitored and kept at physiological levels as heart rate 400-500 beats per minute (BPM), respiratory rate 120-180 and body temperature 36-37°C. Limb electrodes were used to obtain electrocardiogram recordings. A Vevo 2100 imaging systems equipped with a MS-400 30 MHz transducer (Visual Sonics, Toronto, Canada) was used for Transthoracic echocardiography. Conventional 2D parasternal long, short axis views and M-mode view were recorded. Using the LV-trace mode of the VevoLab software (version 3.1.1), images were assessed to determine systolic function (EF, fractional shortening, and stroke volume) and LV morphological parameters including septum thickness, posterior wall thickness, LV end diastolic diameter (LVEDD). The relative wall thickness (RWT), a concentric remodeling marker was calculated as Septum thickness + posterior wall thickness) / LVEDD.

Pulsed wave (PW) Doppler echocardiography was employed to assess the transverse aortic flow velocity and the pressure gradients across the transverse aorta (Mohammed et al., 2012) using the modified Bernoulli equation (Pressure gradient = $4*\text{Velocity}^2$). 2 days after TAC, Doppler velocity was measured using a 20 MHz probe to quantify the pressure gradient across the TAC/Sham region by transthoracic echocardiography.

Speckle tracking echocardiography was performed as described by Tanabe et al., 2008 and Schnelle et al., 2018 using Vevo2100 Imaging Application 3.1.1. in the parasternal axis view, tracking points (speckles) were placed on the endocardial and epicardial borders which were subsequently used for framewise tracking throughout the whole cardiac cycle. From the motion of these speckles on the borders, LV volume and EF were measured. The application divides the LV into six specific segments: two basal, two mid, and two apical to calculate parameters of deformation (strain, strain rate) and motion (displacement and velocity), as a separate segment value or an overall mean. The data presented here are the averages from these six different values per mouse. The peak longitudinal strain rate during early LV filling defined as the reverse longitudinal strain rate (rLSR) was measured to assess the diastolic function. Echocardiography was performed by Marcel Zoremba from the SFB1002 service team (Cardiology and Pneumology, University Medical Center Göttingen). Echo measurements and analyses were performed with blindness towards cohort assignment.

6. LV Pressure-Volume Analysis

Pressure volume loops form the basis of cardiac physiological and functional assessment. LV catheterization was performed surgically according to the procedures described by Pacher et al., 2008. The mouse to be analyzed was placed in an induction chamber with 2-3% isoflurane supplied with 0.5-1 L/min of 100% O_2 briefly for 30-60 seconds then transferred to the operating area. Here the mouse was kept on a heating pad and anesthesia was maintained with 1.5% isoflurane through an inhalation mask. A rectal probe was used to monitor body temperature which was kept constant at 37°C and a hydrating ophthalmic ointment was applied on the corneas to prevent drying and discomfort. Upon confirmation of complete anesthesia, a midline incision was made in the neck, tracheal muscles were gently teased apart to expose the trachea. An endotracheal tube connected to a respirator was guided through the mouth ensuring goof visualization into the trachea. The left salivary gland was then laterally displaced to expose the jugular vein which was very carefully cannulated using a home-made setup. An incision was then made in the xiphoid process ≈ 1.5cm laterally across the chest. Once the diaphragm was visible, a small incision was made to expose the apex of the heart. Then carefully a stab wound was made into the center of apex using a 26G needle and a murine ventricular catheter SPR-839 1.4F (Mikro-Tip® catheters, Millar instruments, USA) was inserted into the LV. 100-150 microliters of (10%) human albumin in (0.9%) NaCl was injected intraperitoneally to balance the loss of fluids during the invasive surgery. 15 minutes were allowed for the catheter to measure baseline hemodynamics, a pause or a sigh in ventilation was employed here to avoid respiratory artefacts (MPVS-Ultra Single Segment Pressure-Volume System for Mice, Millar ADInstruments, UK). Transient inferior vena cava (IVC) occlusion was done by briefly obstructing the vena cava by gently passing a surgical thread underneath it and pulling it upwards as illustrated in **figure 8**. This reduced the preload and gave load independent parameters of LV contractile function. Catheter based PV loop technologies employ a pressure transducer and the measurement of conductance to estimate LV volume which is governed by the changes in an electrical field generated by the catheter. The conductance signal has two components: conduction through blood and conduction on the ventricular wall (parallel conductance). To calculate the parallel conductance, 10 µl of hypertonic saline (10%) was injected into the animal through the jugular vein cannula. This briefly changes the conductivity of the blood, whereas the conductivity of the wall remains constant. This data can be used to determine parallel conductance which is converted to a volume function (Vp), and subtracted from the total signal to determine the absolute ventricular volume.

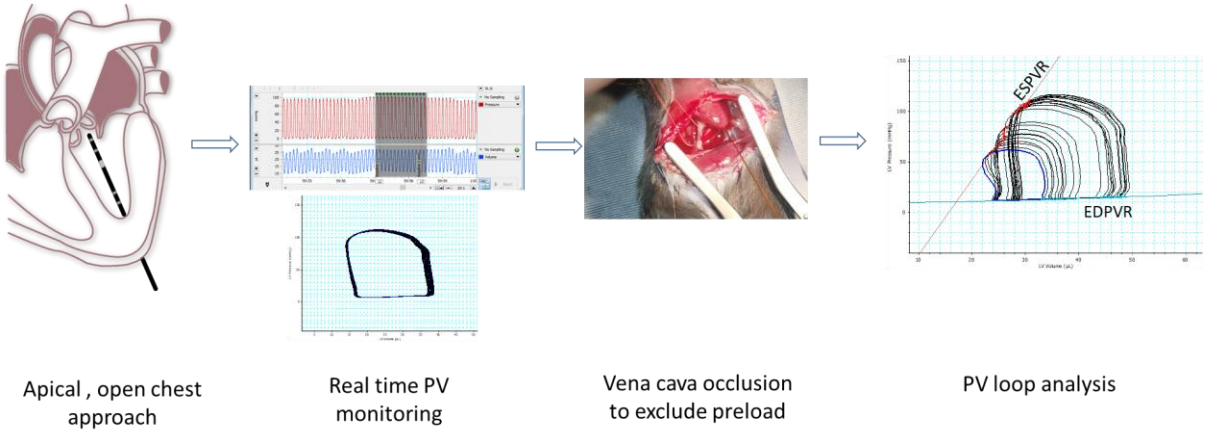

Fig. 8. Analysis of Pressure- Volume relationship using left ventricle catheterization.
A murine catheter was inserted in to the LV through a stab wound in the apex. Pressure and volume were measured to establish baseline. Subsequently, brief vena cava occlusion was done using a surgical thread to quantify load independent parameters. End systolic and End diastolic pressure volume relations (ESPVR and EDPVR) were calculated from the resulting PV loops.

At the end of the recording, the LV catheter was withdrawn, blood was aspirated from the LV using a heparinized syringe to be used for volumetric cuvette calibration. The animal was sacrificed and the heart tissue was obtained for further histological and molecular analysis. Data was processed and analyzed using PowerLab 8/35 with LabChart Pro software. The following parameters were then calculated.

Physiologically relevant parameters of systolic function:

a. ESPVR: This denotes the maximum pressure generated by the ventricle at a given volume in LV. Its slope represents end-systolic elastance (Ees) and is a marker for myocardial contractility.
b. dp/dt max: Used as an index of ventricular compliance and denotes the maximum rate of change of pressure in ventricle.
c. Pre-load Recruitable stroke work (PRSW): It is an empirical relationship between stroke work and end-diastolic volume (EDV) and reflects myocardial contractility independent of preload and afterload.

Physiologically relevant parameters of diastolic function:

a. EDPVR: it represents the passive filling properties of the ventricle and is a standard marker for impairment in ventricular relaxation.
b. Tau: Constant for isovolumic relaxation or Tau denotes the exponential decay of ventricular pressure during isovolumic relaxation. It is independent of preload.
c. End diastolic pressure (EDP): Ventricular pressure at the end of diastole.

d. dp/dt min: Used as an index of ventricular compliance and denotes the minimum rate of change of pressure in ventricle.

7. Organ harvesting

Animals were anesthetized with isoflurane and cervical dislocation was done for sacrifice. Body weight was measured and the thorax was cut to visualize the beating heart. Intra-cardiac injection of 500 µl 5% potassium chloride (KCl) was administered to suspend the heart in diastole. The heart was then excised near the aorta and transferred to ice cold Phosphate buffered saline (PBS). Retrograde perfusion was done by placing a 21-guage needle in the aorta with sterile saline. The heart was dried and weighed using a fine balance (Sartorius, Germany), the right ventricle, both atria were cut aside and weighed and finally LV weigh was measured. The LV was then cut transversely into three parts, the apex and base was quickly frozen in liquid nitrogen to be used for protein and RNA isolation respectively. The middle part was stored overnight in 4% paraformaldehyde (PFA) for fixation and used for histology. Peripheral organs like lungs, kidney and liver were also weighed. Tibia was isolated and measured with an electronic gauge to normalize organ weights as a function of mouse size.

8. Protein extraction

LV tissue snap frozen liquid nitrogen (20-30 mg) was placed in RNAse-free 2 ml Eppendorf having a 5mm stainless steel bead (Qiagen, 69989) and RIPA lysis buffer (Thermo Fischer, 89900) along with cOmplete™ protease inhibitors (Sigma, 11873580001) and phosphatase inhibitor tablets (Sigma, 4906837001). The mixture was then lysed and homogenized using tissue Lyser LT (Qiagen, 85600) for 5 min with 50 Hz. The lysate was briefly centrifuged at 4°C and placed on a cooled overhead rotor at for 30 minutes before they were again centrifuged for 15 min at 16,000 x g and transferred into a fresh 1.5 ml Eppendorf tube. Photometric determination of protein concentration was performed by measuring absorbance at 562 nm using Pierce™ BCA Protein Assay Kit (Thermo Fischer, 23225) and a 96-well plate reader (Biotek). These lysates were then aliquoted and stored at -80°C.

9. Western Blotting

Protein lysates as per the required concentration (20-30 µg) were denatured by conventional cooking at 95°C for five minutes in 4x Laemmli buffer (Invitrogen, NP0007) and 0.2M DTT (Sigma-Aldrich, D9779) and then separated on 4–12% SDS-PAGE (NuPAGE Novex Bis-Tris 4-12% Gel, Invitrogen, NP0321) in MES running buffer (Invitrogen, NP0002) at 120 Voltage for 90 minutes. Pre-stained protein standard was run in parallel lanes to aid in molecular mass estimation of proteins (Precision Plus protein™ All Blue pre-stained protein standards, Bio-Rad, 1610373). Separated proteins were blotted on 0.45 µm nitrocellulose membranes (Amersham™ Protran™, Sigma-Aldrich, GE10600002) at a constant current of 0.5A in transfer buffer (25 mM Tris-HCl, pH 8.3; 150 mM Glycine; 20% Methanol)

for 2 hours while constantly being kept cold. As per the manufacturer's instructions, samples used for phospho-PLN detection were not cooked but instead incubated at 37°C for 30 minutes, separated on 10-15% SDS-PAGE and transferred on 0.2µm PVDF membranes (Amersham™ Hybond™, SigmaAldrich, GE106000021). After successful blotting, the membranes were briefly stained with Ponceau Red solution. Unbound sites on the membranes were then blocked for 1 h with 5% non-fat milk (Roth, 68514-61-4) in 0.1% Tween-20 (Sigma-Aldrich, P2287) in TBS (20 mM Tris-base, 50 mM NaCl, pH=7.5), and probed at 4°C overnight with respective primary antibody diluted in 1% milk TBS-Tween. Membranes were then washed three times with TBS-Tween 10 minutes each, followed by incubation with a secondary peroxidase-conjugated antibody for one hour at room temperature. Antibodies used in this dissertation are listed in table 6. Afterwards, membranes were washed three times with TBS-Tween 10 minutes each. Signals were detected using SuperSignal™ West Femto Maximum Sensitivity Substrate (Thermo Fisher, 34095) chemiluminescent kit and Chemidoc XRS™ + imager. Signals were analyzed using Image Lab software 5.1 (Bio-rad).

Table 6. Antibodies used for immunoblotting experiments

Target Protein	Manufacturer	Dilution used
Phospho-Erk1/2 (Thr202/Tyr204)	Cell Signaling, 9106	1:1000 in 1% milk
Total Erk1/2	Cell Signaling, 9102	1:5000 in 1% milk
Phospho-AKT (Ser473)	Cell Signaling, 4060	1:1000 in 1% milk
Total AKT	Cell Signaling, 9272	1:5000 in 1% milk
Phospho-p38 (Thr180/Tyr182)	Cell Signaling, 9211	1:1000 in 1% milk
Total p38	Cell Signaling, 9212	1:5000 in 1% milk
Phospho-JNK (Thr183/Tyr185)	Cell Signaling, 9251	1:1000 in 1% milk
Total JNK	Cell Signaling, 9252	1:5000 in 1% milk
Phospho- CaMKII beta/gamma/delta (Thr 287)	ThermoFisher, PA5-37833	1:1000 in 1% milk
Total CaMKII delta	ThermoFisher, PA5-22168	1:5000 in 1% milk
Phospho-Troponin I (Ser23/24)	Cell Signaling, 4004	1:1000 in 1% milk
Total Troponin I	Cell Signaling, 4002	1:5000 in 1% milk
Phospho-PLN (Ser16)	Badrilla, A010-12AP	1:5000 1% milk
Phospho-PLN(Thr17)	Badrilla, A010-13	1:5000 1% milk
Total PLN	Cell Signaling, 14562	1:5000 1% milk
Phospho-RyR2 (Ser2808)	Badrilla, A010-30	1:5000 1% milk
Phospho-RyR2 (Ser2814)	Badrilla, A010-31	1:5000 1% milk
Total RyR2	Sigma-Aldrich, HPA016697	1:1000 1% milk
Phospho-RKIP(Ser153)	Santa Cruz Biotechnology, sc-135779	1:5000 in 1% milk
Total RKIP	Abcam, ab76582	1:5000 in 1% milk
NOX2	Abcam, ab129068	1:1000 in 1% milk
GAPDH	Merck Millipore, MAB374	1:10000 in 1% milk
Rabbit IgG HRP- secondary antibody	Cell Signaling, 7074	1:10000 in 1% milk
Mouse IgG HRP- secondary antibody	GE Healthcare, NA931	1:10000 in 1% milk

10. RNA isolation, cDNA synthesis and quantitative real-time polymerase chain reaction (RT-qPCR)

10.1. In-silico oligonucleotide design

Primers for RT-qPCR were designed using Primer-BLAST (https://www.ncbi.nlm.nih.gov/tools/primer-blast/). The settings used were, product size: 100-200 bp; exon junction span: may not span exon-exon junction; intron inclusion: yes (if possible); organism: Mus musculus (taxid:10090); allow splice variants: yes. Melting temperatures were calculated using the Thermo Fisher Tm Calculation platform All oligonucleotides were synthesized by Eurofins Genomics.

10.2. RT-qPCR

Tissue samples were lysed using a proprietary lysis buffer from RNeasy Fibrous tissue Mini kit (Qiagen, 74704) and 7mm stainless steel beads for 5 min with 50 Hz. RNA purification from the lysate was performed using the same kit as per manufacturer´s instructions. Total RNA was then eluted in 30 µl nuclease free water. Absorbance at 260 nm was measured to quantify RNA concentration using the Nanodrop 2000 (Thermo Fisher). Quality control absorbance ratios of 260/280 and 260/280 were also measured. The RNA was then used for reverse transcription or stored at -80°C for prolonged storage. Complementary DNA synthesis was done using iScript cDNA synthesis kit (Bio-Rad, 1708891) according to manufacturer's protocols. Relative gene expression was quantified via qRT-PCR performed on a Biorad iQ-Cycler using SYBR Green Supermix (BioRad). **Table 7** shows the constituents of reaction master mix (A) and the program (B) while **table 8** shows all the primer pairs used.

Table 7. Components of RT-qPCR reaction mix (A), PCR program protocol (B).

Reagents	Volume (µl)
Nuclease-free H_2O	7.8
Forward primer (10 pmol/µl)	0.6
Reverse primer (10 pmol/µl)	0.6
SsoAdvanced SYBR Green Mix	10
cDNA (2.5 ng)	1

A

Step	Temp. (°C)	Time
Denaturation	95	3 min
Amplification (x45)	95	10 sec
	60	30 sec
Meltcurve (x81)	55-95	6 sec/step

B

Table 8. Primers used for qPCR

Primer	Forward sequence	Reverse sequence
Nppa (ANP)	GAGACGGCCGCATCTTCTT	CAATCTCCACTTTGCCACTGC
Nppb (BNP)	ACAAGATAGACCGGATCGGA	ACCCAGGCAGAGTCAGAAAC
Serca2-α	GGGCAAAGTGTATCGACAGG	TCAGCAGGAACTTTGTCACC
Acta1(α-skeletal actin)	CTCACTTCCTACCCTCGGC	GCCGTTGTCACACACAAGAG
Mhc-β	TCCCAAGGAGAGACGACTGTG	CCTTAAGCAGGTCGGCTGAGT
Mhc-α	CCGGGTGATCTTCCAGCTAAA	GCTCAGCACATCAAAGGCACT
TGF-β	TGATACGCCTGAGTGGCTGTCT	CACAAGAGCAGTGAGCGCTGAA
TNF-α	GGTGCCTATGTCTCAGCCTCTT	GCCATAGAACTGATGAGAGGGAG
IFN-γ	CAGCAACAGCAAGGCGAAAAAGG	TTTCCGCTTCCTGAGGCTGGAT
IL-1 β	TGGACCTTCCAGGATGAGGACA	GTTCATCTCGGAGCCTGTAGTG
IL-6	TACCACTTCACAAGTCGGAGGC	CTGCAAGTGCATCATCGTTGTTC
VCAM-1	GCTATGAGGATGGAAGACTCTGG	ACTTGTGCAGCCACCTGAGATC
ICAM-1	AAACCAGACCCTGGAACTGCAC	GCCTGGCATTTCAGAGTCTGCT
PECAM-1	CCAAAGCCAGTAGCATCATGGTC	GGATGGTGAAGTTGGCTACAGG
FN1	CCCTATCTCTGATACCGTTGTCC	TGCCGCAACTACTGTGATTCGG
ET1	CTACTTCTGCCACCTGGACATC	CGCACTGACATCTAACTGCCTG
GAPDH	GAGACGGCCGCATCTTCTT	CAATCTCCACTTTGCCACTGC

11. Histology

LV sections pre-fixed in 4% PFA (8-12 hours) were dehydrated through an increasing concentration gradient 60% ethanol, 2x 75% ethanol, 2x 96% ethanol, 2x 100% ethanol, 2x xylol, and 3x paraffin, each for 90 min using an automated system (Leica, TP1020). Paraffin blocks were prepared using an embedding station (Leica, EG1150H) and 3-5 µm thick LV cross-sections were made using a Microtome (Leica RM 2165). Cryosectioning was done for lipid quantification using the Leica CM1950 cryostat. Prior to staining, sections were dewaxed in xylene, followed by graded serial rehydration in ethanol 100% → 96% →80%→70%→50%→30%→ water (five minutes/ incubation). The sections were then subjected to the respective staining protocols:

Picro Sirius Red staining: To measure the levels of deposition of connective tissue, slides were immersed in Picro-Sirius Red solution (Abcam, ab 150681) for 1 hour. They were then removed and rinsed twice in 0.5% acetic acid solution and once in absolute ethanol. At the end, slides were mounted with Permount (Fischer Scientific, SP15-100) medium. Images were captured using the Olympus CK 40 microscope. Collagen components were stained red/pink and non-collagen deposits appeared yellow. Percentage fibrotic area was calculated by red staining density relative to the total area of the LV tissue slice using Image J (Bethesda, USA). Two random sections per LV were quantified.

Fluorescein-conjugated wheat germ agglutinin (WGA): For assessment of cross-sectional area (CSA), LV sections were first washed three times in Hank's balanced salt solution (HBSS) and then incubated in 5.0µg/ml fluorescein-conjugated WGA solution (Invitrogen, W11262) in HBSS for 15 minutes at RT. Slides were then washed twice in PBS and mounted with ProLong® Gold antifade with DAPI (Thermo Fischer, P36935). Images were captured using a fluorescence microscope (Leica DF350 FX). At least 350-400 random cardiomyocytes (Inclusive of all sizes) per animal were measured using Image J (Bethesda, USA).

TUNEL (TdT-mediated dUTP-biotin nick end labelling) staining: cells undergoing apoptosis were detected using the In-Situ Cell Death Detection Kit (Roche, 11684795910) according to the manufacturer's protocols. At the end, sections were mounted using ProLong® Gold antifade with DAPI (Thermo Fischer, P36935). In principle, terminal deoxynucleotidyl transferase (TdT) catalyzes the conjugation of fluorescein labelled deoxyuridine triphosphate nucleotides to the 3´OH end of DNA strand breaks. Fluorescein-dUTP helps in identifying apoptotic cells directly after the TUNEL reaction. TUNEL-positive apoptotic cells were detected with a fluorescence microscope (Leica DF350 FX) in 5-8 randomly selected fields versus total number of cells/LV using Image J (Bethesda, USA).

Staining of neutral lipids by oil red O (ORO): The lysochrome ORO ($C_{26}H_{24}N_4O$) is a fat soluble diazol dye. It has an absorbance maxima at 518 nm. The advantage is that ORO stains only neutral lipids and cholesteryl esters but not membrane lipids, making it ideal to study lipid accumulation of steatosis in dyslipidemic tissue samples. The principle involves first diluting the highly hydrophobic ORO in water, when it reaches the tissues it follows the lipophilic gradient and accumulates in lipid deposits. The protocol described by Mehlem et al., has been followed. Cryosectioned LV tissue was briefly stained with ORO working solution and washed under running tap water for 30 minutes. Sections were mounted with a water based mounting medium and images were acquired through a bright field microscope.

Immunocytochemistry: Epitopes were unmasked using an antigen retrieval step. Slides were incubated with antigen retrieval solution (S2369 Dako Target Retrieval Solution) and incubated at 60-65°C for 15-20 minutes. Tissue permeabilization was the achieved by using permeabilization buffer having 1% goat/rabbit serum and 0.4% Triton X-100 in TBS (TBS-T). Non-specific sites were blocked with 5% serum in TBS-T for 30 minutes at room temperature. Primary antibody was diluted in 1% animal serum TBS (with 0.05-0.1 % Triton X 100) and added to the sections overnight at 4°C in humidified chamber. The next morning, sections were washed twice with 1% serum TBS-T for 10 minutes each. Then a fluorescent-probe conjugated secondary antibody in 1% serum in TBS (with 0.05-0.1% Triton X 100) was added and incubated at room temperature for 1-2 hours. Sections were

washed twice with 1% serum TBS-T for 10 minutes each. The slides were then mounted in medium containing DAPI (ProLong™ Gold Antifade, Thermofisher P36931), dried and sealed with a coat of clear nail-polish. The antibodies used are mentioned in **table 9.**

Table 9. Antibodies used for immunocytochemistry.

Antibody	**Manufacturer**	**Dilution used**
Rabbit- anti CD45	Abcam, ab10558	1:500
Alexa Fluor® 633 Goat anti-Rabbit IgG (H+L)	ThermoFisher, A-21070	1:1000

12. Next Generation Sequencing

12.1. mRNA library preparation

Sequencing of RNA-seq samples and initial data analysis was conducted at the Microarray and Deep-Sequencing Facility Göttingen (Transcriptome and Genome Analysis Laboratory, TAL, headed by Dr. Gabriela Salinas). TruSeq RNA Library Preparation Kit v2 was used to generate RNA-seq libraries using the RS-122-2001 protocol from Illumina starting with 500 ng of total RNA. Quality and integrity of RNA was ascertained with the Fragment Analyzer from Advanced Analytical by using the standard sensitivity RNA Analysis Kit (DNF-471). All samples selected for sequencing had an RNA integrity number over 8.5. Ligation step was optimized by optimizing the adapter concentration to increase ligation efficiency (>94%), and finally the number of PCR cycles was reduced to avoid PCR duplication artifacts as well as primer dimers in the final product in library. For quantification of cDNA libraries, a fluorometric analysis system, the QuantiFluor™ dsDNA System from Promega, was used. The size of final cDNA libraries was determined by using the dsDNA 905 Reagent Kit (Fragment Analyzer from Advanced Bioanalytical) having a means sizing of 300 bp. Libraries were pooled and sequenced on an Illumina HiSeq4000 (Illumina) generating 50 bp single-end reads (30-40 Mio reads for each sample).

12.2. Raw read and Quality check

Sequence images were transformed with Illumina software BaseCaller to BCL files, which was demultiplexed to fastq files with bcl2fastq v2.17.1.14. The sequencing quality was found out using FastQC (Andrews et al., 2010).

12.3. Mapping and Normalization

Sequences were aligned to the reference genome Mus musculus (mm10 version 89, https://www.ensembl.org/Mus_musculus/Info/Index) using the STAR aligner (Dobin et al., 2013) (version 2.5.2a) allowing for 2 mismatches within 50 bases. Subsequently, read counting was performed using featureCounts (Liao et al., 2014).

12.4. Differential expression analysis

Read counts were analyzed in the R/Bioconductor environment (version 3.4.2, www.bioconductor.org) using the DESeq2 (Love et al. 2014) package version 1.14.1. Candidate genes were filtered using an absolute log2 fold-change >0.5 and FDR-corrected pvalue <0.05. Gene annotation was performed using Mus Musculus entries via biomaRt R package version 2.32.1 (Durinck et al., 2009). Pathway analysis and over representation assessment was done using WebGestalt platform. Pathway mapping was done through KEGG website.

13. Statistics and data analysis

All statistical analyses were performed using GraphPad Prism version 8.0 (GraphPad Software, Inc, California, USA) with two-tailed unpaired Student's t-test, one-way or two-way analysis of variance (ANOVA) where appropriate along with Bonferroni post-test correction where suitable. Kaplan–Meier survival analysis was performed, and significance was determined through a Log-rank test. Data are presented as mean ± standard error of mean (SEM). Differences between groups were considered statistically significant if the p-value was <0.05.

Results 1: High fat Diet+ Low grade TAC model

1. Survival after low-grade TAC

The first model we wanted to assess was based on the combination of dyslipidemia induced by high fat diet (HFD) and low grade pressure overload (PO) through transverse aortic constriction (TAC) surgery. Normal diet (ND) and TAC operated animal were used as controls. Sham operated mice were included in each dietary group.

To ensure consistency of TAC constriction, pressure gradient across the transverse aorta was measured through echocardiography. Gradients between the ND TAC and HFD TAC group were comparable showing consistent aortic constriction. A 20 fold increase in TAC dependent pressure gradient was observed in ND group ($p<0.01$, sham n=10-12, TAC n= 15-17) from about 3.1 mmHg at baseline to 64.7 mmHg at TAC. HFD group showed a 21 fold increase ($p<0.01$, sham n=15, TAC n= 17-20) from about 2.9 mmHg at baseline to 61 mmHg at TAC. TAC mediated mortality between the groups was similar and comparable 15.3% in ND-TAC and 16.04% in HFD-TAC operated mice as shown in **figure 9.A.** In either groups mortality was similar on comparing sham vs TAC ($p>0.05$, Log-rank Mantel-Cox test, n=13-17) as shown in **figure 9.B**.

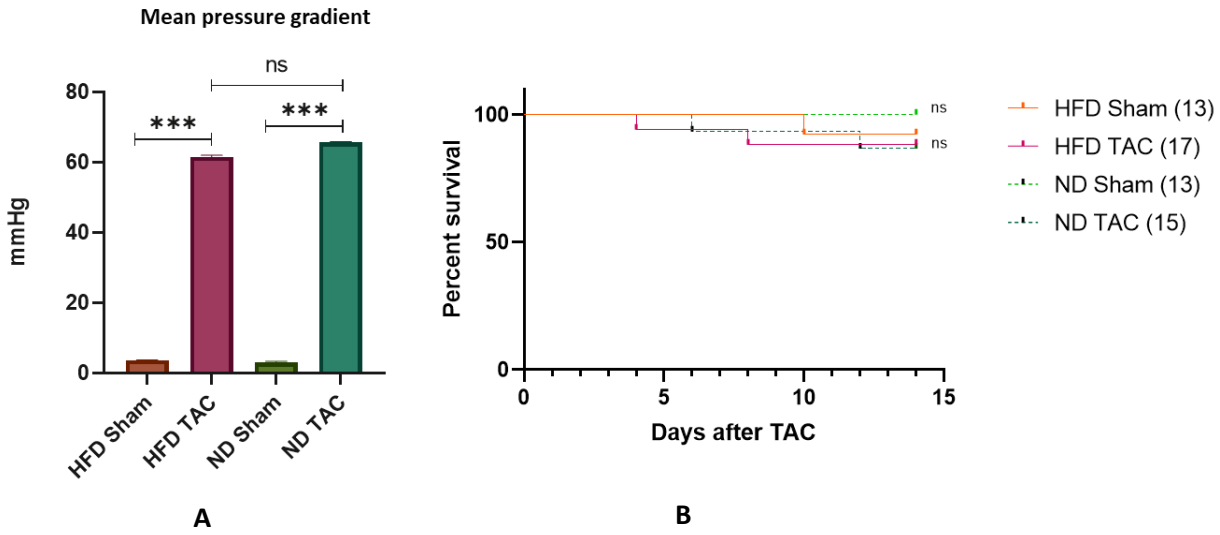

Fig. 9. Gradient echocardiography and survival.
A: Pressure gradient across the aorta before and after TAC procedure, ***$p<0.001$. B: Kaplan-Meier-survival curves representing the survival percentage after TAC (transverse aortic constriction) or sham in HFD (high fat diet) vs ND (normal diet) groups. Mortality within 24 hours of TAC was considered as a death from surgical complications, and thus was excluded from long-term survival of TAC vs. corresponding sham using Log-rank Mantel-Cox test, numbers in brackets represent animals examined.

2. Morphometric analysis

2.1. Organ weights

All weight measurements were normalized to the respective tibia length (TL) as shown in **figure 10**. Despite the clear increase in average body weight in HFD (28 g) as compared to ND (20 g), both groups showed similar increase in heart weight ($p<0.01$) and LV hypertrophy after TAC ($p<0.01$). Both groups showed a trend towards higher lung congestion (HFD-Sham 11.02 mg/mm vs HFD-TAC 13.35 mg/mm; ND-Sham 10 mg/mm, ND-TAC 10.4 mg/mm) after TAC, failing to reach significance ($p>0.05$).

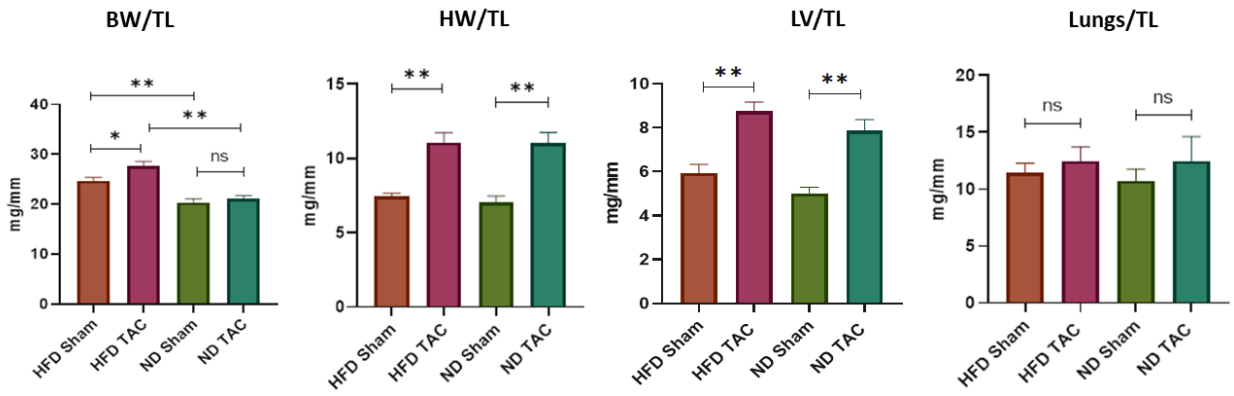

Fig. 10. Morphometry of HFD and ND mice following 2 weeks of TAC.
BW/TL, Body weight; HW, Heart weight; LV; Left ventricular weight; TL, tibia length and lung weight-to-tibia length ratios. Data are expressed as mean ± SEM. *p <0.05, **p <0.01 vs. corresponding group using one-way ANOVA with Bonferroni post-test, n=13/group.

2.2. LA hypertrophy

In human subjects, LA hypertrophy has been linked to adverse remodeling in HFpEF and a high-risk marker for AF, stroke and MI (Kuo et al., 2022)**.** LA hypertrophy was almost significantly increased in the HFD sham vs TAC group ($p>0.05$, n=13/group), **figure 11**. However, the results were highly variable among the animals, 20% mice showed on average a 10 fold increase in LA/TL. It was not prominent in ND-TAC group.

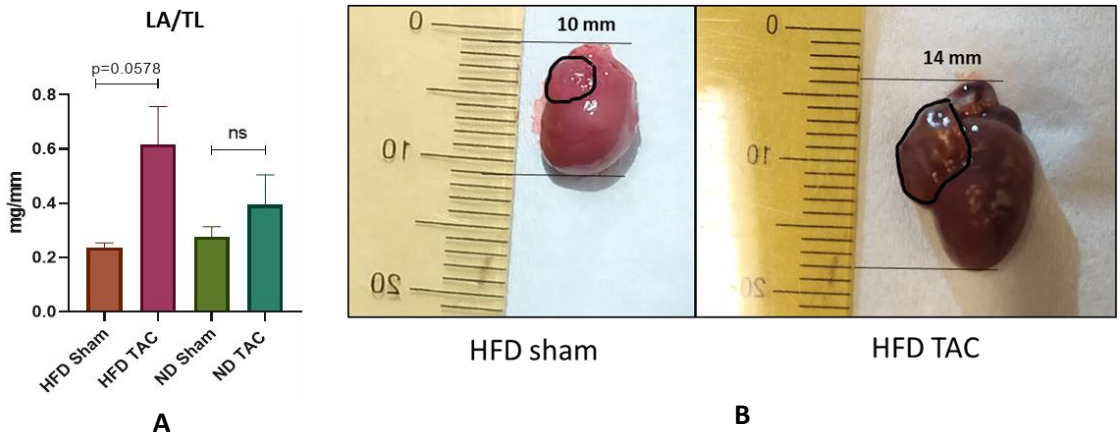

Fig. 11. Left atrial remodeling.
Analysis of left atrial (LA) hypertrophy 2 weeks after TAC. A:LA weight normalized to tibia length (TL) using 2-way ANOVA with Bonferroni post-test , n=13/group. B: representative images from HFD sham and TAC groups, black border traces the LA area.

2.3. Cardiomyocyte hypertrophy

WGA-stained LV cross sections were used to determine the diameter of individual cardiomyocytes by measuring their cross-sectional area (CSA). Both dietary groups showed a similar increase in cardiomyocyte hypertrophy after TAC; HFD ($p<0.001$) and ND ($p<0.001$) as demonstrated by two-way ANOVA analysis. It was interestingly found that despite similar HW as described in section 2.1, the HFD-sham group showed a higher cardiomyocyte CSA when compared to ND-sham suggesting that HFD is sufficient to model the cellular profile independent of TAC ($p<0.05$). the difference in both TAC groups showed a non-significant trend towards higher CSA in HFD-TAC, **figure 12**.

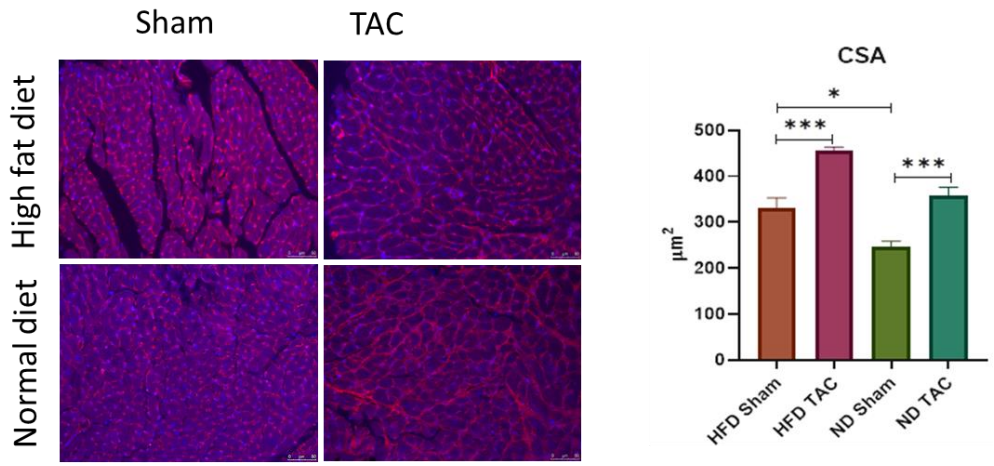

Fig. 12. Hypertrophy at cellular level.
Left ventricular cardiomyocyte cross sections stained with wheat germ agglutinin (WGA) after TAC. Mean data for cross-sectional area (CSA) are shown. Data are presented as mean ± SEM. *p < 0.05, ***p<0.001 between groups using 2-way ANOVA with Bonferroni post-test, n=7/group.

3. Echocardiographic evaluation after TAC

3.1. LV remodeling

Non-invasive echocardiographic evaluation was done on all mice that underwent TAC and sham surgeries. The animals were serially analyzed once a week for two weeks. A look at geometric dimensions as in **figure 13,** revealed significant differences in sham vs TAC in both the groups. In ND group, septum thickness was significantly increased in the first week itself ($p<0.05$, sham n=15, TAC n= 17-20) and was consistent in the second week. ND group however, showed rising septum thickness only after the first week, hinting at a delayed but similar response to cardiac remodeling as HFD ($p>0.05$, sham n=15, TAC n= 17-20). Left-ventricular end-diastolic dimension was however, unchanged during the course of two weeks for both the dietary groups. The relative wall thickness (RWT), a marker for concentric remodeling (can also be used as a marker for eccentric hypertrophy if reduced), was then calculated as previously mentioned in methods. It was found that both groups exhibited a higher RWT in both weeks post PO. ND ($p>0.01$, sham n=15, TAC n= 17-20) and HFD ($p>0.01$, sham n=15, TAC n= 17-20) leading to an evidence of concentric hypertrophy of the left ventricle.

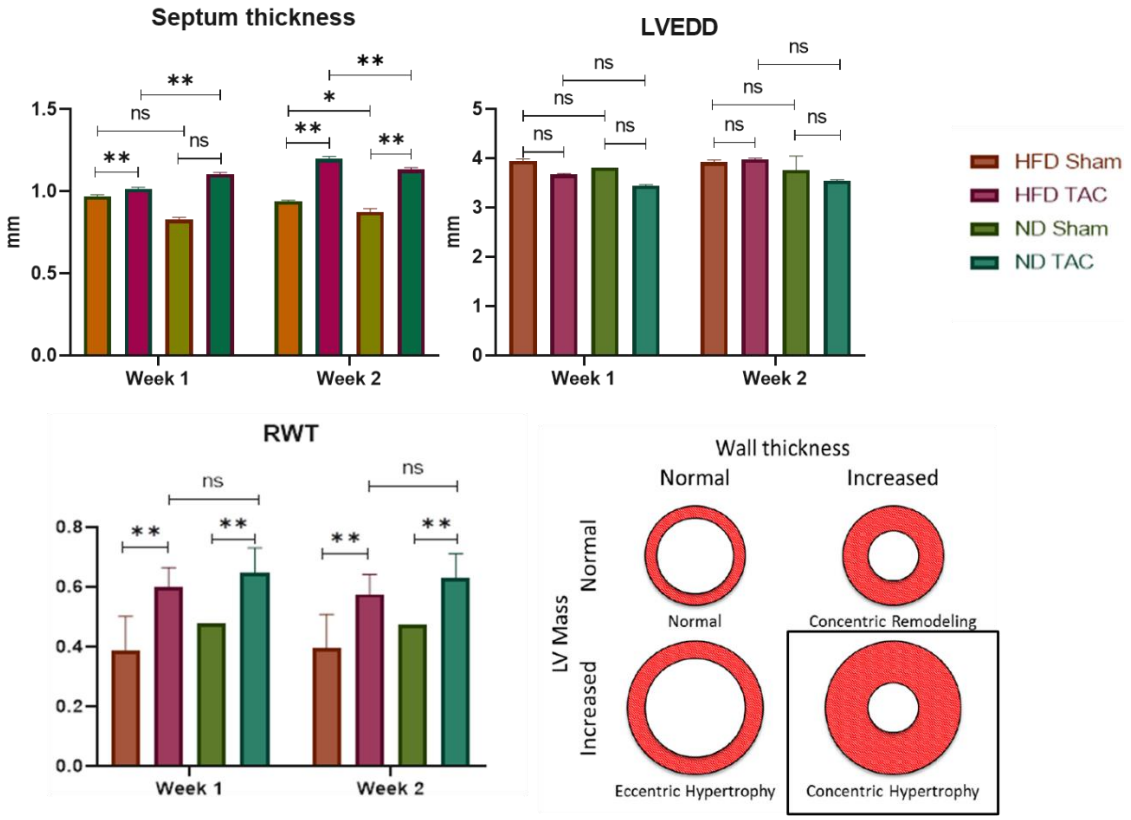

Fig. 13. Left ventricular hypertrophy in HFD versus ND mice following two weeks of PO.
Echocardiographic assessment of left ventricular remodeling. Septum thickness ; LVEDD, Left ventricular end-diastolic diameter and RWT, relative wall thickness. Data are presented as mean ± SEM. *p < 0.05, **p<0.01 between respective groups using one way ANOVA followed by Bonferroni post-hoc test for multiple comparisons. n=15-20/group.

3.2. Systolic function assessment

With comparable heart rates, it was found that EF and fractional shortening (FS) were differentially presented in the two dietary groups. Remarkably, when HFD sham vs TAC were compared, it was found that EF and FS appeared to be well conserved in both weeks. In the ND cohort, TAC vs sham EF was reduced in the first week itself by 20% (p<0.001) and the change was further exacerbated in the second week of evaluation. FS in ND followed a similar trend with a 15% drop in first (p<0.05) and 21 % in the second week (p<0.01). This led us to believe that the condition of dyslipidemia induced by HFD is an important component that shifts the spectrum of HF towards a preserved state after low grade PO. Ultimately, at the end of two weeks of serial echocardiographic evaluation, ND+TAC mice were at an average EF of less than 40% while HFD+TAC mice EF was well preserved at 55 %. SV was also slightly decreased in both groups at the end of two weeks after PO, data not shown(P>0.05). Data is summarized in **figure 14.**

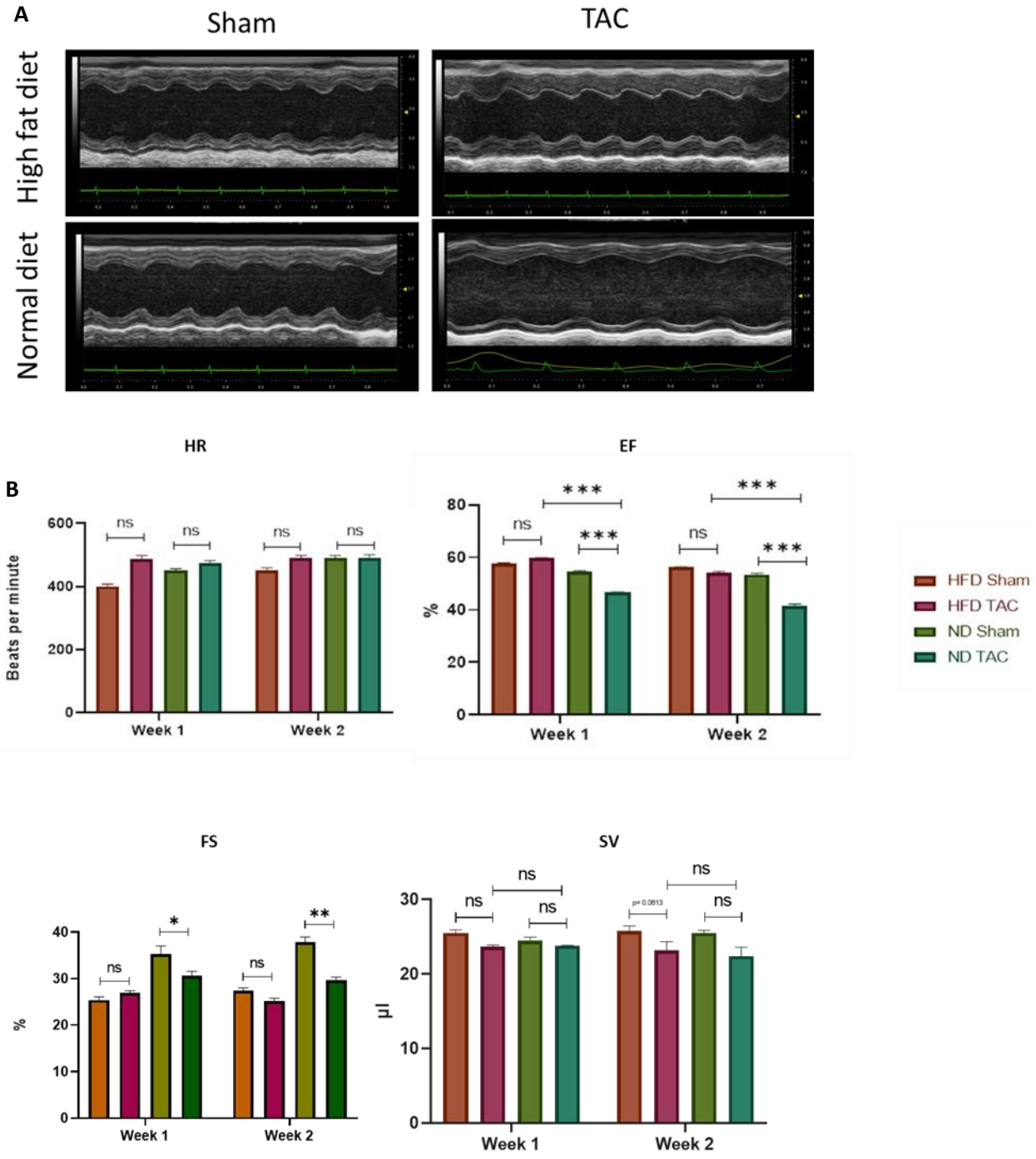

Fig. 14. Differential systolic function in HFD vs ND mice during two weeks of low grade PO.
A: Respective AM-mode images from echocardiography show a representation of LV function and geometry. B: Heart rate (HR), ejection fraction (EF), fractionation shortening (FS) and stroke e volume (SV) between the groups. Data are expressed as mean ± SEM. *p <0.05, **p <0.01, ***p<0.001 vs. corresponding group using two-way ANOVA with Bonferroni post-test for multiple comparisons. n=13/group.

Henceforth, in this dissertation, HFD+TAC is considered to be a ''HFpEF like'' model while ND+TAC is reflective of a ''HFrEF like '' scenario. Further diastolic and systolic function measurements to ascertain this hypothesis are described in the following sections.

3.3. Strain echocardiography to ascertain diastolic dysfunction

To truly be able to say that HFD exhibits a HFpEF like state, we needed to demonstrate that along with preserved systolic function, there is a clear indication of diastolic dysfunction. Strain echocardiography was employed for this purpose to measure finer aspects of diastolic dysfunction. Speckle tracking echocardiography was performed as described previously by Bhan et al., 2014. Vevo2100 Imaging Software 1.5.0 was used to place a series of tracking points on the endocardial and epicardial borders of LV in parasternal long-axis views. Then though an automated frame by frame tracking for one whole cardiac cycle allowed for calculation of calculation of EF and strain parameters like strain and strain rates.

The program divided the left ventricle into six segments from which strain rate values were quantified for each segment. Using the "reverse peak" option during strain analysis, the peak longitudinal strain rate (r-LSR) was also measured as depicted in **figure 15**.

Fig. 15. Speckle tracking echocardiography.
A: Note the position of tracking points of epicardial and pericardial borders. B: Vevo2100 allows for automatic measurement of reverse strain rates by using the reverse peak function. C: A typical longitudinal strain rate profile is shown for WT mouse with color coded ventricular segments. Reverse longitudinal strain rate and longitudinal strain rate peaks are shown that corelate temporally with early LV filling. Adapted from Schnelle, M et al., 2018.

EF was kept consistent with the B-mode measurements to keep a control on strain quantification. It was found that for HFD+TAC, r-LSR was decreased in the second week when sham vs TAC comparisons were made suggesting diastolic dysfunction ($p<0.05$, sham n=7, TAC n= 7), while first week showed no change. ND group showed no change in strain rate in first week or second week as shown in **figure 16**. Pressure volume loop was then employed to further assess systolic and diastolic functions in detail as described in the subsequent section.

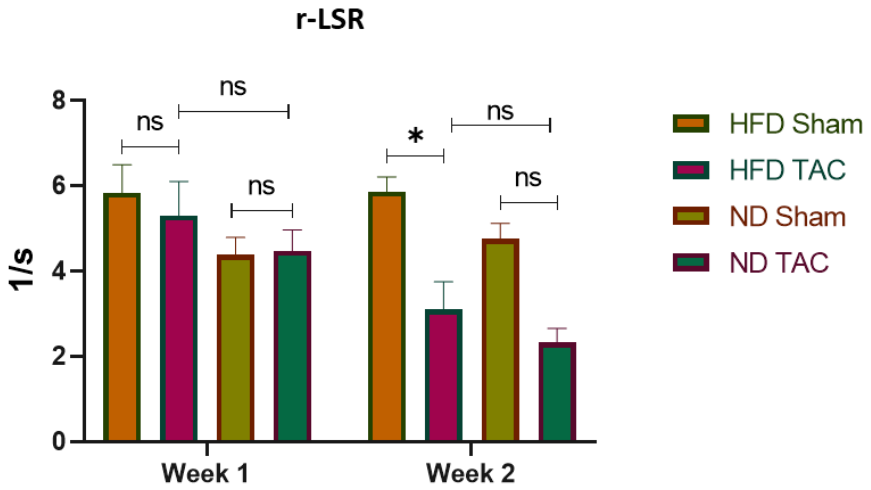

Fig. 16. Reverse-Longitudinal strain rate (r—LSR) in HFD vs ND during two weeks of low grade PO.
Data are expressed as mean ± SEM. *p <0.05 vs. corresponding group using two-way ANOVA with Bonferroni post-test, n=7/group.

4. Pressure Volume loop analysis for in depth cardiac function characterization

Since the data from speckle tracking analysis post PO pointed towards diastolic dysfunction, we wanted to further explore this aspect in depth. We employed the analysis of pressure volume relationship in the mice undergoing TAC in both dietary groups. Real time measurement of pressure and volume within the ventricle and plotting them against each other for several time-points during a cardiac cycle generates a PV loop. PV loops can be used to calculate several physiologically relevant hemodynamic can be calculated like stroke volume, cardiac output, end systolic pressure volume relationship (ESPVR), end diastolic pressure volume relationship (EDPVR) etc. At the end of experiment prior to harvesting organs, PV loop analysis was performed as described in section 6 of methods. In sync with echo data, HFD mice showed preserved systolic function (**figure 17)** as denoted by an unchanged ESPVR and dp/dt_{max} in sham vs TAC ($p>0.05$). However, in ND cohort, ESPVR was markedly increased by 110% hinting at a non-preserved systolic function ($p<0.05$, sham n=4, TAC n=5). PRSW similarly showed a load-independent increase ($p<0.05$, sham n=4, TAC n=5). dp/dt_{max} did not show any change in either of the groups. The main takeaway for this part is that HFD TAC operated mice exhibited a preservation of systolic function as compared to ND group.

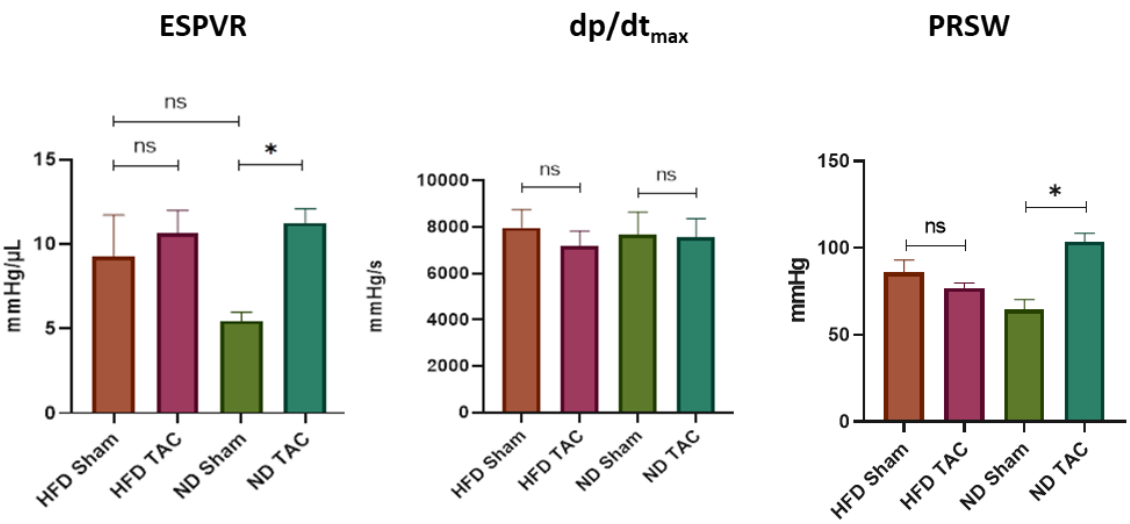

Fig. 17. Systolic LV function in HFD vs ND mice at the end of two weeks of low grade PO.
ESPVR: End systolic pressure volume relationship, dp/dtmax: maximal rate of pressure fall with time, PRSW: Preload recruitable stroke work. Data are expressed as mean ± SEM. *p <0.05 vs. corresponding group using one-way ANOVA with Bonferroni post-test. n=4-5/group.

Looking at diastolic dysfunction (**figure 18)** indices, it was found that the load independent parameter of EDPVR was significantly elevated in HFD group after PO; HFD ($p<0.001$, sham n=4, TAC n=5) and ND ($p>0.01$, sham n=4, TAC n=5) reflective of increased LV stiffness and restrictive pattern of filling. The isovolumic relaxation time (Tau) was prolonged in both groups HFD ($p<0.01$, sham n=4, TAC n= 5) and ND ($p<0.05$, sham n=4, TAC n=5). EDP was elevated in both groups HFD and ND ($p<0.001$, sham n=4, TAC n= 5) as a result of similar PO. The peak rate of decline of pressure dp/dt_{min} was decreased in HFD group only ($p<0.01$, sham n=4, TAC n=5) showing the sustained elevation of high pressure state in contrast to ND where the parameter remained unchanged. This shows that despite a different pattern of systolic function, both dietary groups showed a dysfunction in diastolic properties albeit with minor differences. Representative PV loops as baseline and vena cava occlusion are shown in **figure 19.**

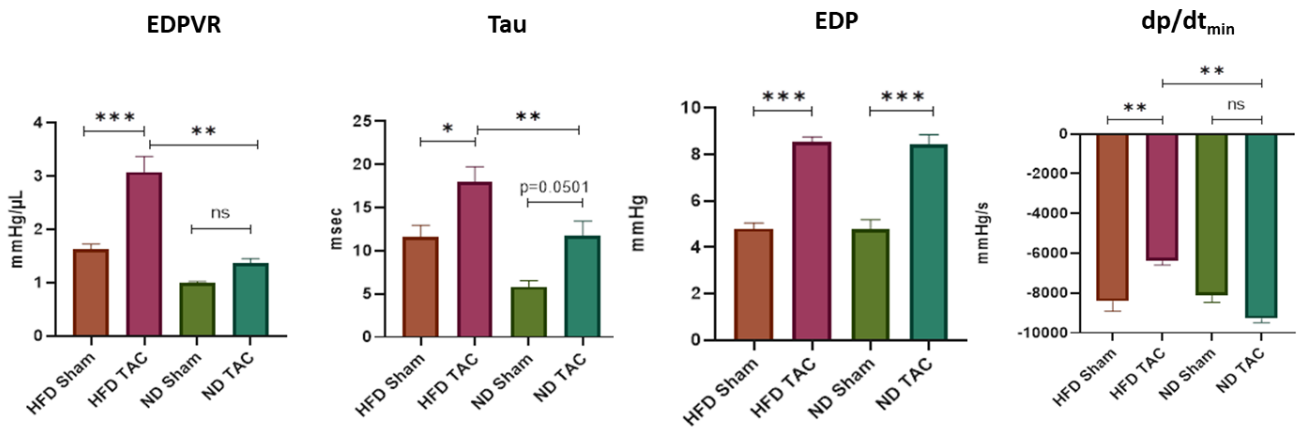

Fig. 18. Diastolic LV function in HFD vs ND mice at the end of two weeks of low grade PO.
EDPVR: End diastolic pressure volume relationship, Tau: time constant of isovolumetric relaxation, EDP: end diastolic pressure, dp/dtmix: minimal rate of pressure fall with time. Data are expressed as mean ± SEM. *p <0.05, **p<0.05, ***p<0.001 vs. corresponding group using one-way ANOVA with Bonferroni post-test. n=4-5/group.

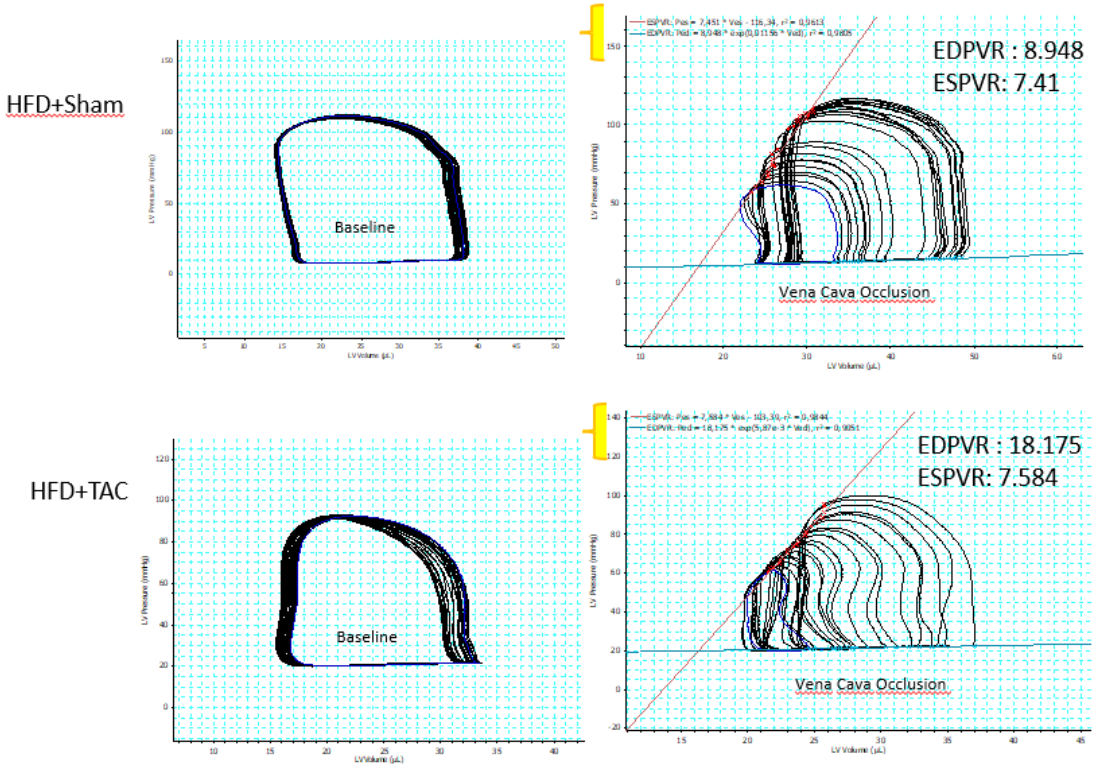

Fig. 19. Representative PV loops of HFD group.
Sham vs TAC comparison of HFD cohort at baseline and vena cava occlusion to account for preload. Note the changes in ESPVR and EDPVR values.

5. Gene expression of cardiac stress markers in HFpEF and HFrEF

Myocardial gene expression for cardiac stress markers (**figure 20)** was investigated two weeks after TAC subsequent to PV analysis using RT-qPCR. A pattern reminiscent of the fetal gene program was seen in both dietary groups. Common stress markers were increased but in a differential manner. The transcript levels of Natriuretic peptides A and B (nppa, nppb) were found to be similarly and consistently increased in ND and HFD sham vs TAC mice ($p<0.05$, n=7/group). ANP was 3.6 fold higher in HFD sham vs TAC and 2.7 fold higher in ND sham vs TAC. BNP was almost 3 fold higher in both dietary groups. This confers with previous findings that PO can lead to re-activation of fetal gene program and increase the levels of stress related markers. mRNA level of α-skeletal actin (Acta1) which is known to be a marker of compensated cardiac hypertrophy was increased after PO to a much higher extent in HFD group (12.3 fold, $p<0.001$, n=7/group) vs ND group (6 fold, $p<0.05$, n=7/group). Sarcoplasmic/Endoplasmic Reticulum Ca2+ ATPase-2α (Serca2-α) was decreased in both groups but it was much lower in ND (0.2 fold, $p<0.01$, n=5/group) vs only a trend to decrease in HFD groups 0.6 fold ($p>0.05$). Myosin heavy chain (Mhc) often undergoes an isoform shift during the fetal gene program, and it was observed that both dietary groups showed a shift from α-myosin heavy chain to β-myosin heavy chain after TAC; HFD (184 fold, $p<0.01$, n=7/group) and ND (95 fold, $p<0.05$, n=7/group).

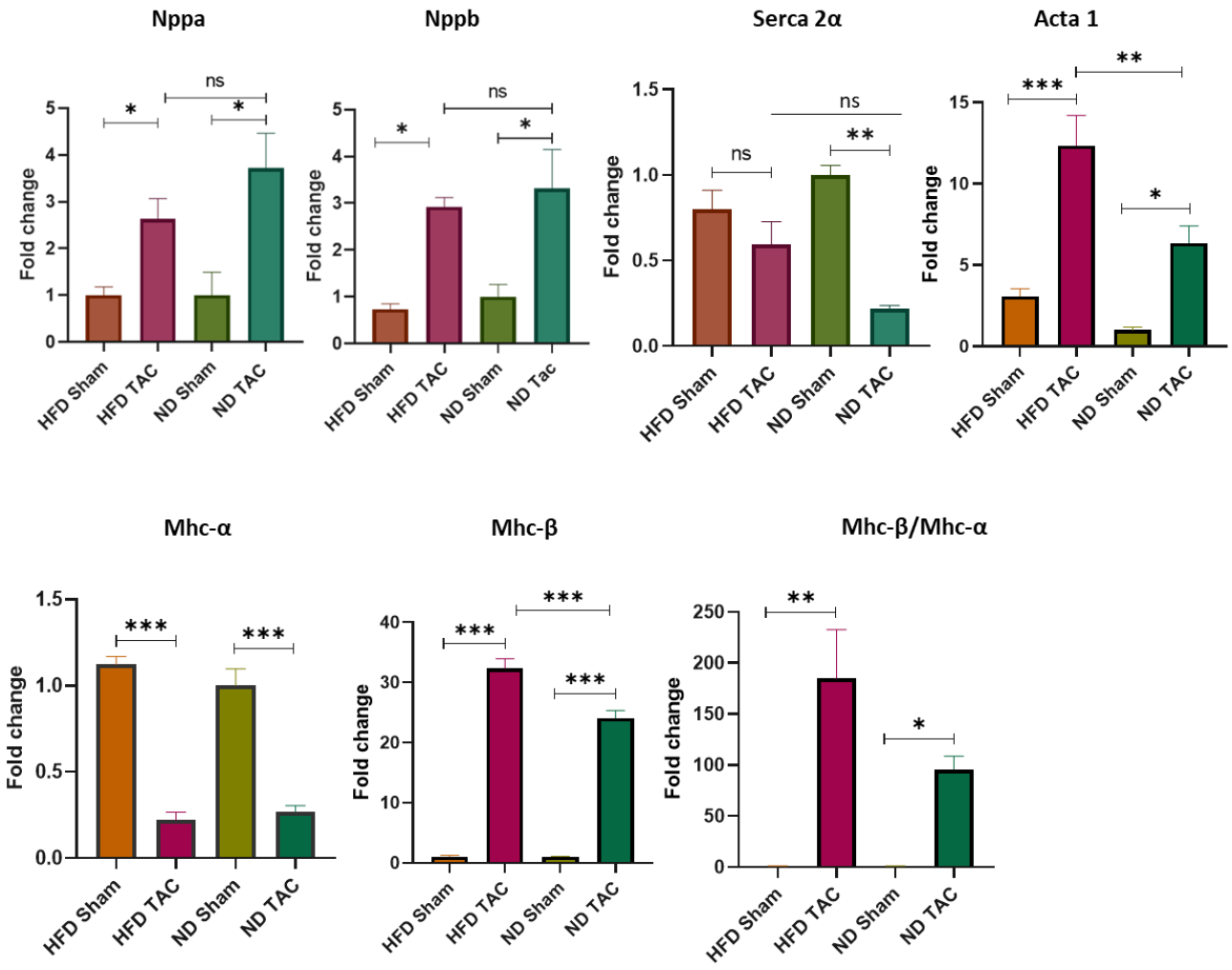

Fig. 20. Cardiac gene expression of stress markers in HFD and ND following two weeks of low grade PO. Cardiac mRNA levels of Nppa, natriuretic peptide A; Nppb, natriuretic peptide B; Serca2-α, Sarcoplasmic/Endoplasmic Reticulum Calcium ATPase-2α; Acta, α-skeletal actin; Mhc-α, myosin heavy chain-α; Mhc-β, myosin heavy chain-β and Mhc-β/ Mhc-α ratio were measured using RT-qPCR. Values are presented as fold change normalized to ND-sham controls. Gapdh was used for normalization. Data are presented as mean ± SEM. *p<0.05, **p < 0.01, ***p<0.001 vs. corresponding groups using one-way ANOVA followed by Bonferroni post-hoc test for multiple comparisons, n=7/group.

6. Steatosis in ventricular cryosections

Excess accumulation of lipid in peripheral tissues is a key feature in a variety of metabolic disorders and pathophysiologies involving insulin resistance. In order to support the finding of increase in BW subsequent to HFD for 10 weeks, we measured the accumulation of lipid or steatosis within cryosections from snap frozen ventricular tissue. Oil red O staining was employed for this, which stains only the neutral lipids (triglycerides, diacylglycerols and cholesterol esters) present in a specimen which correspond basically to steatotic lipid droplets. It was seen that 10 weeks of HFD was indeed sufficient to induce steatosis in LV sections of HFD group with respect to ND group (p<0.001,

n=5/group). However, sham vs TAC in HFD showed no differences in any group, indicating that lipid accumulation subsequent to HFD is not altered by PO. However, the analysis does support that HFD mice are indeed dyslipidemic. ND group showed no significant lipid deposition as shown in **figure 21**.

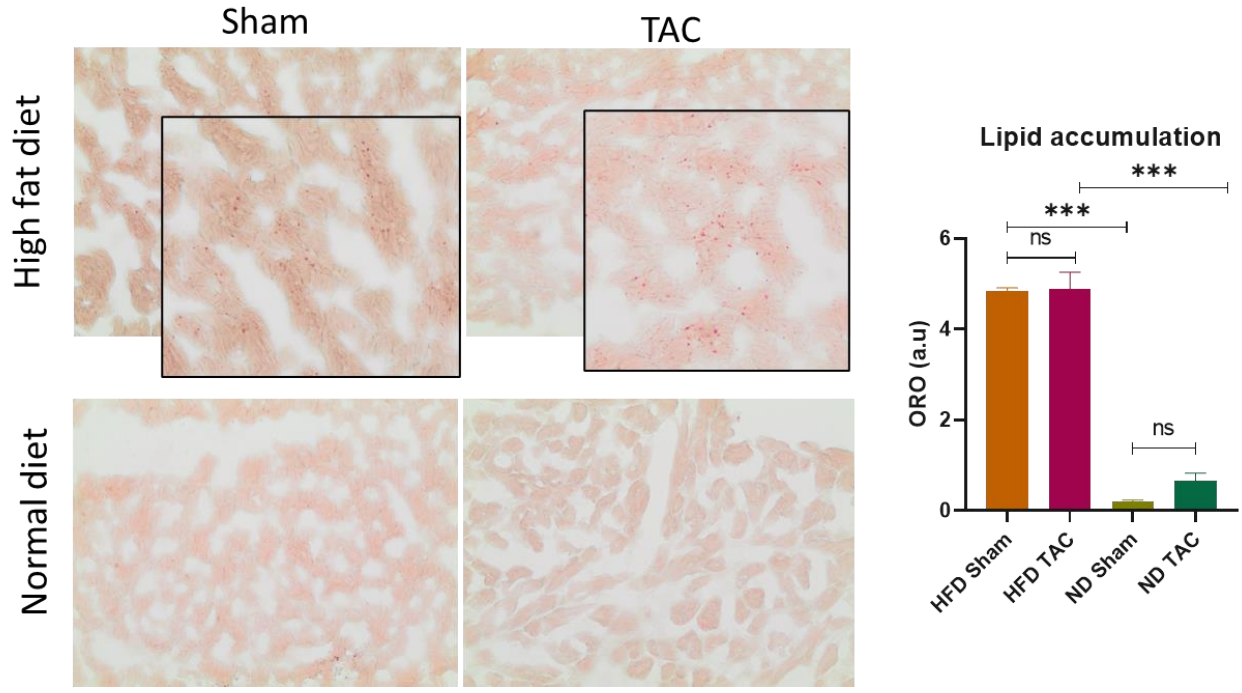

Fig. 21. Lipid accumulation in HFD and ND mice after two weeks of low grade PO.
Oil red O stained cryosections show lipid deposits (as dark pink granules) at 20X magnification. Inlets show five times magnified image to emphasize the staining. Data are presented as mean ± SEM. ***p<0.001 vs. corresponding groups using two-way ANOVA followed by Bonferroni post-hoc test for multiple comparisons, a.u: arbitrary units, n=5/group.

7. Dynamics of collagen induced fibrosis in HFpEF and HFrEF

7.1. Total LV fibrosis

LV myocardial sections were stained with picrosirius red to distinctly identify collagen (pink) from surrounding matrix (yellow). Both groups exhibited enhanced LV fibrosis when shams were compared with TAC; ND ($p<0.05$, n=7/group) and HFD ($p<0.05$, n=7/group). However, the level of fibrosis as shown in **figure 22.A,** in both TAC groups was significantly different, with HFD TAC showing exacerbated collagen content with respect to ND TAC ($p<0.05$).

7.2. Perivascular fibrosis

Upon picrosirius staining, two types of reactive fibroses were seen in the LV tissues, interstitial and perivascular. It has been known that states of disturbed metabolism can lead to increased fibrosis in perivascular regions (de Boer et al., 2019) so we wanted to see if the same holds true for the HFD cohort. To analyze perivascular fibrosis, a similar protocol was followed in stained sections but the region of interest for quantification was limited to only perivascular regions (**figure 22.B)**. It was found that, although there were no changes in perivascular fibrosis between the sham and TAC groups of ND. HFD TAC group had 2 fold higher levels as compared to ND TAC ($p<0.001$, n=8/group) as shown in figure 25.b which may explain the higher levels of fibrosis between the two TAC groups.

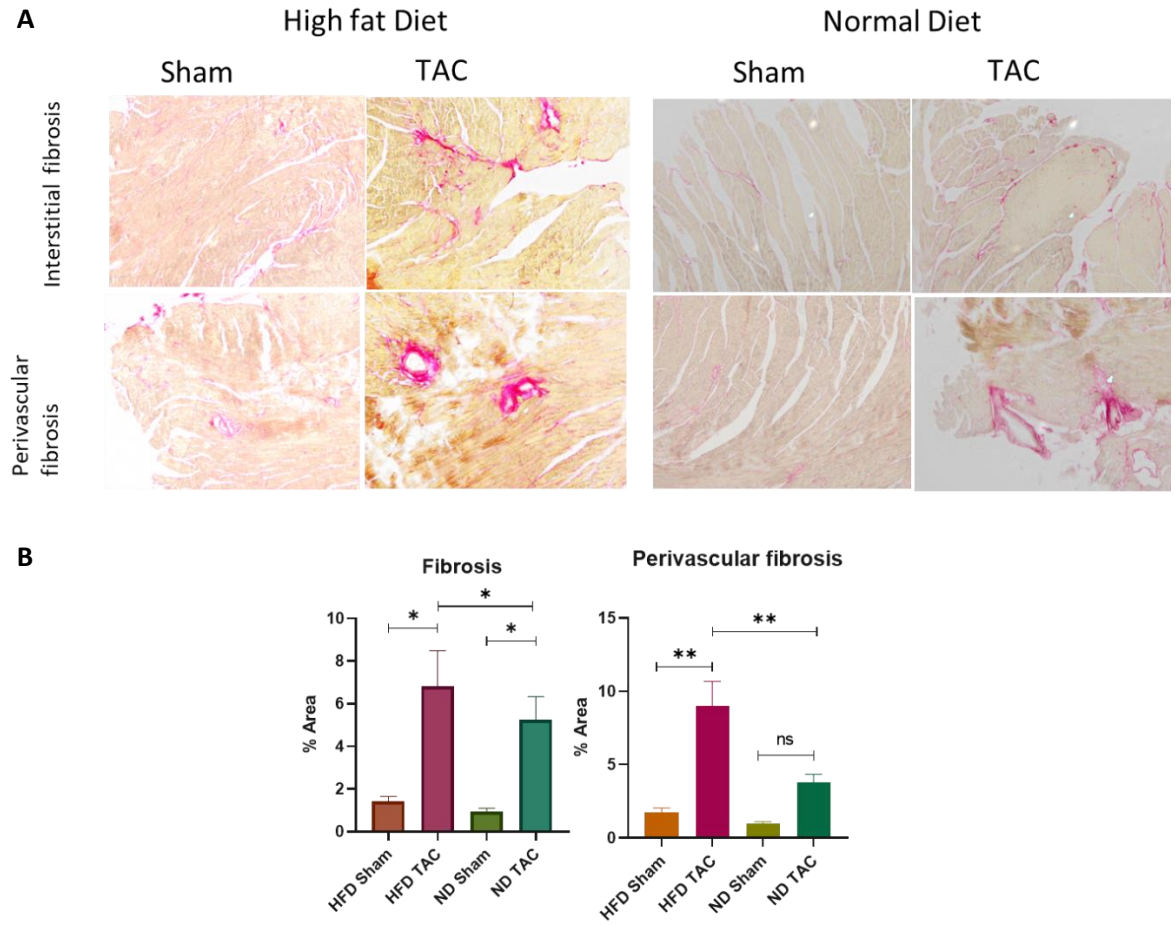

Fig. 22. Left ventricular fibrosis following two week of TAC surgery.
A: Representative histological images of cardiac sections stained with picrosirius red staining to measure fibrotic regions (pink), scale bar = 200 µm. B: Quantification of fibrosis percentage area as mean data for the fibrotic area relative to the total left ventricular section and quantification of fibrosis only around perivascular regions. Data are presented as mean ± SEM, *p < 0.05, **p<0.05 between groups using 2-way ANOVA with Bonferroni post-hoc test for multiple comparisons, n=7/group.

7.3. Collagen subtypes expressed in HFpEF and HFrEF states

Analysis of mRNA transcripts coding for pro-fibrotic proteins, fibronectin-1, collagen I and III through RT-qPCR was subsequently performed, **figure 23**. While fibronectin expression was the same in both groups in sham vs TAC ($p<0.01$, n= 5/group), it was found that both dietary cohorts exhibit a similar profile of collagen subtypes. In HFD group, Col I was found to be 3 fold higher in HFD sham vs TAC ($p<0.05$, n=7/group) group while in ND sham vs TAC group, Col III was abundantly expressed ($p<0.05$, n=7/group). Resultingly, Col I / Col III ratio was higher in HFD group after PO. The differences in dominant collagen subtype may be correlated to the differential pattern of fibrosis seen in HFD group.

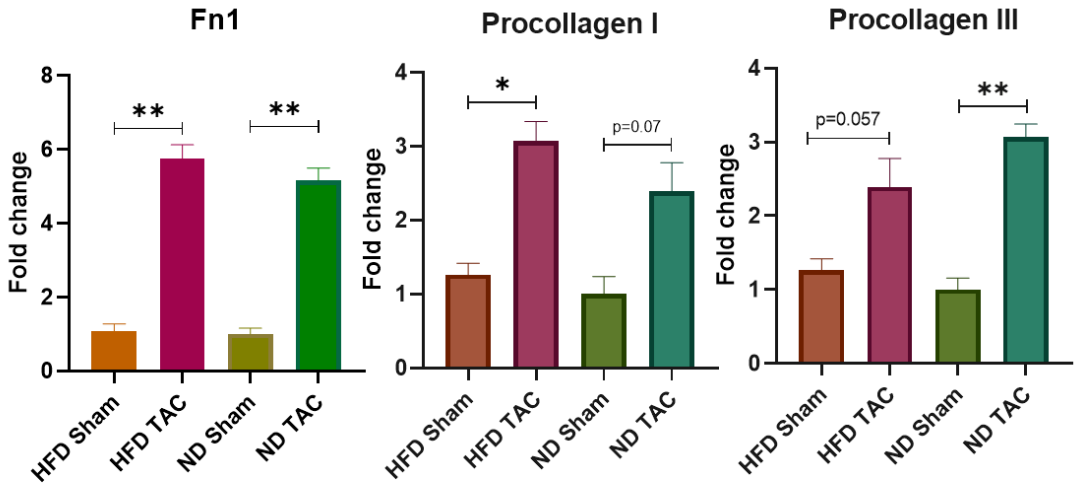

Fig. 23. Cardiac gene expression of pro-fibrotic markers in HFD and ND following two weeks of low grade PO. Cardiac mRNA levels of FN-1, Fibronectin-1; Procollagen I and Procollagen III were measured using RT-qPCR. Values are presented as fold change normalized to ND-sham controls. Gapdh was used for normalization. Data are presented as mean ± SEM. *p<0.05, **p < 0.01 between corresponding groups using one-way ANOVA followed by Bonferroni post-hoc test for multiple comparisons, n=7/group.

8. Inflammation and endothelial dysfunction in HFpEF and HFrEF

8.1. Expression of common inflammatory cytokines in HFrEF vs HFpEF

Metabolic stress caused by dyslipidemia is often driven by cytokine signaling that may lead to further pro-inflammatory cascades. An analysis of common inflammatory cytokines relevant to the myocardial environment revealed a differentially activated pattern, as shown in **figure 24**. mRNA levels of TGF-β and IFN-γ were only upregulated in the HFD sham vs TAC examination with 5 fold ($p<0.05$, n=7/group) and 7 fold ($p<0.01$, n=7/group) higher expression levels in TAC respectively. In ND group, only the level of TNF-α was enhanced 6 fold ($p<0.01$, n=7/group) with respect to sham and in HFD group, it was not significant. IL-1β was found to be upregulated differentially in the HFD group with a 7 fold higher expression ($p<0.001$, n=7/group), IL-6 was not significantly increased in either

group. Interestingly, Endothelin-1 was also only selectively enriched in HFD mice after PO with about 2.5 fold higher expression as compared to sham ($p<0.05$).

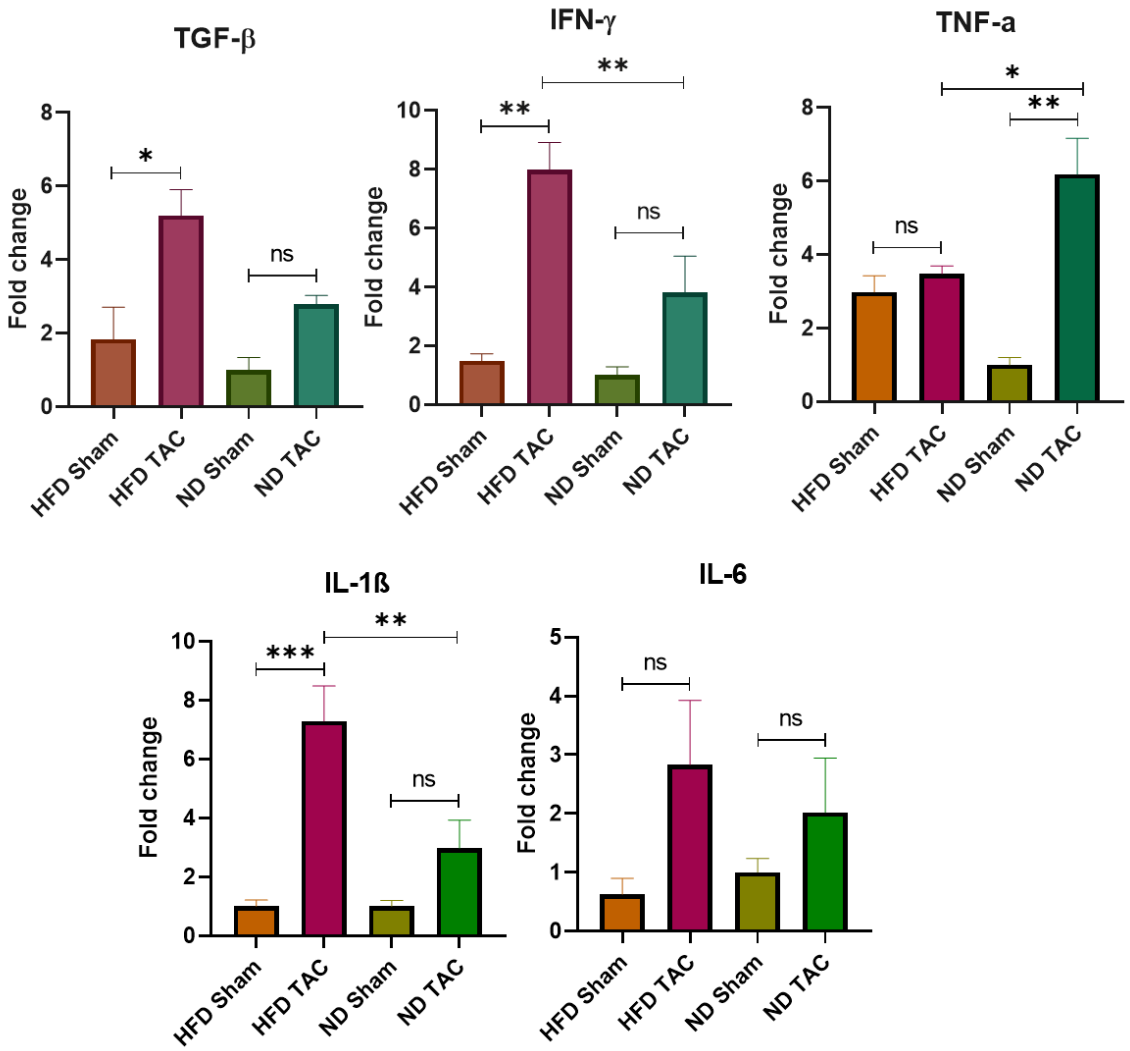

Fig. 24. Cardiac gene expression of pro-inflammatory markers in HFD and ND following two weeks of low grade PO.
Cardiac mRNA levels of TGF-β, transforming growth factor β; IFN-γ, interferon γ and TNF-α, tumor necrosis factor α; IL-1β, interleukin 1 β and IL-6, interleukin 6 were measured using RT-qPCR. Values are presented as fold change normalized to ND-sham controls. Gapdh was used for normalization. Data are presented as mean ± SEM. *p<0.05, **p < 0.01 vs. corresponding groups using one-way ANOVA followed by Bonferroni post-hoc test for multiple comparisons, n=7/group.

8.2. Endothelial dysfunction

Cytokine signaling is multidimensional in aspect, while it may lead to inflammation through one signaling cascade, through the other it can exert a different effect. To analyze markers of endothelial

dysfunction, mRNA levels of Cell adhesion molecules- Vcam-1, Pecam-1 and Icam-1 were assessed. Moreover, the vasopeptide hormone endothelin 1 (Et1) was also examined, as shown in **figure 25**.

It was seen that the dominant active cell adhesion molecules in HFD group were Vcam-1 and Icam-1 with an approximately 2 fold ($p<0.01$, n=7/group) and 2.75 fold ($p<0.01$, n=7/group) higher expression in TAC operated mice . While both Icam-I and Pecam-1 were active in ND TAC mice as well ($p<0.05$, n=7/group), Vcam-1 showed no upregulation.

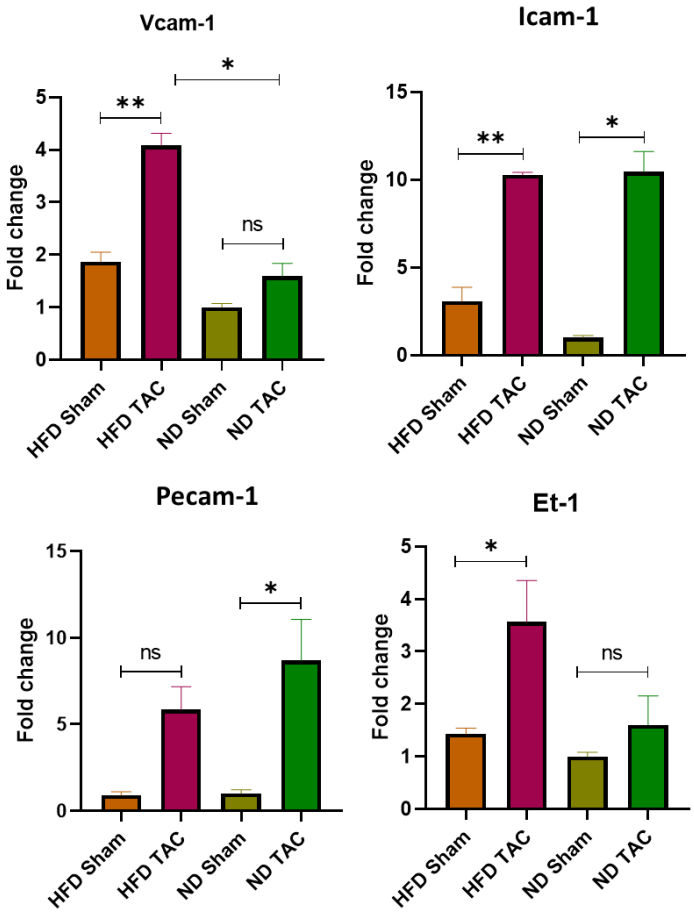

Fig. 25. Cardiac gene expression of pro- endothelial dysfunction markers in HFD and ND following two weeks of low grade PO.
Cardiac mRNA levels of CAMs, cell adhesion molecules namely vascular (VCAM-1), intracellular (ICAM-1), platelet endothelial (PECAM-1) and ET-1, endothelin 1 were measured using RT-qPCR. Gapdh was used for normalization. Data are presented as mean ± SEM. *p<0.05, **p < 0.01, ***p<0.001 vs. corresponding groups using one-way ANOVA followed by Bonferroni post-hoc test for multiple comparisons, n=7/group.

8.3. CD45 mediated inflammation

CD45 or protein tyrosine phosphatase receptor type C (PTPRC) is a marker for hematopoietic cells and it is implicated in lymphocyte mediated myocardial inflammation (Woudstra et al., 2017). Immunofluorescence staining specific to CD45 revealed that it was unchanged in TAC vs sham of both

ND and HFD. However, when the two ND-sham and HFD-TAC were compared, the percentage of CD45 positive cells was higher in HFD-TAC mice ($p<0.05$, n=6/group) indicating that the dual stress of HFD and PO is sufficient to lead to inflammatory pathways originating from lymphocytes, as shown in **figure 26**.

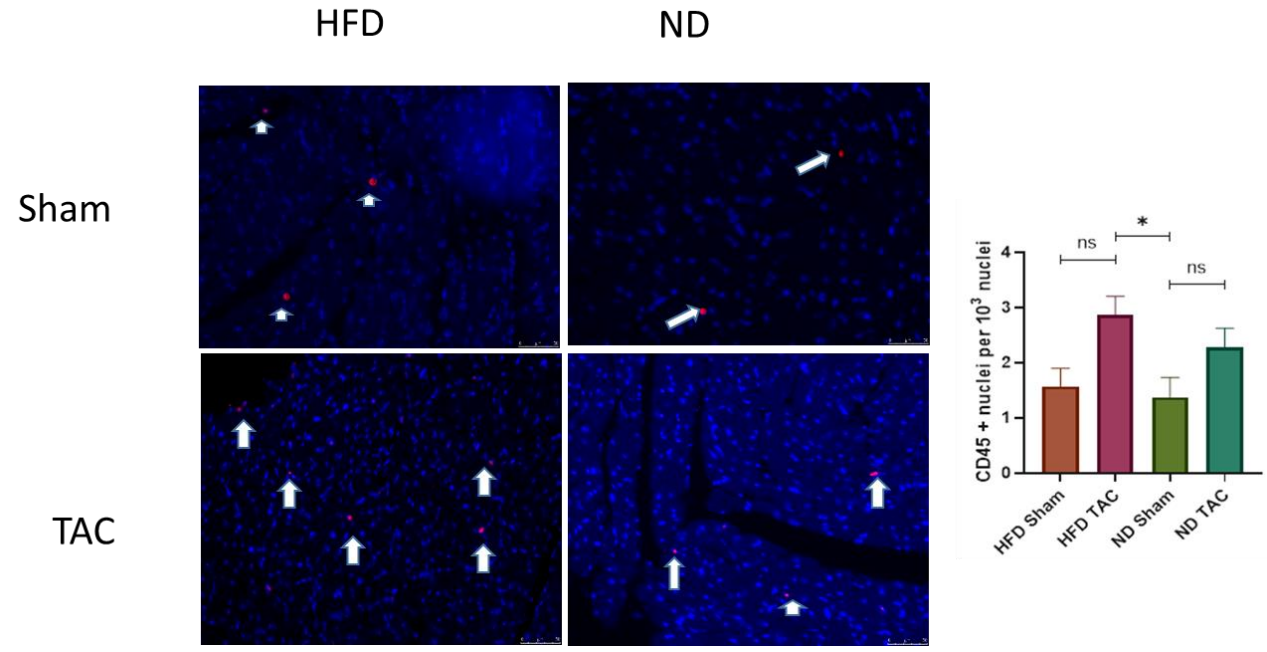

Fig. 26. CD45 levels in HFD and ND mice after two weeks of low grade PO.
LV sections were stained with primary antibody against CD45 antigen and then incubated with fluorophore conjugated secondary antibody (red). Counterstaining with DAPI was done to visualize individual nuclei (blue) at 20X magnification, number of CD45 positive nuclei were measure / 1000 nuclei. Data are presented as mean ± SEM. *$p<0.05$ vs. corresponding groups using two-way ANOVA followed by Bonferroni post-hoc test for multiple comparisons, n=5/group.

8.4. NOX2 expression

NADPH oxidase NOX2 is a major source of ROS within the heart and its overactivation has been implicated in several cardiovascular defects, including PO and diastolic dysfunction (Harvey et al., 2020; Zhang et al., 2012). Since a number of differentially regulated cytokine levels were observed in the two dietary groups, we were curious to see whether ROS mechanisms triggered through NOX2 may be relevant here. Protein expression level analysis through immunoblotting showed higher expression of NOX2 in sham vs TAC in both ND (1.8 fold, $p<0.05$, n=6/group) and HFD group (3 fold, $p<0.05$, n=7/group). Interestingly, the two sham groups also showed a significant difference with 1.8 fold higher expression in HFD sham ($p<0.05$) as compared to ND sham indicating a higher basal level of NOX2 as a consequence of HFD independent of PO (**figure 27)**.

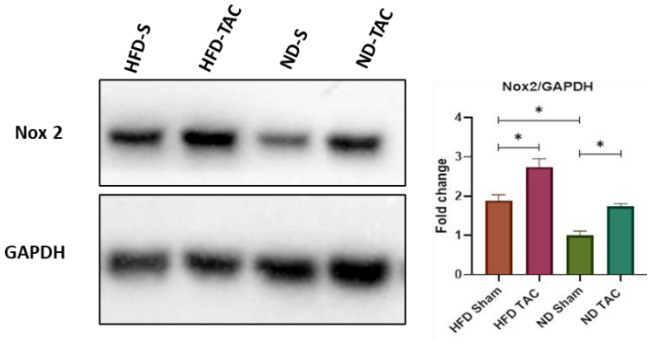

Fig. 27. Expression of NADPH oxidase (Nox-2).
Western blot images for Nox-2 and GAPDH from LV lysates are shown. Values are presented as fold change normalized to ND sham controls. Data are presented as mean ± SEM. *p < 0.05 between respective groups using one way ANOVA followed by Bonferroni post-hoc test for multiple comparisons. n=6-7/group.

8.5. HDAC-4 phosphorylation

HDAC-4 belongs to the class-IIa of histone deacetylase family and it is strongly associated to be positively correlated with indices of obesity (Shanaki et al., 2022). It has been known to induce maladaptive hypertrophy in several cardiomyopathies. We measured the levels of phosphorylation at Serine246 by comparing P-HDAC4 normalized to HDAC-4 and found that it was unequivocally higher in the HFD-TAC vs sham (p>0.05, sham n=6, TAC n=7) while remaining unchanged in ND sham vs TAC animals as shown in **figure 28.**

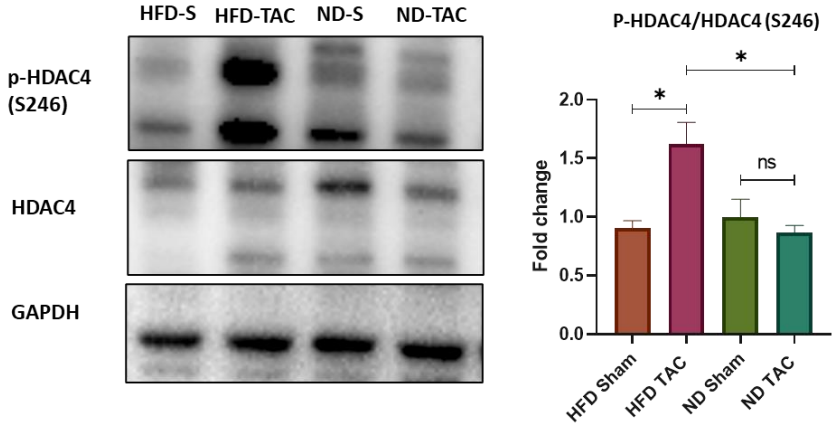

Fig. 28. Phosphorylation of HDAC-4 in HFD vs ND mice following two weeks of low grade PO.
Western blot images for phospho-HDAC-4 (Ser246) (p-HDAC-4), total HDAC-4, and GAPDH from LV lysates are shown. Values are presented as fold change normalized to ND sham controls. Data are presented as mean ± SEM. *p < 0.05 between respective groups using one way ANOVA followed by Bonferroni post-hoc test for multiple comparisons. n=6-7/group.

9. Programmed cell death in HFpEF and HFrEF

Immunohistochemistry with terminal deoxynucleotidyl transferase (TdT)-mediated dUTP-biotin nick end-labelling (TUNEL) of LV myocardium cross sections from both dietary groups was performed to analyse the levels of programmed cell death or apoptosis. As shown in figure 31, the number of TUNEL positive cells was 8.5 fold higher in HFD TAC ($p<0.01$, n=6/group) compared to sham littermates and 5.2 fold higher in ND sham vs TAC mice ($p<0.01$, n=6/group). No difference was seen in intergroup comparisons, indicating that differential activation of apoptosis is not a discriminating factor in the two states as shown in **figure 29.**

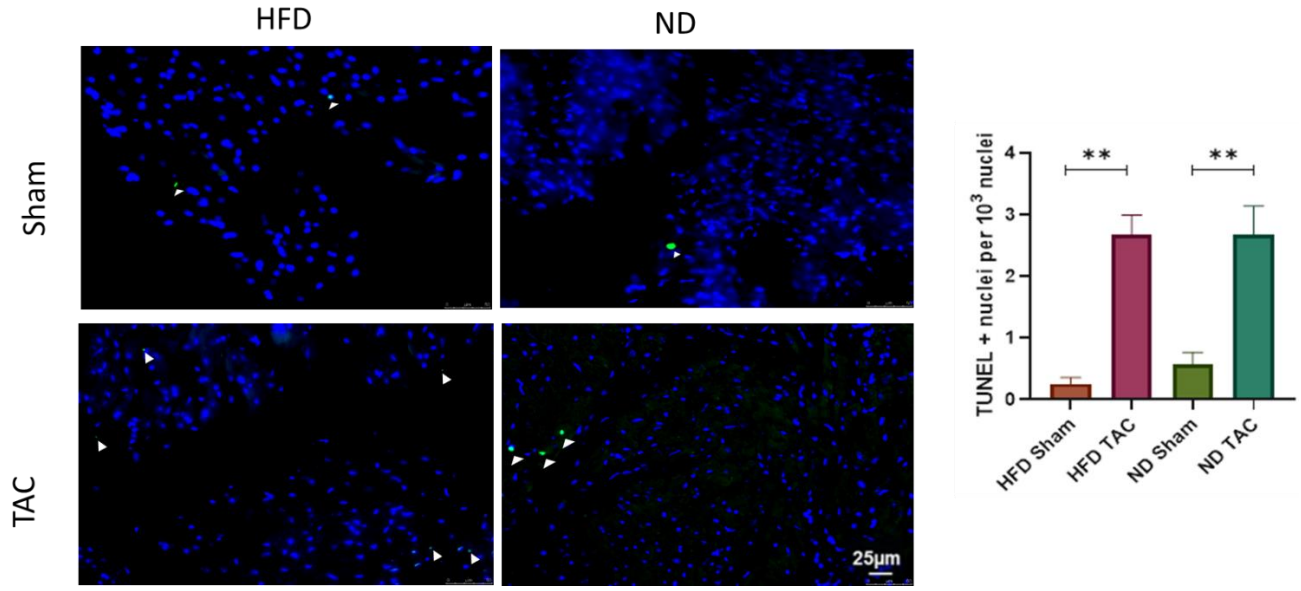

Fig. 29. LV apoptosis in HFD and ND cohorts following two week of TAC surgery.
TdT-mediated dUTP-biotin nick end-labelling (TUNEL) staining of LV sections and white arrows indicate TUNEL-positive cardiomyocytes (scale bar = 25 µm) and subsequent quantification of TUNEL-positive cells per 1000 DAPI-positive nuclei. Data are presented as mean ± SEM. **p < 0.01 vs. corresponding groups using two way ANOVA with Bonferroni post-hoc test for multiple comparisons, n=6/group.

10. Cardiac kinases in HFpEF and HFrEF states

Protein kinases in the myocardium are involved in several signal transduction pathways that regulate important cardiac function. We wanted next to investigate signaling kinases that could be conferring the aforementioned striking differences between the HFpEF and HFrEF like states afforded by HFD and ND after the induction of low grade PO. Total protein lysates from the LV were probed through immunoblotting to assess the levels of active phosphorylated forms of each of these kinases.

Serine/threonine kinase protein kinase B (Akt) is a downstream of phosphatidylinositol 3-kinase (PI3K) and it has been shown to be activated in response to a pathological event where it leads to compensatory hypertrophy and remodeling. Moreover, it is also implicated in regulation of cardiac growth, myocardial angiogenesis, glucose metabolism, and apoptosis in cardiac myocytes (Chaanine

et al., 2011). Upon comparing the sham and TAC of our dietary groups, it was found that active phosphorylation of Akt was unchanged in the ND group, however HFD group showed significant activation of this kinase in TAC mice with approximately 2.6 fold higher upregulation ($p<0.001$, sham n=6, TAC n=6). The data is shown in **figure 30.**

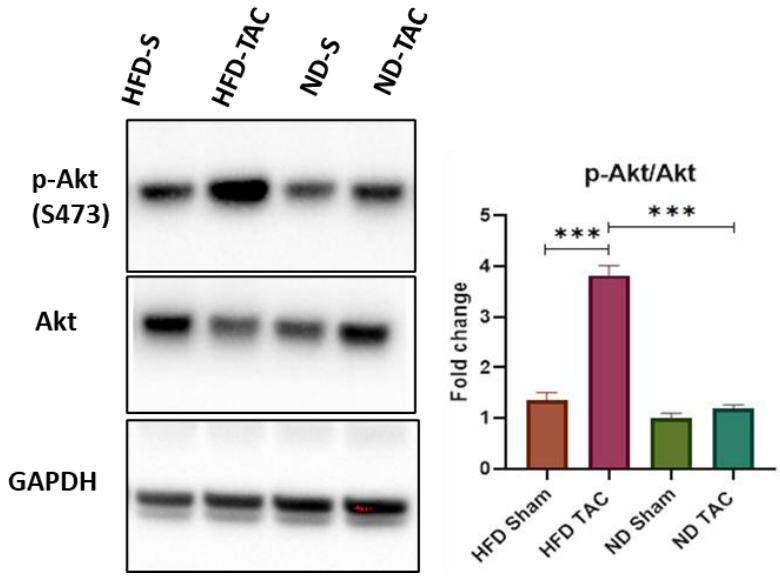

Fig. 30. Phosphorylation of cardiac Akt in HFD and ND mice following two weeks of PO.
Representative Western blot images for phospho-Akt (Ser473) (p-Akt), total Akt, and GAPDH from LV lysates two week after intervention are shown alongside quantification of phosphorylated Akt to total Akt abundance. Values are presented as fold change normalized to corresponding ND sham controls. Data are presented as mean ± SEM. ***p < 0.001 between corresponding groups using one way ANOVA with Bonferroni post-hoc test for multiple comparisons, n=6-7/group.

Mitogen-activated protein kinase (MAPK) and its downstream effector kinases namely extracellular signal-regulated kinases 1/2 ERK (ERK1/2), p38 kinases and c-Jun N-terminal kinases (JNK) are involved in a wide variety of cellular responses to a pathological injury. They play pivotal roles in regulation of cell proliferation, development, differentiation, inflammation, cell death and overall response to stress (Rose et al., 2010). ERK1/2 phosphorylation at at TEY (Thr-Glu-Tyr) motif followed a similar trend as P-Akt and was highly upregulated in the HFD group post PO with upto 2.75 fold higher expression ($p<0.01$, sham n=7, TAC n=7) while maintaining basal levels in ND- TAC mice ($p>0.05$, sham n= 7, TAC n=7). The levels of p38 phosphorylation at Threonine180/Tyrosine182 remained unchanged between sham vs TAC comparison of both HFD and ND but a comparison of respective TAC operated mice exhibited a significant 1.4 fold upregulation in HFD ($p<0.01$). The levels of JNK phosphorylation at Threonine183/Tyrosine185 was however, unchanged in both groups ($p>0.05$) as shown in **figure 31**.

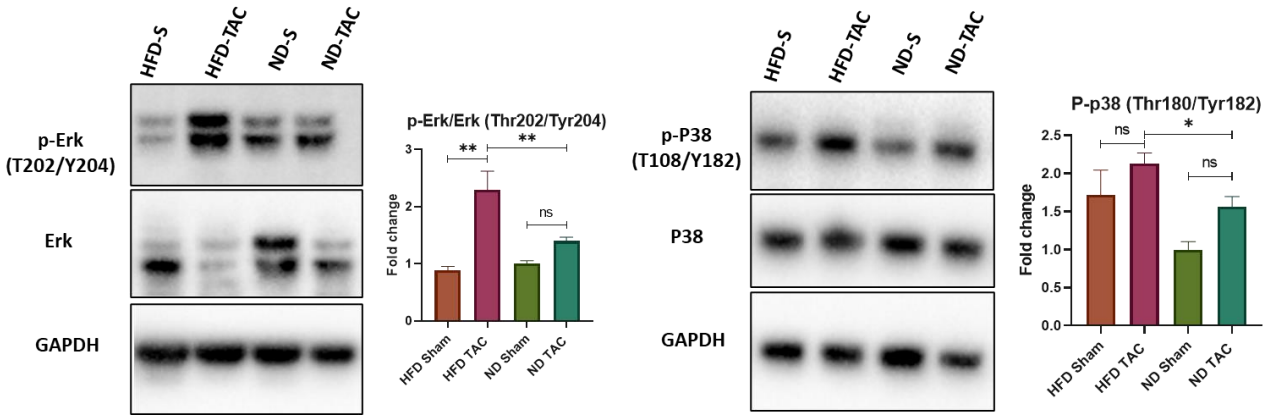

Fig. 31. Assessment of cardiac MAPK activation levels in HFD and ND mice following two weeks of PO.
Representative blots of phosphorylation levels of ERK1/2 (at TEY motif) and p38 (at Threonine180/Tyrosine182) with GAPDH as a loading control. Values are presented as fold change normalized to ND sham group. Data are presented as mean ± SEM. *p < 0.05, **p < 0.01 vs. corresponding groups using one- way ANOVA with Bonferroni post-hoc test for multiple comparisons, n=7/group.

11. Calcium handling in HFpEF vs HFrEF

Calcium handling and signaling cannot be ignored when we talk about the global effects of PO in the myocardium. The levels of Ca2+/calmodulin-dependent protein kinase type II (CaMKII) phosphorylation were not significantly enhanced in any group but there was an upwards trend in HFD-TAC vs sham comparisons (p=0.08, sham n=6, TAC n=6), **figure 32**.

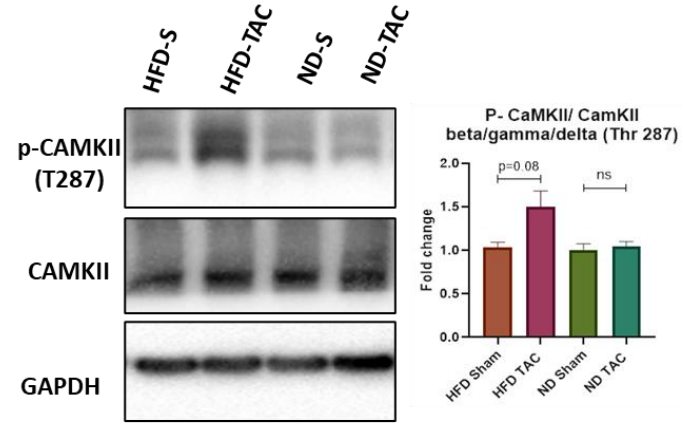

Fig. 32. Activity of CaMKII in HFD and ND cohorts following two weeks of low grade PO.
Cardiac protein levels of phosphorylated CaMKII beta/gamma/delta (Thr287) were assessed by immunoblotting vs. CaMKII delta (CaMKII δ), the major CaMKII isoform expressed in the heart, GAPDH was loading control. Quantification of p-CaMKII abundance to CaMKIIδ/GAPDH is shown alongside. Values are presented as fold change normalized to corresponding shams. Data are presented as mean ± SEM using one -way ANOVA with Bonferroni post-hoc test for multiple comparisons, n=6/group.

The non-significance was a little conflicting because an important downstream target of CaMKII, RyR2 appeared to be selectively phosphorylated at Ser2814 again only in the HFD-TAC vs sham group by 1.4

fold (p<0.05, sham n=6, TAC n=6). In ND group, there was no change in levels of phosphorylation. Another important target is phospholamban (PLN) and levels of phosphorylation at Thr17 followed the same trend as RYR2 phosphorylation at Ser2814 with 1.3 fold upregulation in HFD group after TAC as compared to its sham littermates (p<0.05, sham n=7, TAC n=6) as shown in **figure 33.A and B**. Additionally, the phosphorylation of another downstream target, RyR2 at Ser2808 and the respective PLN at Ser16 were unchanged in both groups, **figure 34.A and B**.

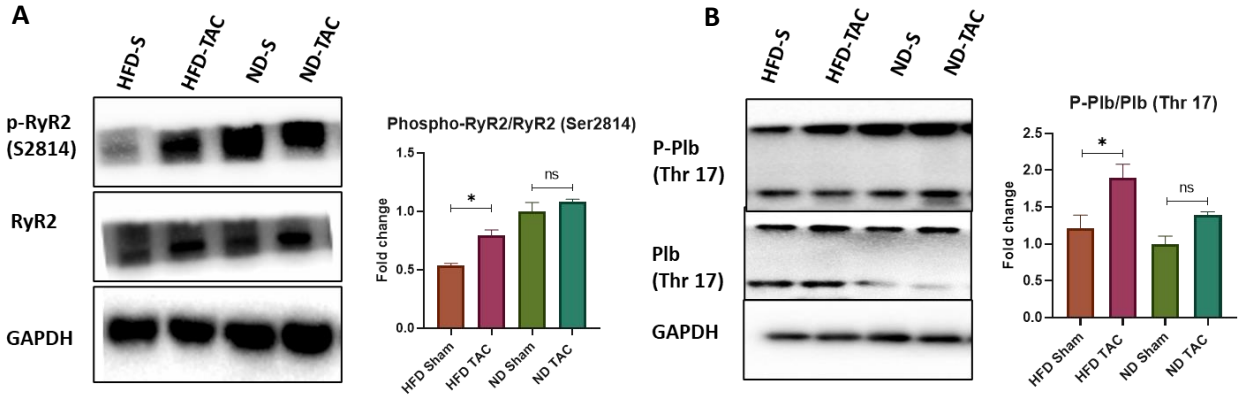

Fig. 33. Immunoblot assessment of CaMKII dependent phosphorylation sites of ryanodine receptors and phospholamban in HFD and ND mice following two weeks of low grade TAC.
Cardiac protein levels of A: Serine 2814-phosphorylated ryanodine (p-RyR2 Ser 2814), and for B: threonine 17-phosphorylated phospholamban (p-PLN Th17) were assessed at two weeks post PO, GAPDH used as loading control. Densitometric quantification of phosphorylated proteins to total protein are shown alongside. Values are presented as fold change normalized to ND sham controls. Data are presented as mean ± SEM. *p < 0.05 between groups using one-way ANOVA with Bonferroni post-hoc test for multiple comparisons, n=6-7/group.

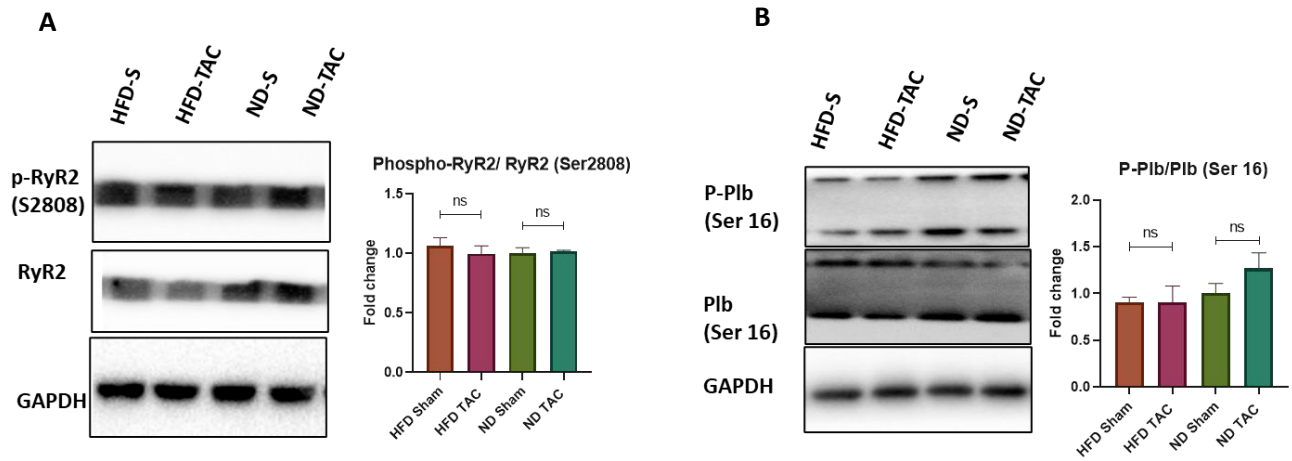

Fig. 34. Immunoblot assessment of PKA dependent phosphorylation sites of ryanodine receptors and phospholamban in HFD and ND mice following two weeks of low grade TAC.
Cardiac protein levels of A: Serine 2808-phosphorylated ryanodine (p-RyR2 Ser 2808), and for B: threonine 16-phosphorylated phospholamban (p-PLN Th16) were assessed at two weeks post PO, GAPDH used as loading control. Densitometric quantification of phosphorylated proteins to total protein are shown alongside. Values are presented as fold change normalized to ND sham controls. Data are presented as mean ± SEM. *p < 0.05 between groups using one-way ANOVA with Bonferroni post-hoc test for multiple comparisons, n=6-7/group.

Furthermore, phosphorylation levels of cardiac troponin (cTnI) at the Ser22/23, another PKA target that decreases the myofilament Ca^{2+} sensitivity thereby leading to enhanced effects on cardiac relaxation, were also assessed. It was found that P-cTnI levels were selectively reduced in the ND group after PO by upto 0.4 fold (p<0.001, sham n=6, TAC n=6) but remained unchanged in HFD, **figure 35**.

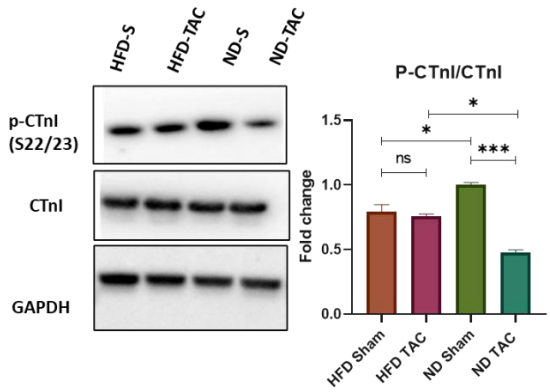

Fig. 35. Immunoblot assessment of Troponin I in HFD and ND mice following two weeks of low grade-TAC.
Cardiac protein levels of phosphorylated cardiac troponin, p-CTnI at Ser22/23 with respect to total cardiac troponin, CTnI. Densitometric quantifications are shown alongside. GAPDH was used as loading control. Values are presented as fold change normalized to ND sham controls. Data are presented as mean ± SEM. *p<0.05, ***p < 0.001 between groups using one- way ANOVA with Bonferroni post-hoc test for multiple comparisons, n=6/group.

Results 2: Natural aging model

1. Morphometric analysis

1.1 Organ level and cellular analysis of hypertrophy

In contrast to the findings from the first model, we found that aged mice (18-20 months) showed no significant change in heart, LV and LA size when compared with young ones (6-8 weeks old) as shown in **figure 36**. All weights normalized to tibia length were non-significant in young vs old except for a slight upwards trend in LV mass ($p>0.05$, young n= 10, aged n=13). Lungs from old mice however, showed on average 30 times more hypertrophy than young mice($p<0.05$) indicating evidence for pulmonary congestion. Analysis of LV CSA with WGA staining also showed no presence of hypertrophy on the cellular level (**figure 37)**.

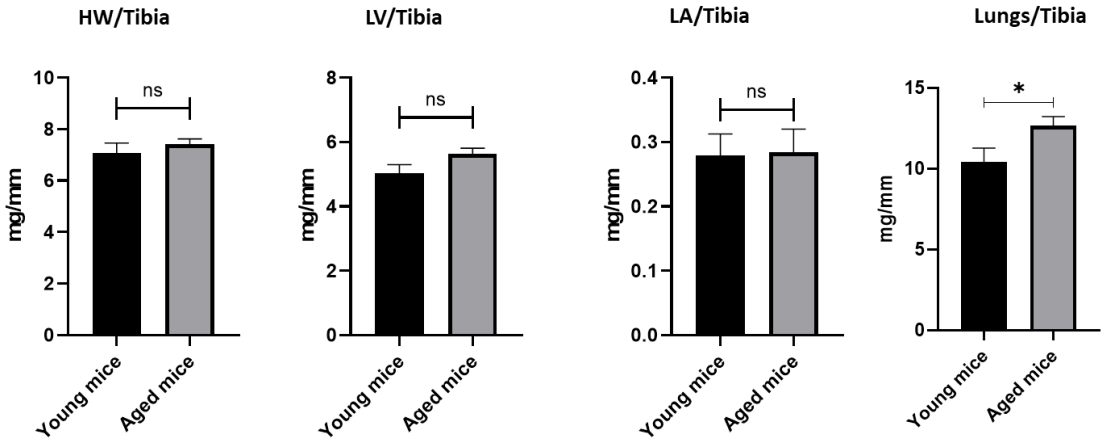

Fig. 36. Morphometry of young and aged mice.
BW/TL, Body weight; HW, Heart weight; LV; Left ventricular weight; TL, tibia length and lung weight-to-tibia length ratios. Data are expressed as mean ± SEM. *p <0.05 vs. corresponding group using unpaired Student's t-test, n=10-13/group.

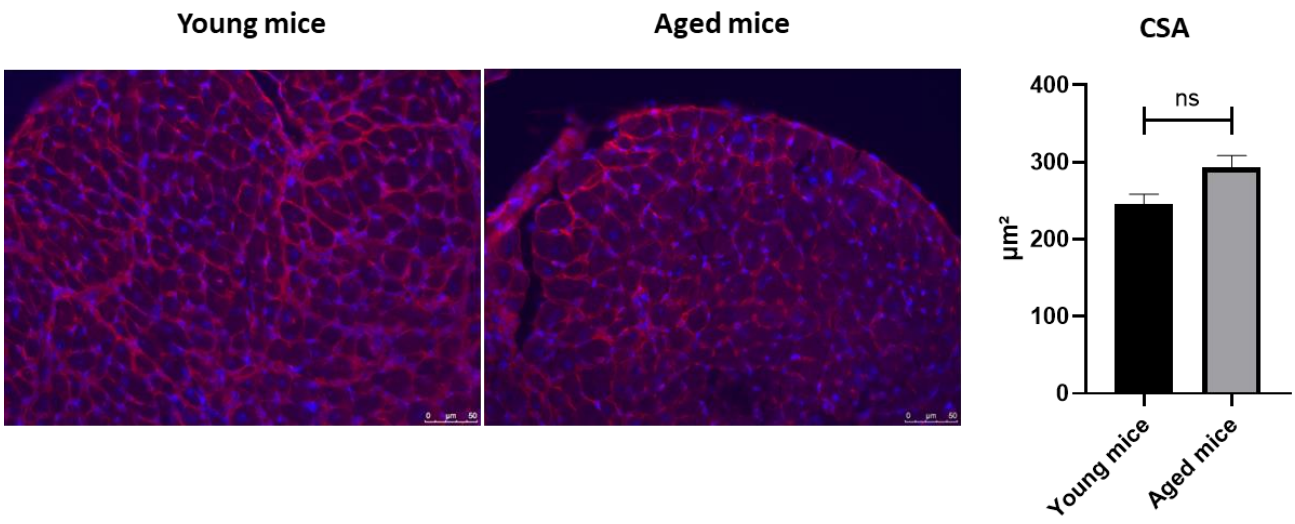

Fig. 37. Hypertrophy at cellular level and natriuretic peptide expression in young vs aged hearts.
A: Left ventricular cardiomyocyte cross sections stained with wheat germ agglutinin (WGA). Mean data for cross-sectional area (CSA) are shown. Data are presented as mean ± SEM between groups using unpaired Student's t-test, n=7/group. B**:** Cardiac mRNA levels of Nppa, natriuretic peptide type A and Nppb, natriuretic peptide type B were measured using RT-qPCR. Values are presented as fold change with respect to young mice. Gapdh was used for normalization. Data are presented as mean ± SEM. *p< 0.01 vs. between groups using unpaired Student's t-test, n=7-8/group.

2. Echocardiographic evaluation

2.1. Cardiac remodeling at 18-20 months

The comparison of septum thickness, LVEDD and subsequently, RWT did not show any signs of hypertrophy (concentric or eccentric) in old mice. However, left ventricular posterior wall dimension at diastole LVPW,d was slightly enhanced by 1.2 fold with respect to young controls ($p<0.05$, young n=10, aged n= 13) . This could suggest the beginning stages of a concentric remodeling phase which has not yet lead to significant hypertrophy. The data is shown in **figure 38.**

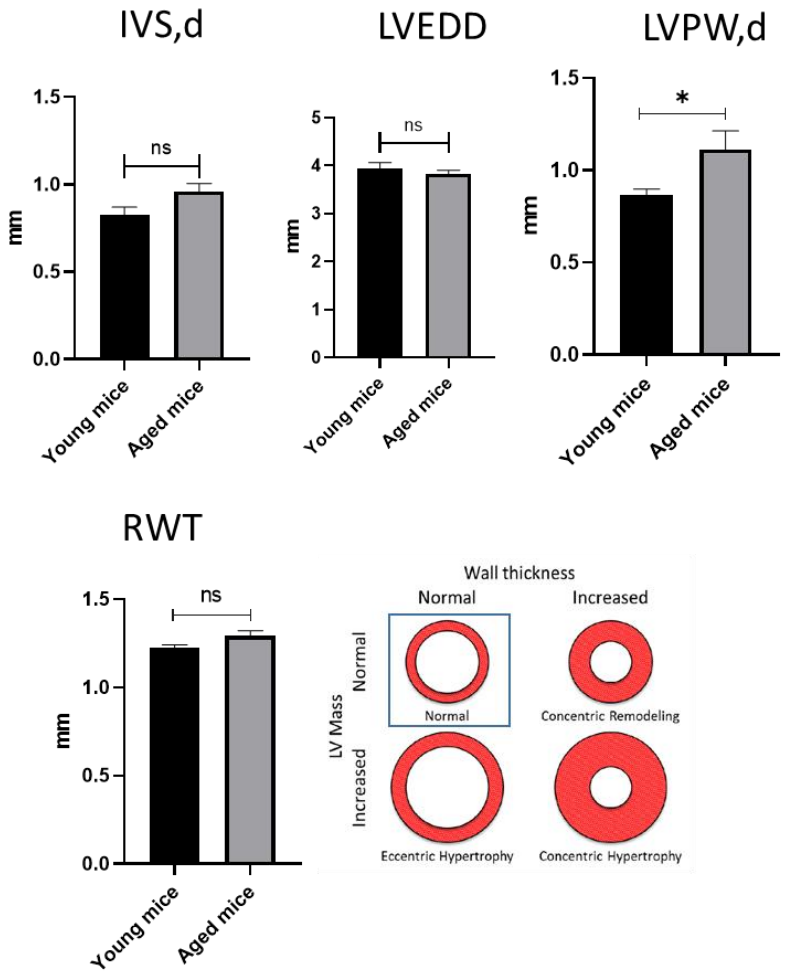

Fig. 38. Left ventricular hypertrophy in young versus aged mice.
Echocardiographic assessment of left ventricular remodeling. Interventricular septum thickness IVs ; LVEDD, Left ventricular end-diastolic diameter, LVPW,d, left ventricular posterior wall dimension at diastole and RWT, relative wall thickness. Data are presented as mean ± SEM. *p < 0.05 between respective groups using unpaired Student's t-test. n=10-13/group.

2.2. Systolic function at 18-20 months

Echocardiographic analysis revealed that EF was preserved (at similar heart rates) between young and aged mice averaging around 50-55%. At the age of 18-20 months, the mice still were in a preserved systolic function stage. However, other cardiac function parameter like SV, CO and FS were perturbed in old mice indicating some level of functional disturbance. SV was reduced by 19% ($p<0.01$), CO was 8.25% less ($p<0.05$) and FS was reduced by 18.5% ($p<0.001$) when compared to young controls (young n=7, aged n=13). The presence of dysregulated cardiac function parameters hints that these mice are undergoing aging related cardiac complications such as diastolic dysfunction even though systolic function remains preserved. This is shown in **figure 39.A-C.**

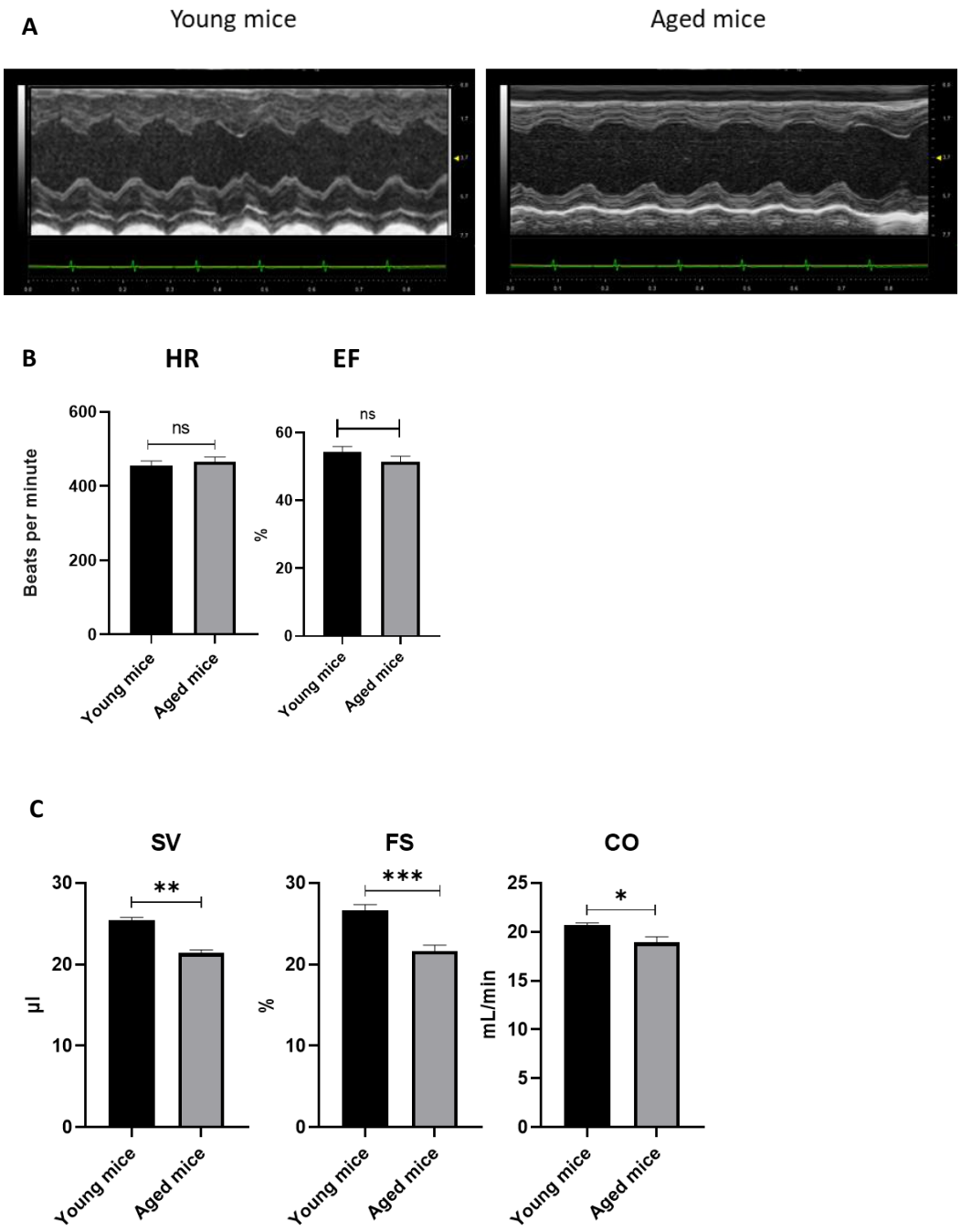

Fig. 39. Differential systolic function in young vs. aged mice.
A: Respective AM-mode images from echocardiography show a representation of LV function and geometry. B: Ejection fraction (EF) for comparable heart rates (HR) between the groups. C: Other perturbed heart function parameters SV, stroke volume; FS, fractionation shortening; CO, cardiac output. **p<0.01,***p<0.001 Data are expressed as mean ± SEM. between corresponding group using unpaired Student's t-test. n=10-13/group.

2.3. Strain echo for evidence of diastolic dysfunction in aging

Strain analysis through speckle tracking was similarly applied as the previous model to look at diastolic dysfunction in detail. r-LSR was significantly decreased by 24% in the aging group (p<0.05, young n=6,

aged n=7) as shown in **figure 40**. This shows further evidence of diastolic dysfunction despite preserved systolic function in old mice.

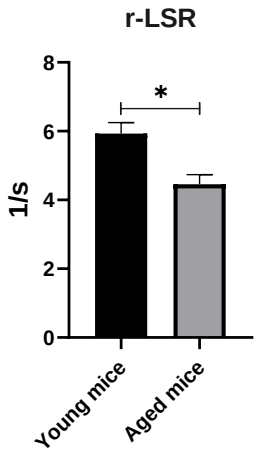

Fig. 40. Reverse-Longitudinal strain rate (r—LSR) in young vs aged mice.
Data are expressed as mean ± SEM. *p <0.05 vs. corresponding group using unpaired Student's t-test, n=6-7/group.

3.Pressure volume loop analysis of aging mice

Similar to the analysis of the previous model, ventricular catheterization was done on aged and young mice prior to organ harvesting to ascertain systolic and diastolic function in a broader detail. in accordance with echo data, we found that systolic function parameters of ESPVR, dp/dt_{max} and PRSW were unchanged in the old mice when compared to younger controls showing a clear preservation of systolic function($p>0.05$, n=4-5/group) as shown in **figure 41**.

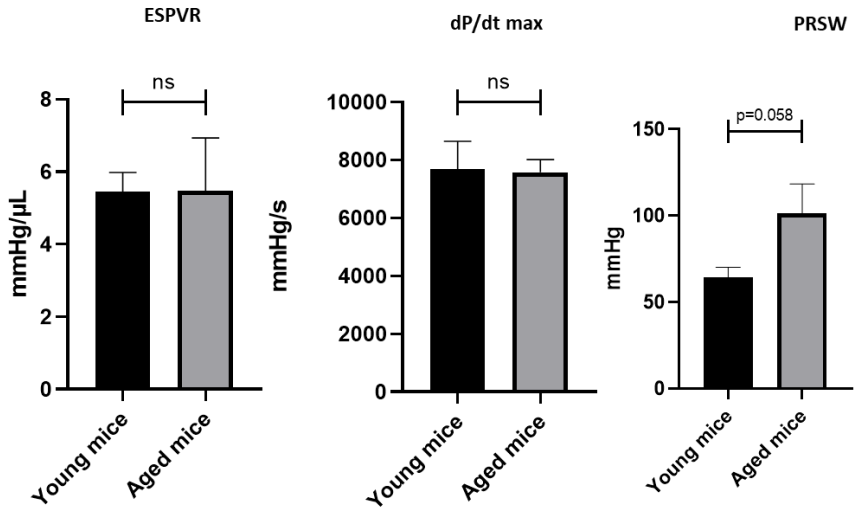

Fig. 41. Systolic LV function in young vs aged mice.
ESPVR: End systolic pressure volume relationship, dp/dtmax: maximal rate of pressure fall with time, PRSW: Preload recruitable stroke work. Data are expressed as mean ± SEM. vs. corresponding group using unpaired Student's t-test, n=4-5/group.

Upon analyzing the diastolic parameters, it was found that all diastolic function markers were perturbed in the aged mice group (**figure 42)**. EDPVR was significantly different and enhanced by 31% indicating clear impairment in relaxation consistent with higher LV stiffness and ventricular filling defects ($p<0.05$ n=4-5/group). The isovolumic relaxation constant- Tau and EDP were also relatively increased in aged mice by 25.6% ($p<0.01$) and 46% respectively ($p<0.05$). Last but not the least, dp/dt_{min} was similarly increased in naturally aged mice by 15.1% ($p<0.05$). Representing PV loops are shown in **figure 43.**

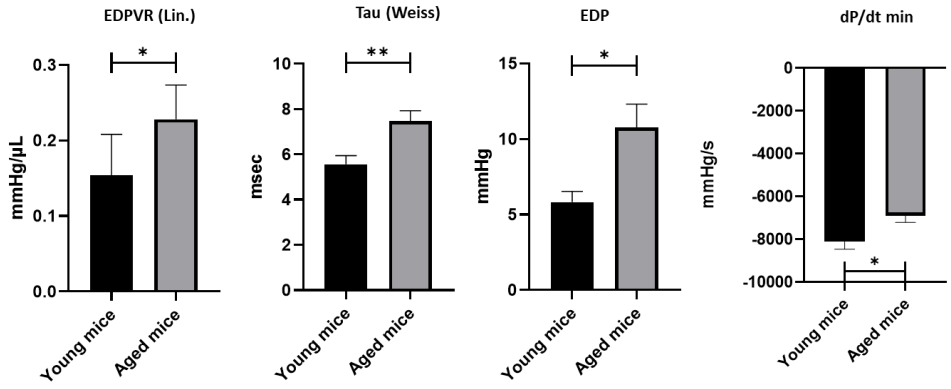

Fig. 42. Diastolic LV function in HFD vs ND mice at the end of two weeks of low grade PO.
EDPVR: End diastolic pressure volume relationship, Tau: time constant of isovolumetric relaxation, EDP: end diastolic pressure, dp/dtmin: minimal rate of pressure fall with time. Data are expressed as mean ± SEM. *p <0.05, **p<0.05, *** vs. corresponding group using one-way unpaired Student's t-test, n=4-5/group.

Young BL6/J 7-9 months

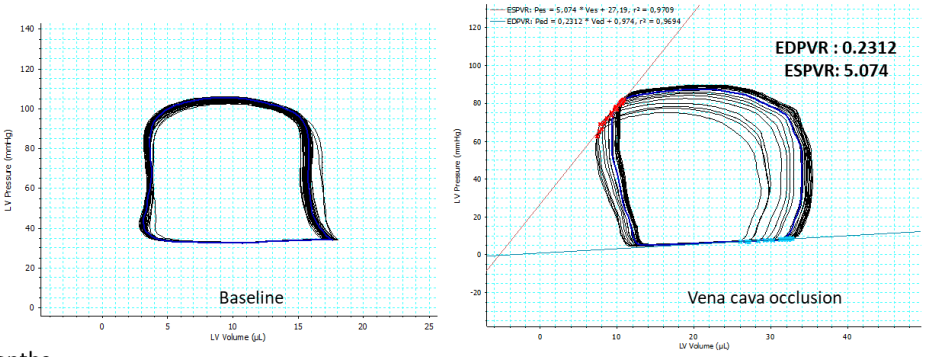

Aged BL6/J 20 months

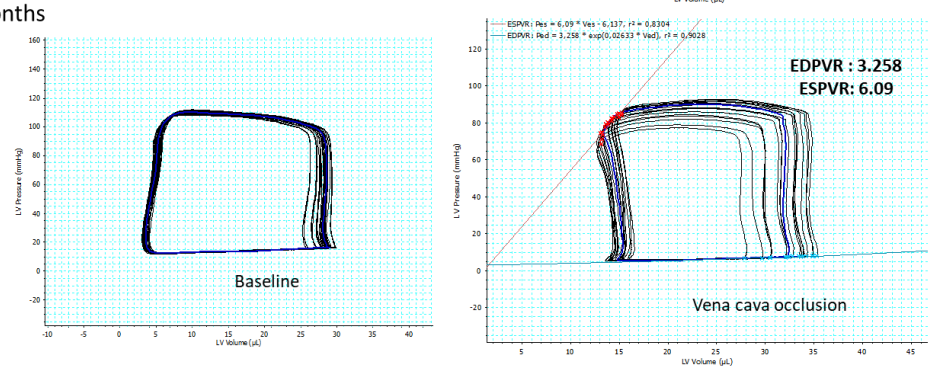

Fig. 43. Representative PV loops of young mice vs. aged mice.
Sham vs TAC comparison of HFD cohort at baseline and vena cava occlusion to account for preload. Note the changes in ESPVR and EDPVR values.

4. Cardiac stress markers in aged mice

Myocardial gene expression was also investigated in naturally aged mice using RT-qPCR. An activation of the fetal gene program where common stress markers are upregulated was seen in senescence. The analysis of natriuretic peptides showed that the levels of BNP were 1.9 fold higher in aged mice ($p<0.05$, young n= 5-6/group) and not ANP when being compared with young controls. mRNA levels of Acta1 a known marker of compensated cardiac hypertrophy was unchanged which is consistent with the absence of hypertrophy but, Serca2-α showed a marked decrease in aged mice to 0.2 fold of the value of young mice($p<0.01$, n=5-6/group). In aged mice, isoform shift from α-myosin heavy chain to β-myosin heavy chain was also significantly observed which was up to 21 fold of basal levels in young mice ($p<0.01$, n=5-6/group). this data is shown in **figure 44.**

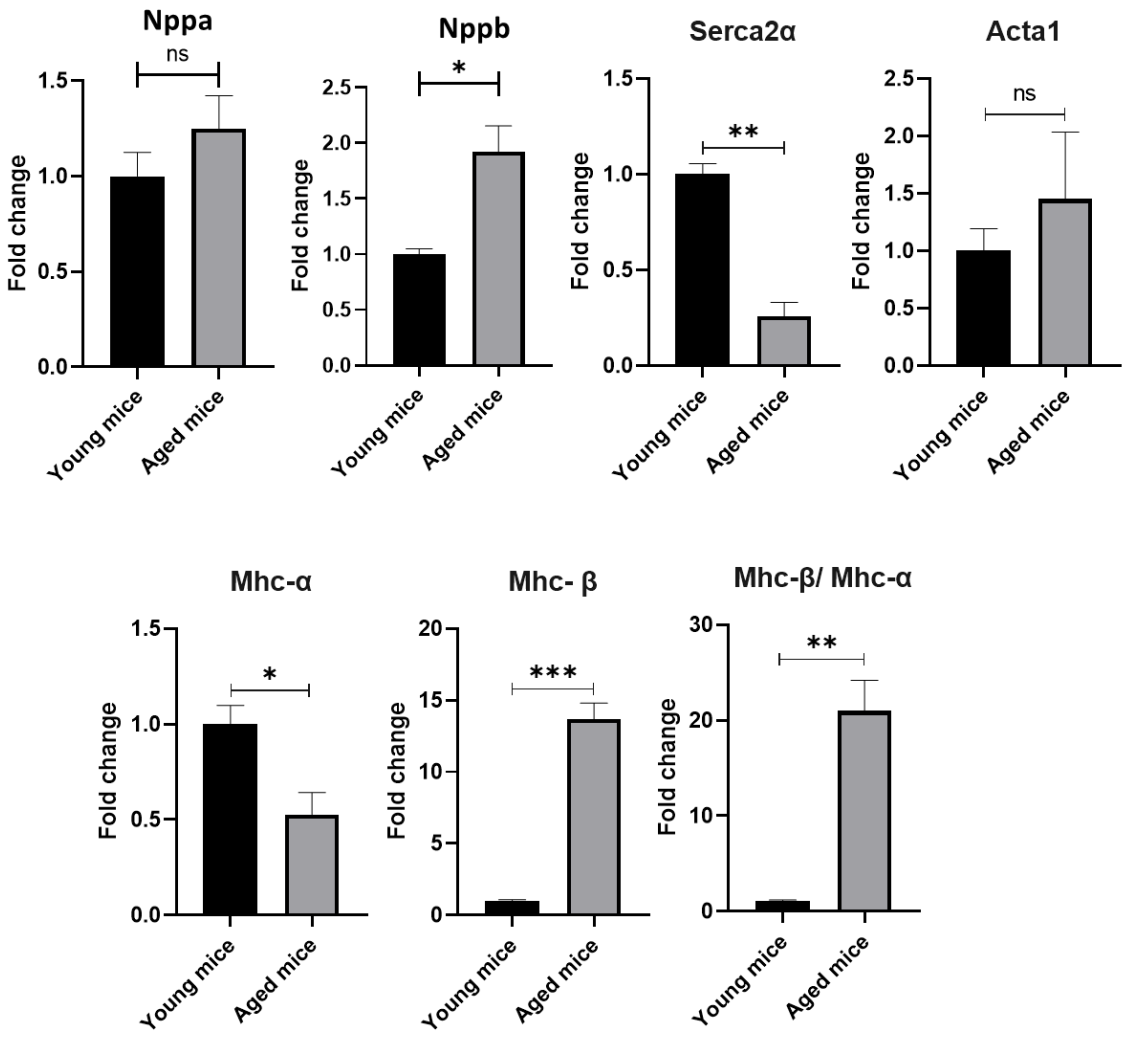

Fig. 44. Cardiac gene expression of stress markers in young and aged mice.
Cardiac mRNA levels of Nppa, Natriuretic peptide A; Nppb, Natriuretic peptide B; Serca2-α, Sarcoplasmic/Endoplasmic Reticulum Calcium ATPase-2α; Acta, α-skeletal actin; Mhc-α, myosin heavy chain-α; Mhc-β, myosin heavy chain-β and Mhc-β/ Mhc-α ratio were measured using RT-qPCR. Values are presented as fold change normalized to young controls. Gapdh was used for normalization. Data are presented as mean ± SEM. *p<0.05, **p < 0.01, ***p<0.001 vs. corresponding groups using unpaired Student's t-test, n=5-6/group.

5. Steatosis in age related HFpEF

We analyzed if natural cardiac aging is also associated with any defects in lipid dynamics in the myocardium (independent of diet). Though some amount of lipid accumulation was evident in aged sections however, we found no significant differences due to high sample inter-variability. Neutral lipid droplets were not significantly larger in size and number as younger controls, as illustrated in **figure 45**.

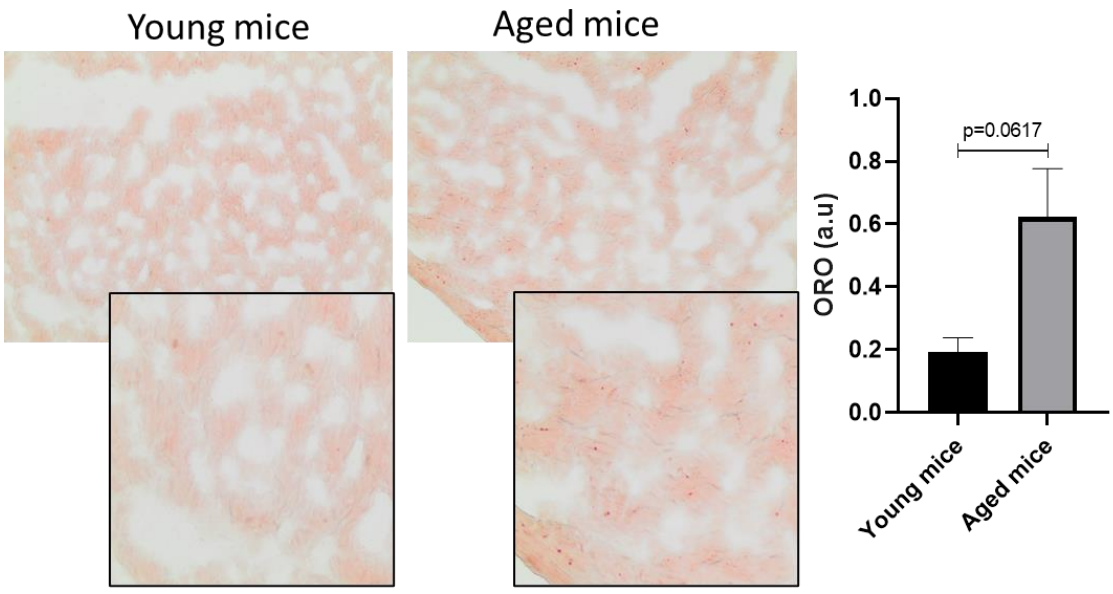

Fig. 45. Lipid accumulation in young vs aged mice.
Oil red O stained cryosections show lipid deposits (as dark pink granules) at 20X magnification. Inlets show five times magnified image to emphasize the staining. Data are presented as mean ± SEM vs. corresponding groups using unpaired Student's t-test, a.u: arbitrary units, n=4/group in duplicates.

6. Fibrosis in aging related HFpEF

6.1. Interstitial and perivascular fibrosis in aging mice

Analysis of total and perivascular fibrosis area with respect to younger mice revealed a marked increase of pro-fibrotic tissue in senescent mice. While interstitial fibrosis was increased by 4 fold ($p<0.001$, n=6-7/group), perivascular fibrosis was similarly up by 4.4 fold ($p<0.001$) as depicted in **figure 46.A and B**.

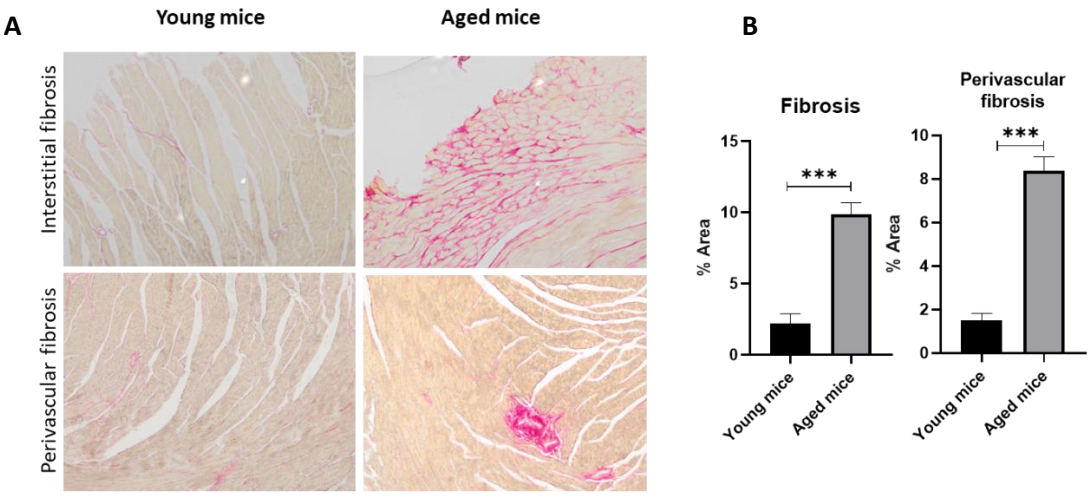

Fig. 46. Left ventricular fibrosis in young vs aged mice.
A: Representative histological images of cardiac sections stained with picrosirius red staining to measure fibrotic regions (pink), scale bar = 200 µm. B: Quantification of fibrosis percentage area as mean data for the fibrotic area relative to the total left ventricular section and quantification of fibrosis only around perivascular regions. Data are presented as mean ± SEM, ***p < 0.001 between groups using unpaired Student's t-test, n=6-7/group.

6.2. Collagen isotypes in aging based HFpEF

In contrast to the dyslipidemic model, no particular dominant isotype was selectively upregulated in aged mice. Col I and Col III showed an increase in expression when compared with younger controls as shown in **figure 47**. Col I was 4.3 fold higher ($p<0.01$) while Col III was 2.4 fold higher ($p<0.05$). Fn-1 was 3.8 fold high ($p<0.01$) in young vs old mice (n=6-7/group).

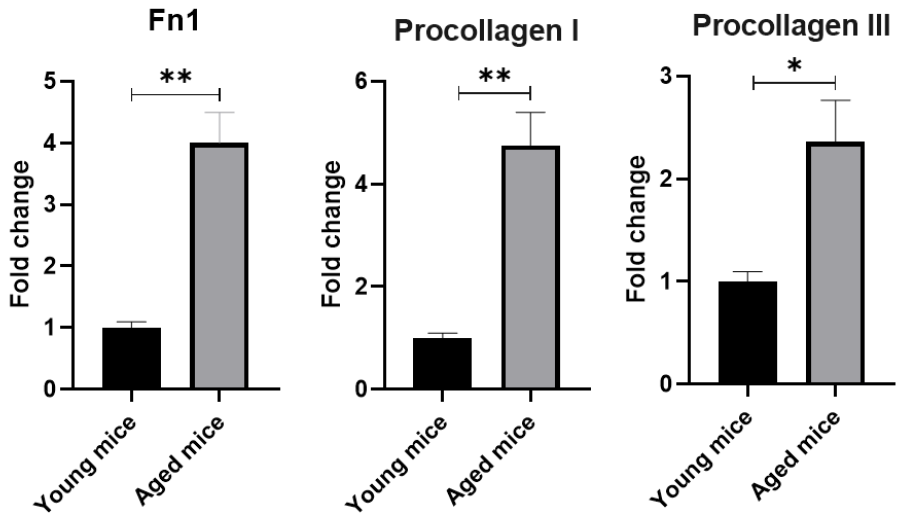

Fig. 47. Cardiac gene expression of pro-fibrotic markers in young and aged mice.
Cardiac mRNA levels of FN-1, Fibronectin-1; Procollagen I and Procollagen III were measured using RT-qPCR. Values are presented as fold change normalized to young controls. Gapdh was used for normalization. Data are presented as mean ± SEM. *p<0.05, **p < 0.01 between corresponding groups using unpaired Student's t-test, n=6-7/group.

7. Inflammatory mechanisms and endothelial dysfunction in aging based HFpEF

7.1. Expression of common inflammatory cytokines in young vs aged mice

Consistent with other studies we found 18-20 months old senescent mice differed significantly in their inflammatory cytokine profile. All cytokines except IFN-γ were highly upregulated with respect to younger controls as shown in **figure 48**. TGF-β ($p<0.001$, n=7/group) and TNF-α were upregulated by 3.8 fold and 2 fold ($p<0.05$, n=7/group) respectively. IFN-γ however, showed no change between the two groups. IL-1β and IL-6 also exhibited a 4.5 fold ($p<0.01$) and 2.9 fold ($p<0.05$) enhanced expression respectively. The pattern of cytokine upregulation is distinct from those described by dyslipidemic HFpEF and HFrEF.

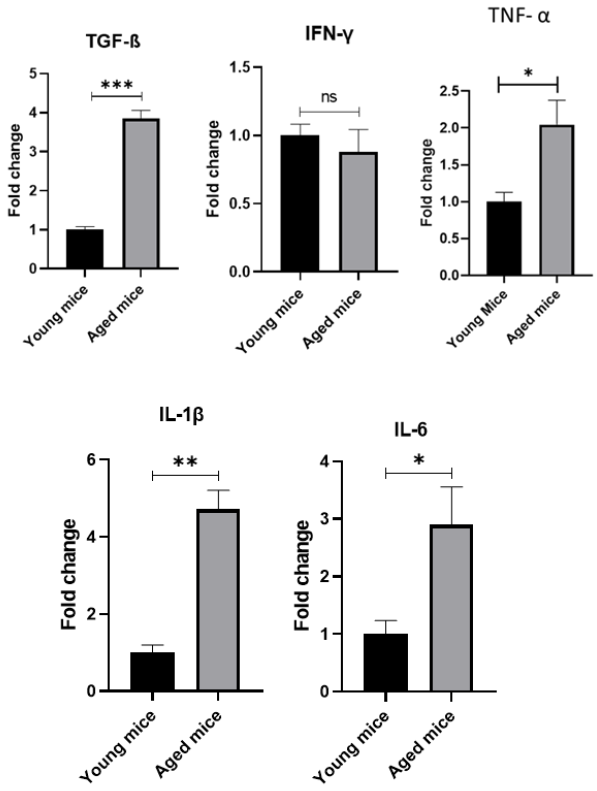

Fig. 48. Cardiac gene expression of pro-inflammatory markers in young vs aged mice.
Cardiac mRNA levels of TGF-β, transforming growth factor β; IFN-γ, interferon γ ; TNF-α, tumor necrosis factor α; IL-1β interleukin 1 beta and IL-6 interleukin 6 were measured using RT-qPCR. Values are presented as fold change normalized to young controls. Gapdh was used for normalization. Data are presented as mean ± SEM. *p<0.05, ***p < 0.001 vs. corresponding groups using unpaired Student's t-test, n=7/group.

7.2. Endothelial dysfunction in aging based HFpEF

Upon investigation of common endothelial dysfunction markers, they were obviously found to be highly upregulated in aging mice. Interestingly, the pattern of upregulated cytokines was quite similar to dyslipidemic HFpEF described in section 8.2 of results 1, with an 8 fold increase in Vcam-1 expression (p<0.001, n=7/group) and 15 fold upregulation in Icam-1(p<0.05, n=7/group). On the other hand, endothelin-1 expression was unchanged in the two groups as shown in **figure 49**.

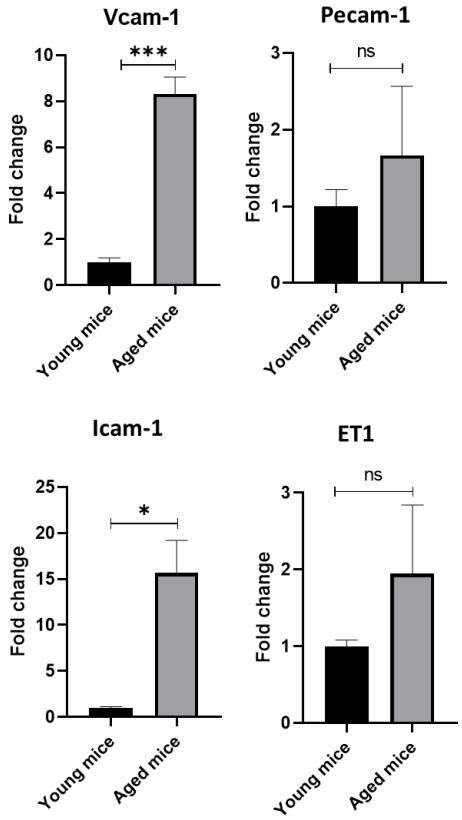

Fig. 49. Cardiac gene expression of pro- endothelial dysfunction markers in young vs aged mice.
A: Cardiac mRNA levels of CAMs, cell adhesion molecules namely vascular (VCAM-1), intracellular (ICAM-1) platelet endothelial (PECAM-1) and ET-1, endothelin 1 were measured using RT-qPCR. Values are presented as fold change normalized to young controls. Gapdh was used for normalization. Data are presented as mean ± SEM. *p<0.05, **p < 0.01, ***p<0.001 vs. corresponding groups using unpaired Student's t-test, n=7/group.

7.3. NOX2 expression is not upregulated on aging

Levels of Nox2 were found to be unchanged when compared with younger controls. NOX2 has been implicated in metabolic complications associated with aging (Fan et al., 2017). It is also known to induce oxidative damage effects on the endothelium but we see a disparity in Nox2 upregulation between the two models as depicted in **figure 50**.

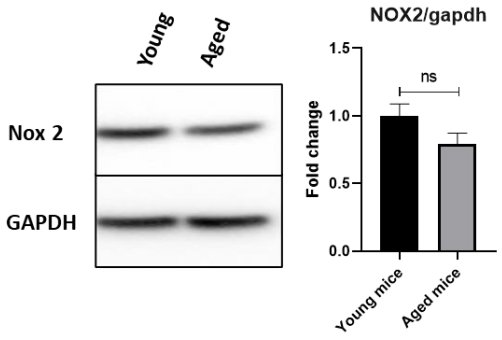

Fig. 50. Expression of NADPH oxidase (Nox-2).
Western blot images for Nox-2 and GAPDH from LV lysates are shown. Values are presented as fold change normalized to young controls. Data are presented as mean ± SEM between respective groups using one unpaired Student's t-test, n=6-7/group.

7.4. HDAC-4 phosphorylation is not present in aged mice

Immunoblot assays revealed no significant difference between the levels of phosphorylation of HDAC-4 when compared with young controls as shown in **figure 51**. This is again in contrast to the findings from HFD sham vs TAC comparisons, hinting that HDAC-4 may be essential in implicating hypertrophic effects exclusively leading to diastolic dysfunction driven by dyslipidemia.

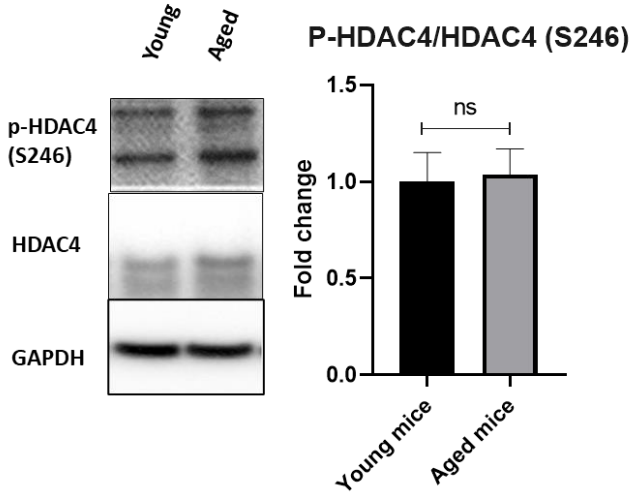

Fig. 51. Phosphorylation of HDAC-4 in young vs aged hearts.
Western blot images for 77hosphor-HDAC-4 (Ser246) (p-HDAC-4), total HDAC-4, and GAPDH from LV lysates are shown. Values are presented as fold change normalized to young controls. Data are presented as mean ± SEM using Student's t-test, n=6-7/group.

7.5. CD45 mediated inflammation is highly prevalent in aging

Previous studies have shown an age associated increase in $CD45^+$ leukocytes in aged human hearts (Trial et al., 2017) and play an important role in ROS driven signaling mechanism from fibroblast activation. The data from aged mice further corroborated this with an 85% percent increase in CD45 positive cells ($p<0.01$, n=5/group) as shown in **figure 52**.

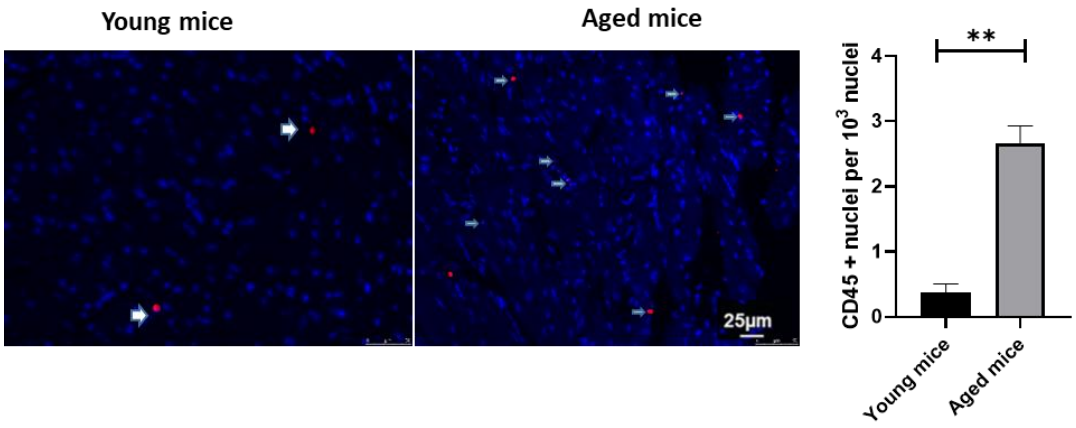

Fig. 52. CD45 levels in young and aged mice.
LV sections were stained with primary antibody against CD45 antigen and then incubated with fluorophore conjugated secondary antibody (red). Counterstaining with DAPI was done to visualize individual nuclei (blue) at 20X magnification, number of CD45 positive nuclei were measure / 1000 nuclei. Data are presented as mean ± SEM. **p<0.01 vs. corresponding groups using unpaired Student's t-test, n=5/group.

8. Apoptosis age related HFpEF

In line with previous studies we also found that senescent mice had highly active programmed cell death (3.6 fold higher, $p<0.01$, n=6/group) when compared to younger controls (**figure 53**). The level was much higher than HFrEF (2.5 fold) as mentioned in section 9 of results 1.

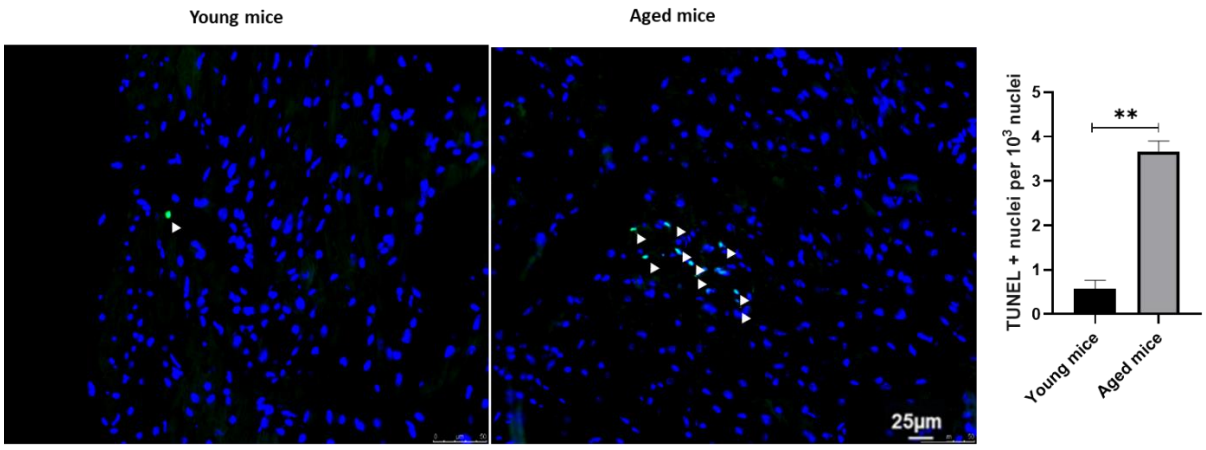

Fig. 53. LV apoptosis in young and aged mice.
TdT-mediated dUTP-biotin nick end-labelling (TUNEL) staining of LV sections and white arrows indicate TUNEL-positive cardiomyocytes (scale bar = 25 µm) and subsequent quantification of TUNEL-positive cells per 1000 DAPI-positive nuclei. Data are presented as mean ± SEM. **p < 0.01 vs. corresponding groups using two unpaired Student's t-test, n=6/group.

9. Cardiac kinases in aging related HFpEF

Cardiac kinases were shown to be differentially regulated in dyslipidemic HFpEF vs HFrEF as described in section 10 of results 1. We further wanted to see which of these cardiac kinases are active in senescent mice. It was found that Akt was not significantly phosphorylated in aged vs young mice as shown in **figure 54. A,** which is contrast to what was seen in HFD-TAC vs sham mice groups (p>0.05, n=6-7/group). However, the level of phosphorylation (MAPK) and its downstream effectors ERK1/2, p38 kinases and c-Jun N-terminal kinases (JNK) at their relevant phosphorylation sites showed significant differences. Erk phosphorylation at T202/Y204 was doubled in aged mice (p<0.05, n=6-7/group). p38 phosphorylation at Threonine180/Tyrosine182 was also two fold higher in aged mice (p<0.05, n=6-7/group). JNK another downstream effector was 2.5 fold more phosphorylated at Threonine183/Tyrosine185 in the aged cohort (p<0.01, n=7/group) as shown in **figure 54.B**.

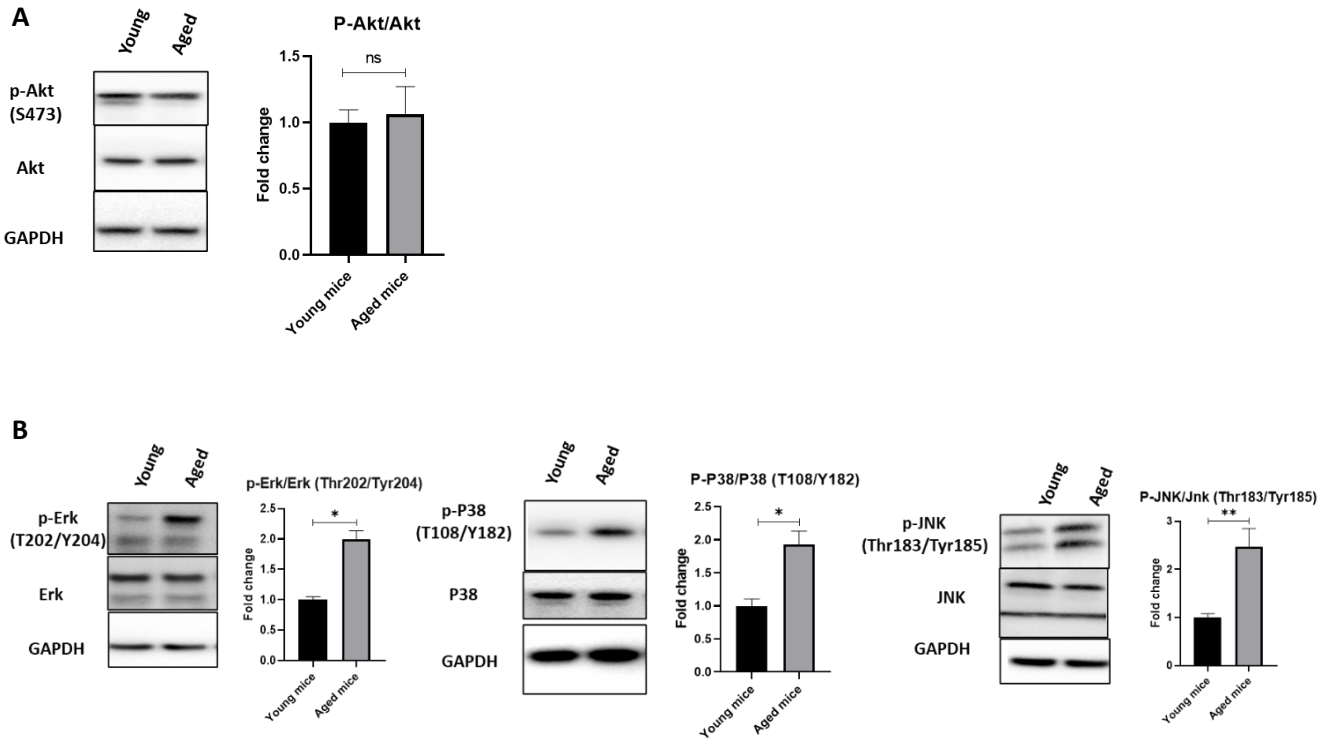

Fig. 54. Phosphorylation of cardiac Akt and assessment of cardiac MAPK activation levels in young vs aged mice.

A: Representative Western blot images for phospho-Akt (Ser473) (p-Akt), total Akt, and GAPDH from LV lysates are shown alongside quantification of phosphorylated Akt to total Akt abundance. B: Representative blots of phosphorylation levels of ERK1/2 (at TEY motif) and p38 (at Threonine180/Tyrosine182) with GAPDH as a loading control. Values are presented as fold change normalized to corresponding young controls. Data are presented as mean ± SEM between corresponding groups using unpaired Student's t-test, n=6-7/group.

10. Calcium handling in aged heart

Looking at the proteins involved in calcium handling, level of CaMKII phosphorylation was significantly enhanced in aged mice by almost three fold ($p<0.01$, n=7/group) which is again in contrast to what was seen in the previous model in section 11 of results 1. This data is shown in **figure 55.**

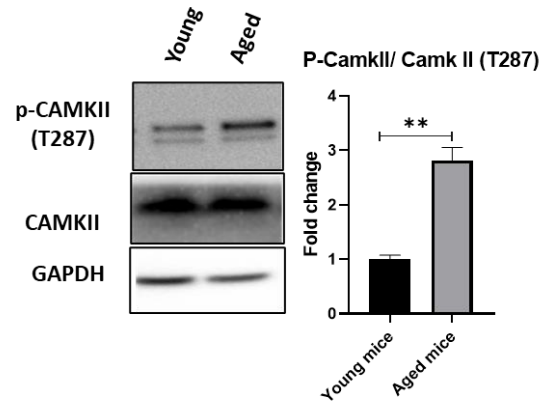

Fig. 55. Activity of CaMKII in young vs aged mice.
Cardiac protein levels of phosphorylated CaMKII beta/gamma/delta (Thr287) were assessed by immunoblotting vs. CaMKII delta (CaMKII δ), the major CaMKII isoform expressed in the heart, GAPDH was loading control. Quantification of p-CaMKII abundance to CaMKIIδ/GAPDH is shown alongside. Values are presented as fold change normalized to young controls. Data are presented as mean ± SEM using unpaired Student's t-test, n=7/group.

Also, in contrast to HFD model, RyR2 appeared to be significantly highly phosphorylated at both Ser2814 by 2.7 fold ($p<0.01$, n=6-7/group) and Ser2804 by 2.5 fold ($p<0.01$, n=6-7/group). PLN phosphorylation reflected a similar pattern as RyR2 phosphorylation with increased levels at both Thr17 and Ser16 in aged mice by 2.5 fold ($p<0.01$) and 1.7 fold ($p<0.01$) respectively as shown in **figures 56.A-D.**

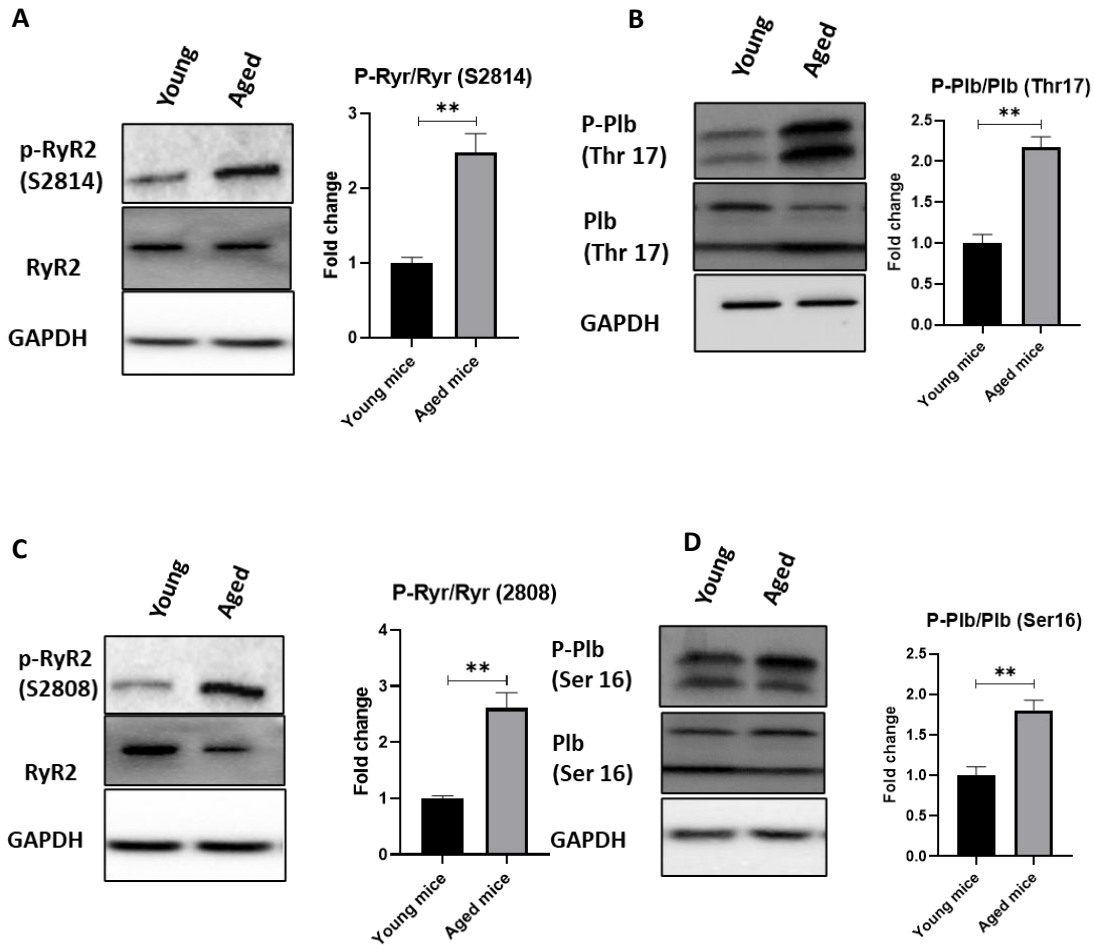

Fig. 56. Immunoblot assessment of CaMKII dependent and PKA dependent phosphorylation sites of ryanodine receptors and phospholamban in young vs aged mice.
A: Cardiac protein levels of A: Serine 2814-phosphorylated ryanodine (p-RyR2 Ser 2814), and for B: threonine 17- phosphorylated phospholamban (p-PLN Th17) were assessed, GAPDH used as loading control. C: Serine 2808-phosphorylated ryanodine (p-RyR2 Ser 2808), and for D: threonine 16- phosphorylated phospholamban (p-PLN Th16) were assessed and GAPDH used as loading control. Densitometric quantification of phosphorylated proteins to total protein are shown alongside. Values are presented as fold change normalized to young controls. Data are presented as mean ± SEM. **p < 0.01 between groups using unpaired Student's t-test, n=6-7/group.

Furthermore, phosphorylation levels of cTnI at the Ser22/23 was again unchanged in aged mice which is similar to what was observed in dyslipidemic HFpEF. In conclusion, except for CTnI, all calcium handling parameters showed a differential regulation in aging when compared with the profiles in dyslipidemia induced HFpEF (**figure 57**).

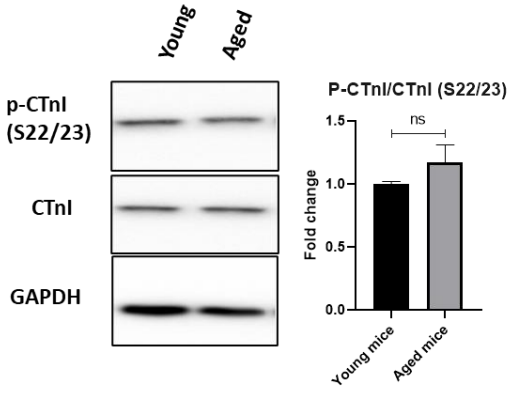

Fig. 57. Immunoblot assessment of Troponin I in young vs aged mice.
Cardiac protein levels of Phosphorylation of cardiac troponin, p-CTnI at Ser22/23 with respect to total cardiac troponin, CTnI. Densitometric quantifications are shown alongside. GAPDH was used as loading control. Values are presented as fold change normalized to young controls. Data are presented as mean ± SEM between groups using unpaired Student's t-test, n=6-7/group.

Results 3: Transcriptomics of different models of HFpEF

The two ''index events'' led to a distinct presentation of HFpEF phenotype in separate mouse models. Sections 1 and 2 deal with these differences in major cardiac structure and function parameters. Overall, dyslipidemia+ low grade pressure overload gave rise to an overall hypertrophic, highly inflammatory, steatotic, apoptotic phenotype with calcium kinetics dysfunction. In contrast, aging induced HFpEF exhibited a non-hypertrophic, non-steatotic, apoptotic phenotype with stark differences in calcium signaling. However, to get a broader understanding of these differences it was necessary to look at the differential regulation of key genes in each group. mRNA sequencing was performed on RNA extracted from snap frozen LV sections. First, the clustering of different experimental groups was analyzed where a total of 15870 variables were tested in 4 mice/group. One outlier from aging group was removed subsequently. The following plot in **figure 58** shows the clustering of cohorts where group A is ND-Sham, group B: ND-TAC, group C: aged mice, group D: HFD-Sham and group E: HFD-TAC. The two dietary group clustered in different regions with distinct demarcation between sham and TAC operated mice. Interestingly, aged mice tended to cluster along with HFD-TAC which proves yet again the shared ''HFpEF like'' phenotype despite different driving factors.

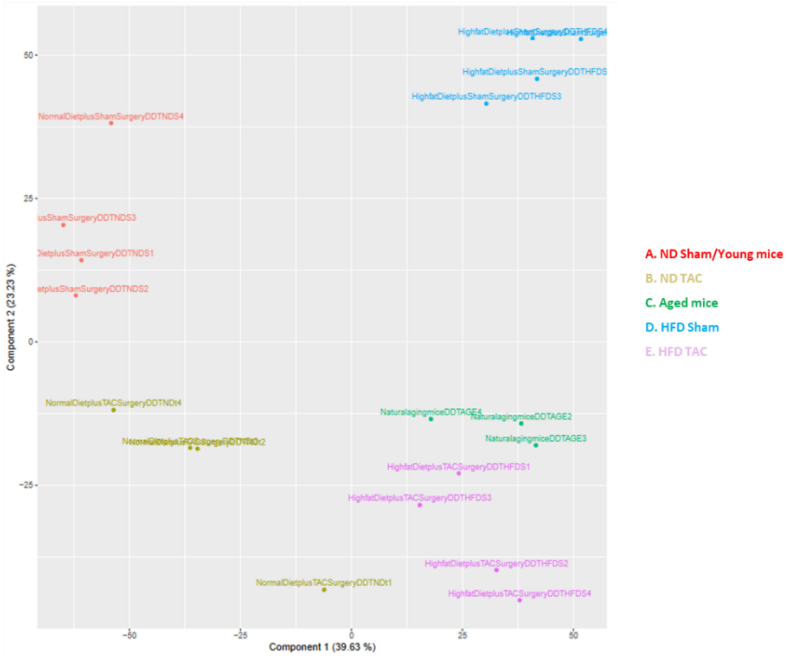

Fig. 58. Principle component analysis (PCA).
PCA plot of the experimental groups based on all mRNAs sequenced using Illumina HiSeq4000 next generation sequencing. A total of 15870 variables were analyzed and compressed into two components plotted against each other, n=4/group (except aged mice where one outlier was removed).

Subsequently, the differentially expressed genes (DEGs) were analyzed. Between **ND sham vs TAC** reflecting the HFrEF phenotype, 2289 DEGs were found (padj<0.05, log2FC±0.5). A volcano scatter between log2foldchange and -logFDR was plotted, a cutoff at -logFDR=2 shows genes that are statistically significant, the most highly significant genes were labelled (**figure 59)**. Kyoto encyclopedia of genes and genomes (KEGG) pathway analysis of deregulated genes showed an enrichment in TNF signaling pathway, dilated/hypertrophic cardiomyopathy, IL-17 signaling, ECM receptor interaction, cytokine/chemokine interaction and PI3-Akt signaling to name a few all with a false discovery rate (FDR) of ≤ 0.05. Gene ontology (GO) term analysis revealed that extracellular matrix, inflammation, leukocyte recruitment and cytokine/chemokine process related genes were highly enriched (FDR≤0.05) as shown in **figure 60**.

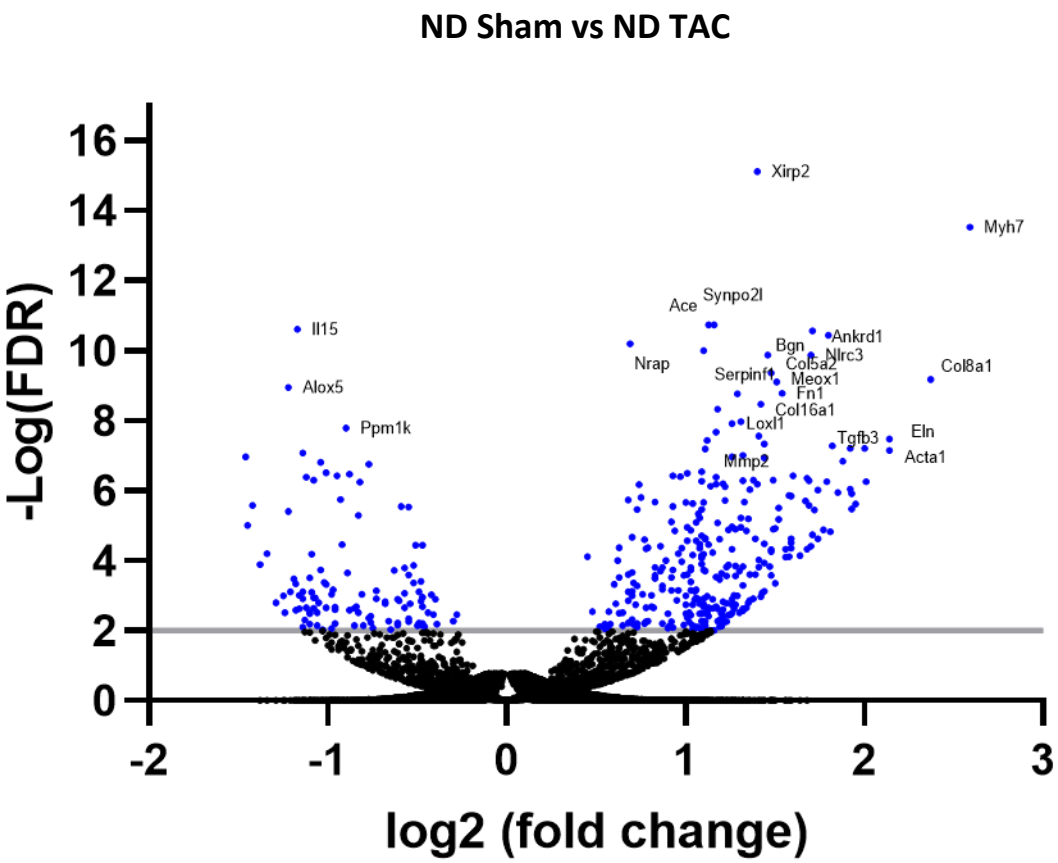

Fig. 59. Volcano plot of differentially regulated mRNAs in ND-Sham vs ND-TAC.
The X-axis represents the log2 fold change $^{\text{ratio (ND-Sham/ND-TAC)}}$ plotted against its significance level -log(false discovery rate-FDR). The cut off of -log(FDR)=2 at the y-axis corresponds to statistically significant deregulation. Left side represents downregulated genes and right side shows the upregulated genes in ND-sham as compared to ND-TAC. Some genes of highest significance are labelled.

ND Sham vs ND TAC

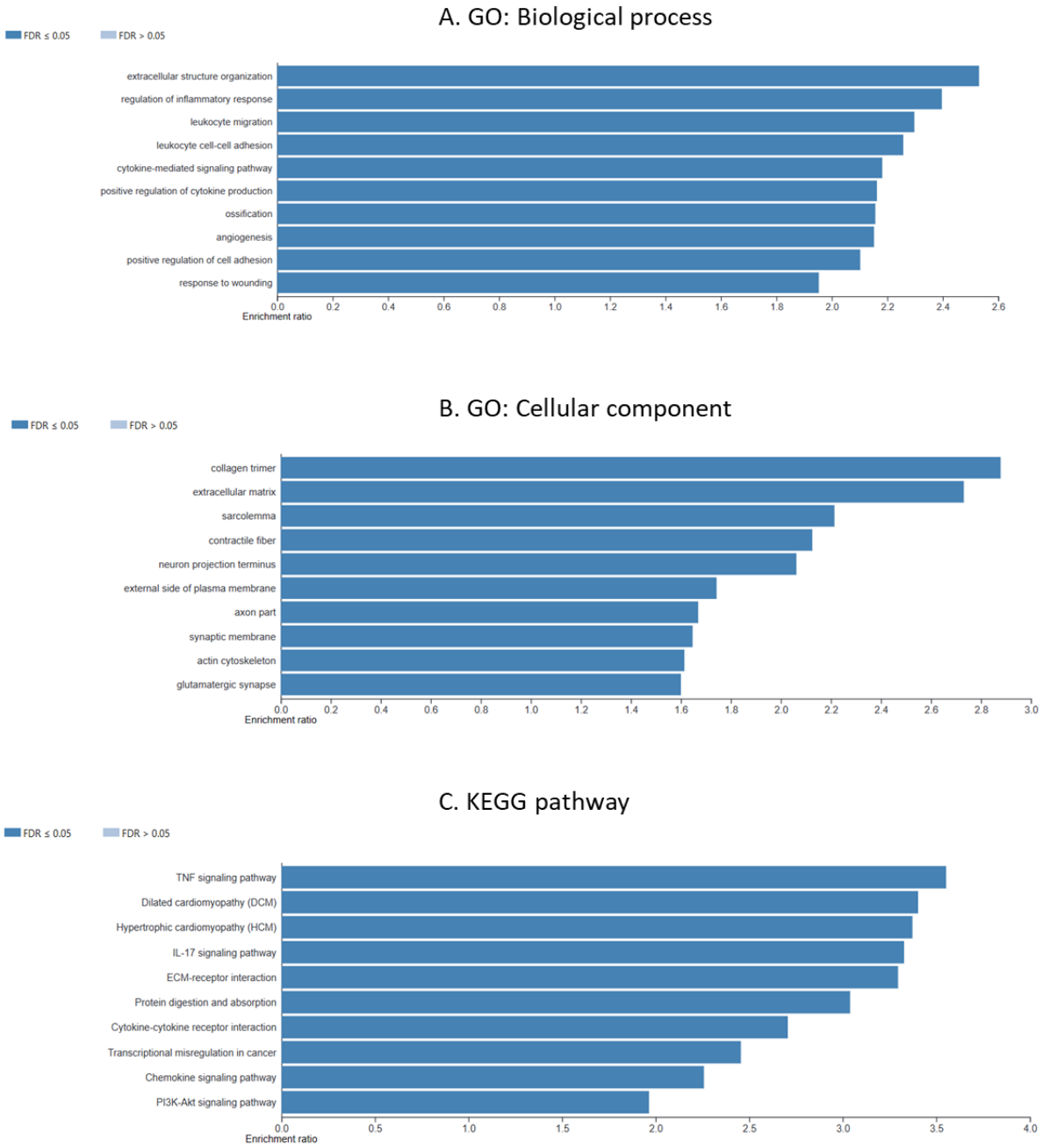

Fig. 60. Significantly over represented gene ontology terms and KEGG pathway analysis of DEGs between ND-Sham and ND—TAC.
Bar charts show the enriched GO terms in the category of biological process (A), cellular components (B)and the list of enriched KEGG pathways (C) for significantly deregulated genes. The numbers on the chart indicate the enrichment ratio. FDR<0.05. Enrichment analysis was done using the WebGestalt platform.

While in the **HFD sham vs TAC** comparisons which is reflective of the HFpEF phenotype, the DEGs represented a different set of genes. GO terms showed enrichment in response to cytokine, lipid, nitrogen and oxygen containing compounds amongst others as shown in **figure 60** (FDR≤0.05). KEGG pathways were enriched in genes associated with TNF-α, MAPK, PI3-Akt and IL-17 signaling pathways (FDR≤0.05). Notably, genes associated with diabetic complications due to Receptors of advanced glycation end products (AGE/RAGE) pathway also popped in the results, which has been highly associated with oxidative damage (**figure 62**). This further supports the 'meta inflammation' hypothesis of HFpEF.

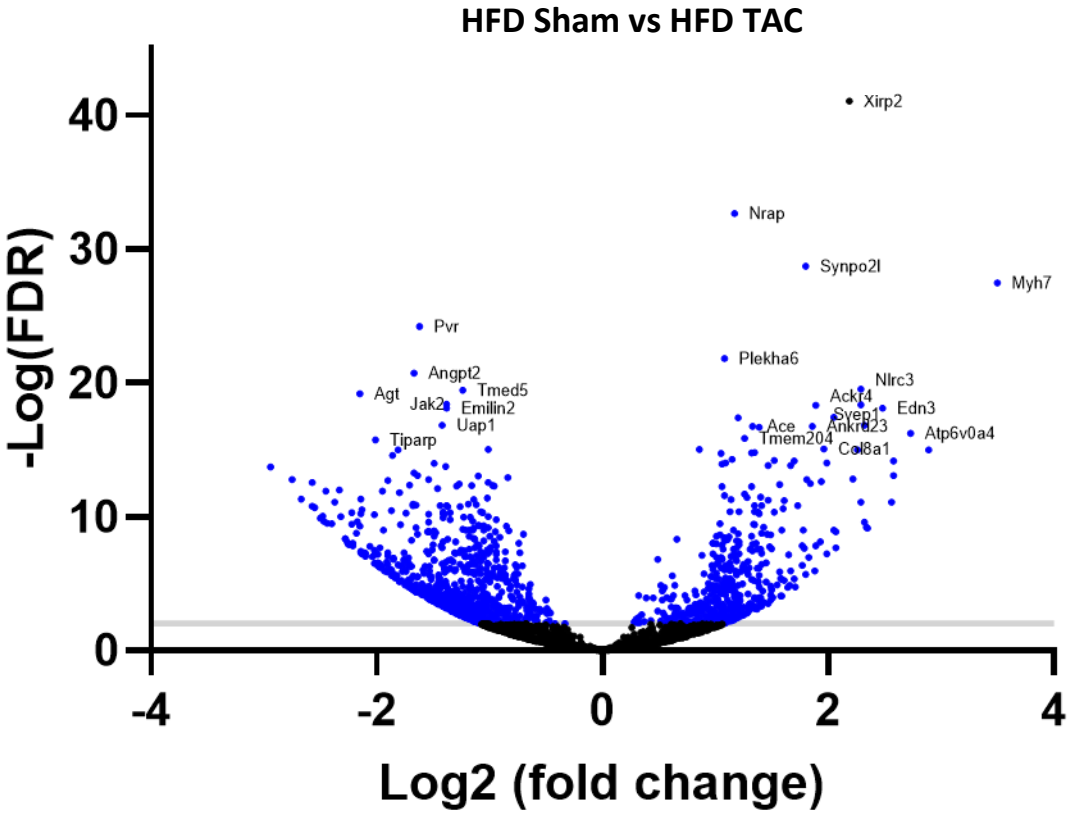

Fig. 61. Volcano plot of differentially regulated mRNAs in HFD-Sham vs HFD-TAC.
The X-axis represents the log2 fold change $^{\text{ratio (HFD-Sham/HFD-TAC)}}$ plotted against its significance level -log (false discovery rate-FDR). The cut off of -log (FDR)=2 at the y-axis corresponds to statistically significant deregulation. Left side represents downregulated genes and right side shows the upregulated genes in HFD-sham as compared to HFD-TAC. Some genes of highest significance are labelled.

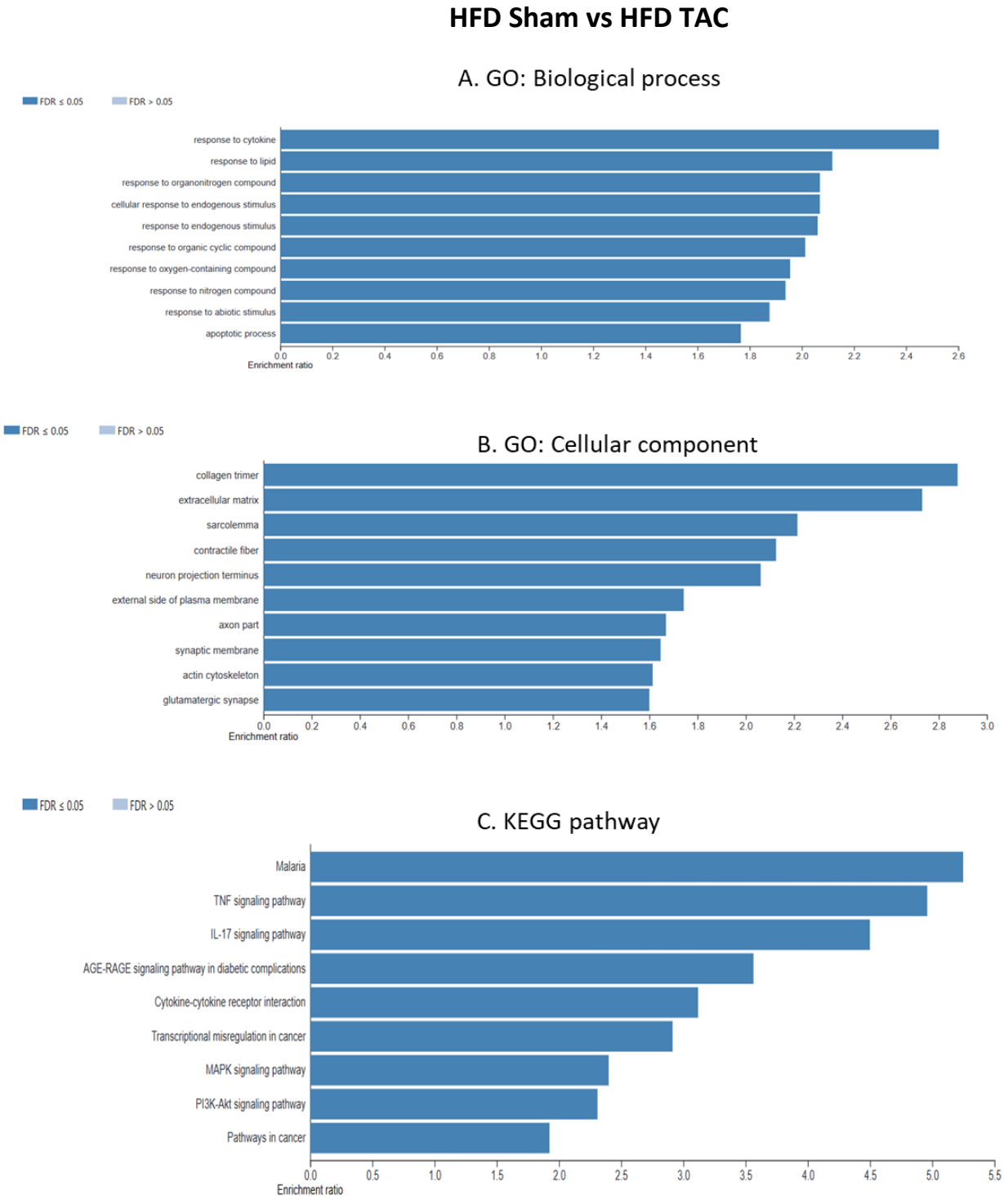

Fig. 62. Significantly over represented gene ontology terms and KEGG pathway analysis of DEGs between HFD-Sham and HFD—TAC.

Bar charts show the enriched GO terms in the category of biological process (A), cellular components (B)and the list of enriched KEGG pathways (C) for significantly deregulated genes. The numbers on the chart indicate the enrichment ratio. FDR<0.05. Enrichment analysis was done using the WebGestalt platform.

The comparison of the third cohort, **young vs aged mice** showing aging associated HFpEF, revealed yet another enriched cluster. While GO term analysis showed a similar trend of enrichment in leukocyte recruitment and inflammation associated process (FDR≤0.05), KEGG pathway analysis showed arrhythmogenic right ventricular cardiomyopathy (ARVC) as the most enriched (FDR≤0.05). This is in contrast to the dietary models. **Figure 63** shows a volcano plot of deregulated genes and subsequent enrichment analysis is shown in **figure 64**. **Figure 65** depicts the highly enriched pathway of ARVC and the genes within it that were deregulated.

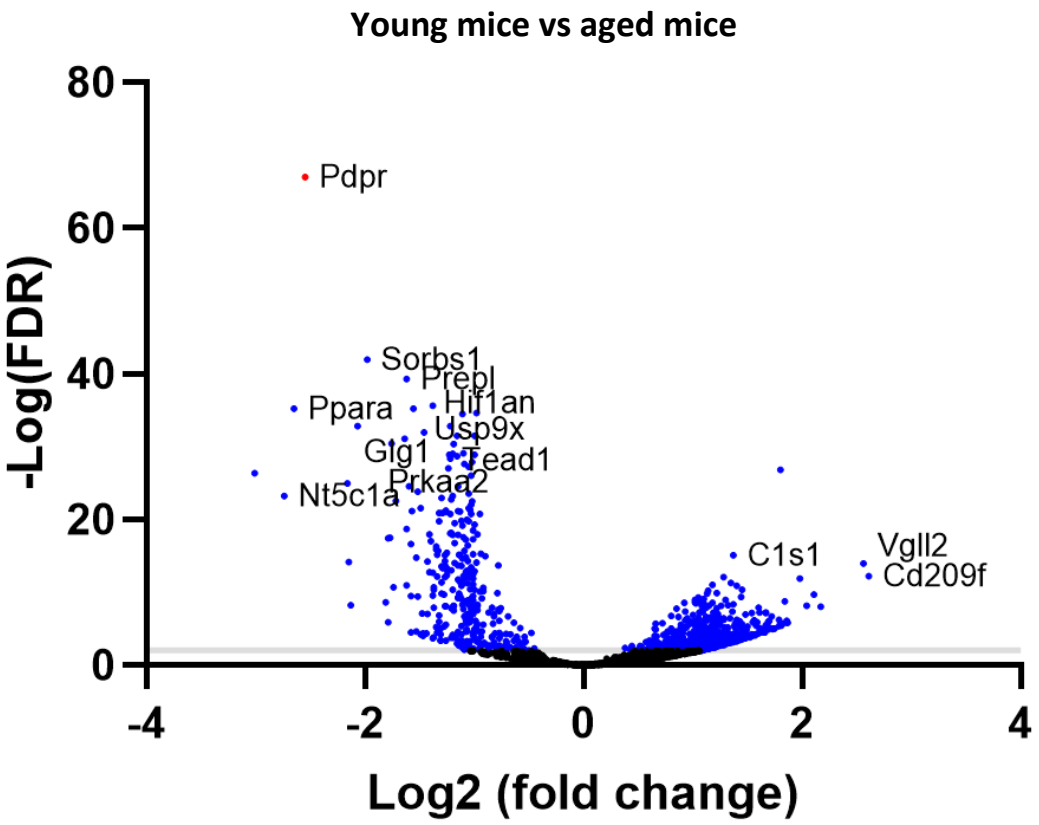

Fig. 63. Volcano plot of differentially regulated mRNAs in young vs aged mice.
The X-axis represents the log2 fold change $^{\text{ratio (young mice/aged mice)}}$ plotted against its significance level -log (false discovery rate-FDR). The cut off of -log (FDR)=2 at the y-axis corresponds to statistically significant deregulation. Left side represents downregulated genes and right side shows the upregulated genes in young mice as compared to aged mice. Some genes of highest significance are labelled.

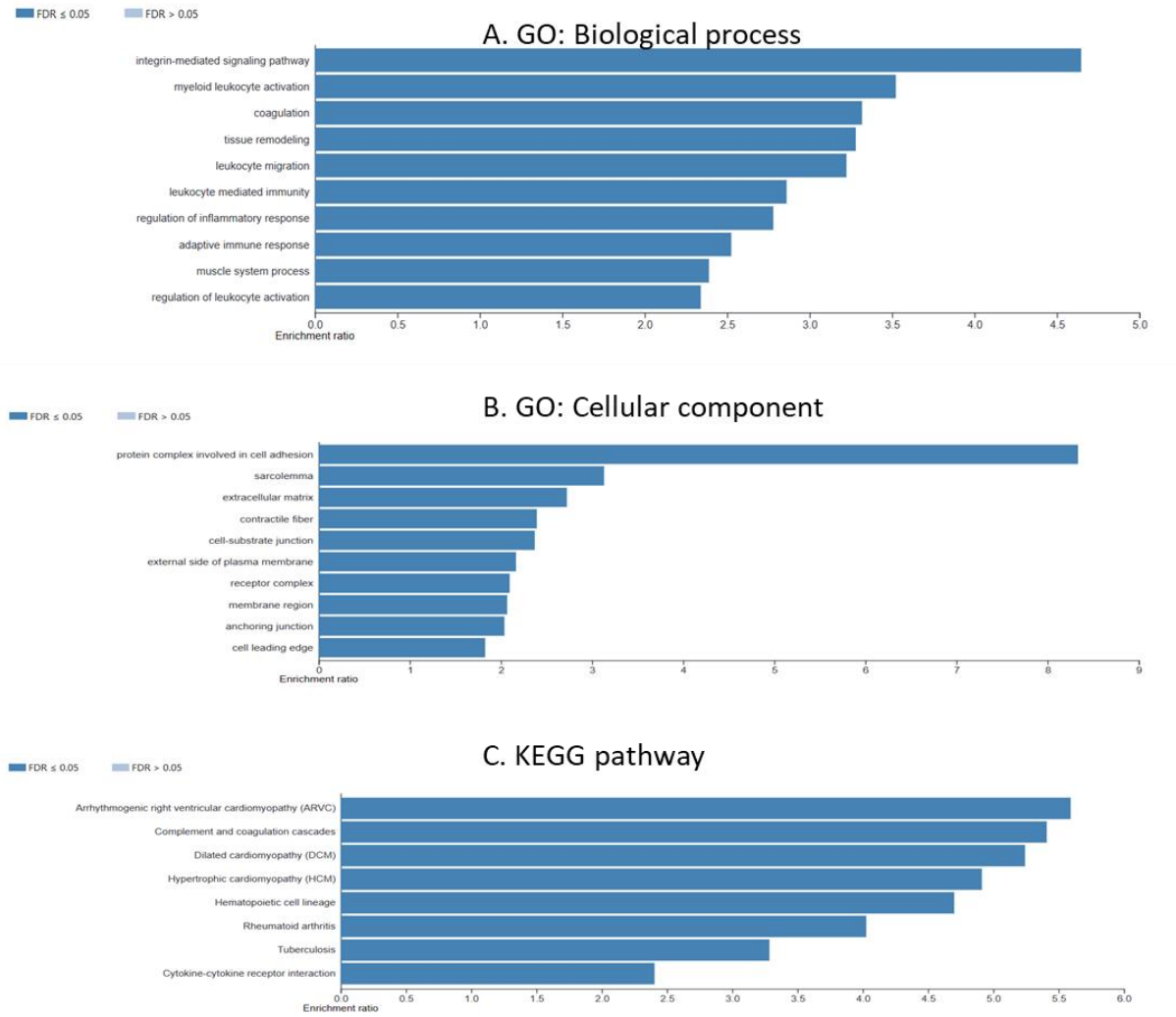

Fig. 64. Significantly over represented gene ontology terms and KEGG pathway analysis of DEGs between young mice and aged mice.

Bar charts show the enriched GO terms in the category of biological process (A), cellular components (B)and the list of enriched KEGG pathways (C) for significantly deregulated genes. The numbers on the chart indicate the enrichment ratio. FDR<0.05. Enrichment analysis was done using the WebGestalt platform.

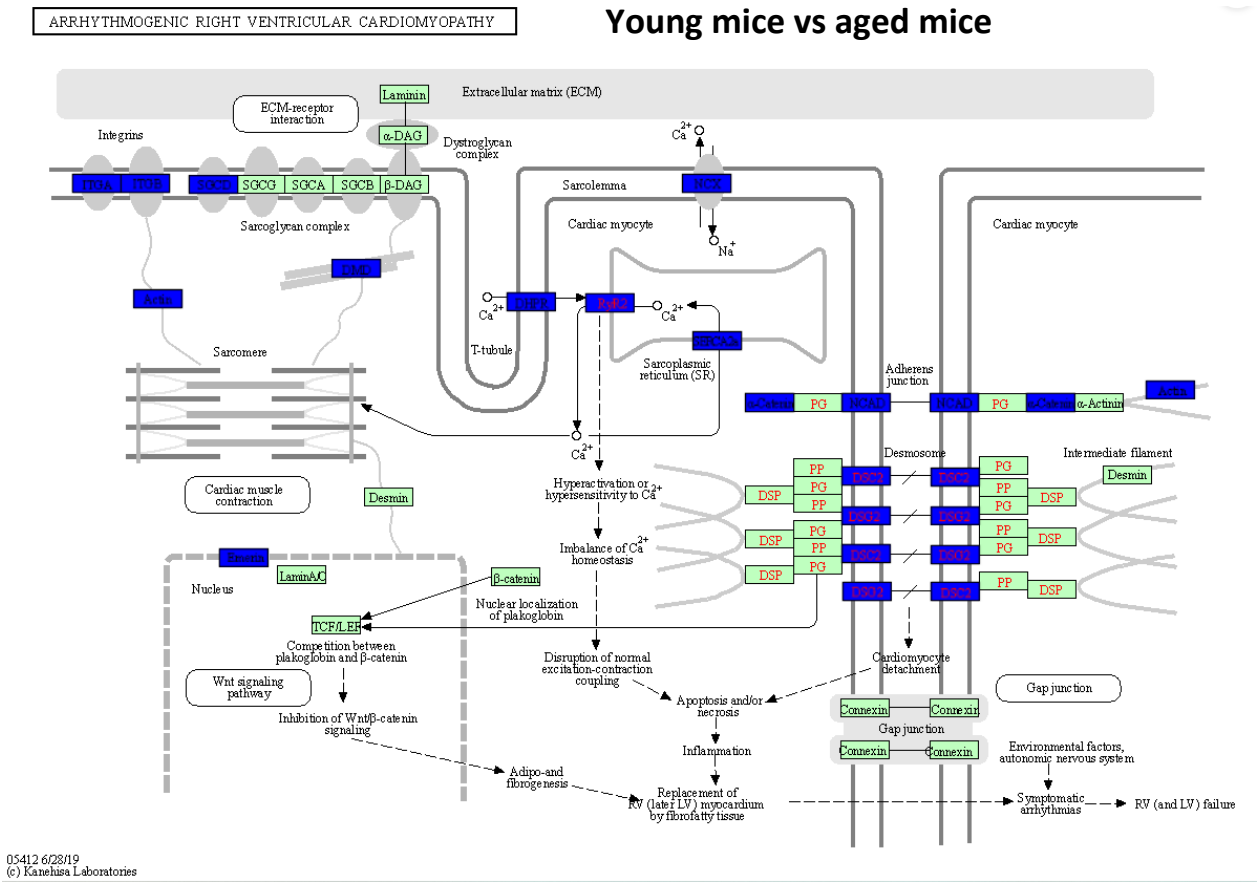

Fig. 65. Young vs aged mice groups exhibit significant expression changes in genes relating to arrhythmogenic right ventricular cardiomyopathy.
Schematic view of a cardiomyocyte with key proteins associated with the KEGG pathway map (05412) for arrhythmogenic right ventricular cardiomyopathy. Differentially expressed genes for young mice versus aged mice (HFpEF) are highlighted in blue. ITG A and B, integrin alpha 1 beta 1; NCX, sodium calcium exchanger; DMD, dystrophin; RR2, ryanodine receptor 2; Serca2α, P-type Ca2+ transporter type 2A; NCAD, N-cadherin and DSG2, desmoglein 2.

Next up, a cross analysis was drawn out between the two TAC cohorts, **ND TAC vs HFD TAC** analysis was done to assess the diet mediated drivers of HFpEF. Volcano plot in **figure 66** shows the distribution of DEGs. In GO terms, remarkable representation of actin filament dependent pathways, cardiomyocyte differentiation along with ECM dynamics were represented with a high significance (FDR≤0.05) suggestive of a potent structural perturbance in HFrEF vs HFpEF. KEGG pathway revealed an enrichment in the adrenergic signaling pathway of cardiomyocytes for which the genes are shown in **figure 67**. The highly enriched pathway of adrenergic signaling in cardiomyocytes was further mapped to visualize the DEGs associated within it as shown in **figure 68**.

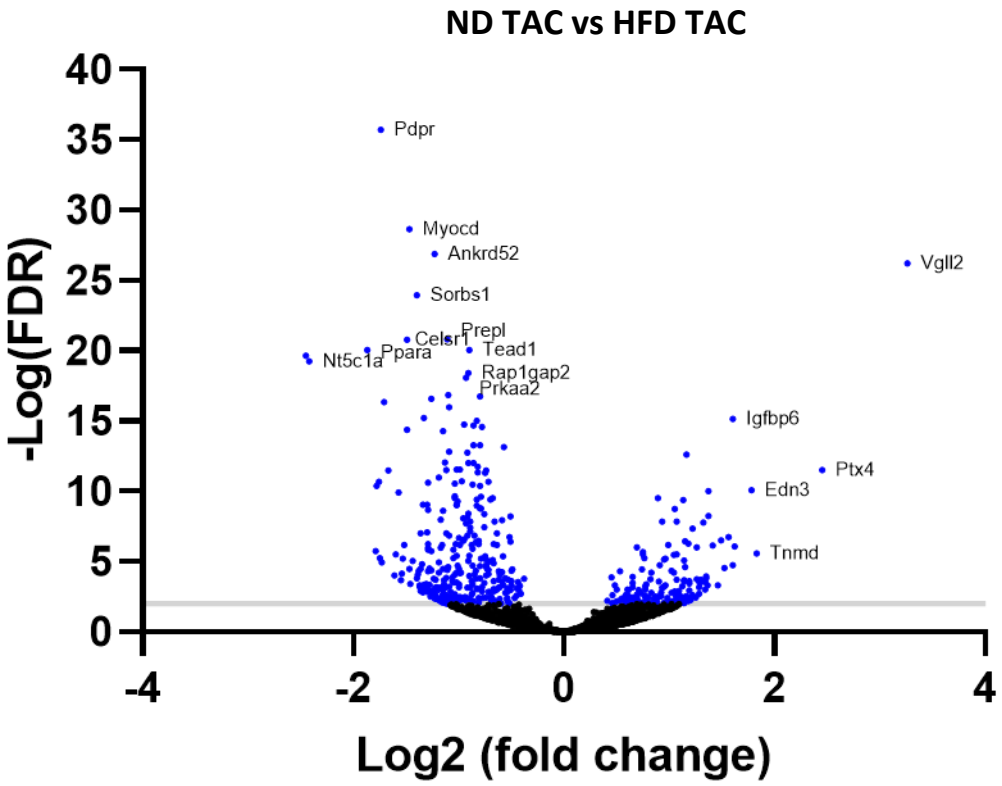

Fig. 66. Volcano plot of differentially regulated mRNAs in ND-TAC vs HFD-TAC.
The X-axis represents the log2 fold change $^{\text{ratio (ND-TAC/HFD-TAC)}}$ plotted against its significance level -log (false discovery rate-FDR). The cut off of -log (FDR)=2 at the y-axis corresponds to statistically significant deregulation. Left side represents downregulated genes and right side shows the upregulated genes in ND-TAC as compared to HFD-TAC. Some genes of highest significance are labelled.

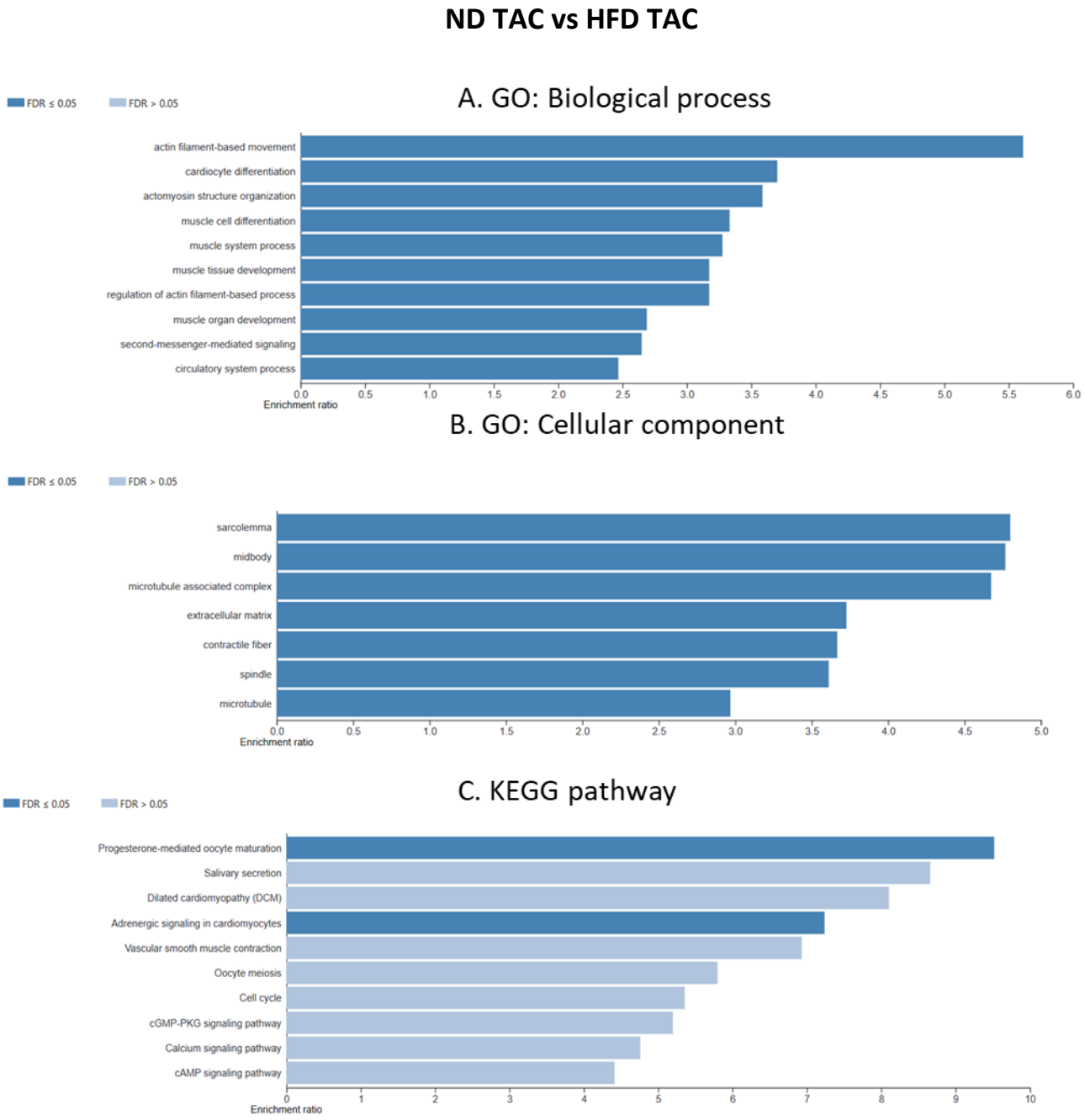

Fig. 67. Significantly over represented gene ontology terms and KEGG pathway analysis of DEGs between ND-TAC and HFD—TAC.
Bar charts show the enriched GO terms in the category of biological process (A), cellular components (B)and the list of enriched KEGG pathways (C) for significantly deregulated genes. The numbers on the chart indicate the enrichment ratio. FDR<0.05. Enrichment analysis was done using the WebGestalt platform.

ND TAC vs HFD TAC

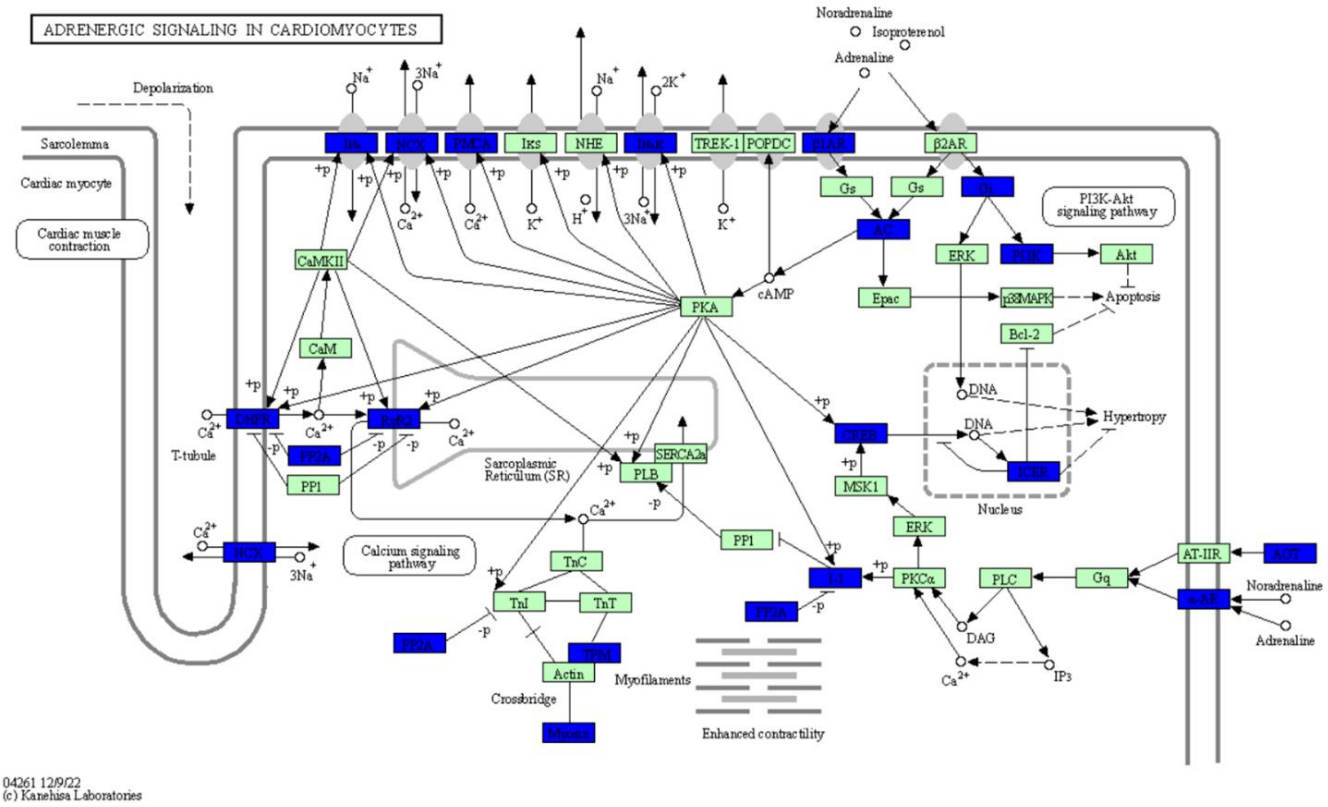

Fig. 68. HFrEF and HFpEF groups exhibit significant expression changes in genes relating to adrenergic signaling in cardiomyocytes.
Schematic view of a cardiomyocyte with key proteins associated with the KEGG pathway map (04261) for adrenergic signaling. Differentially expressed genes for ND-TAC (HFrEF) versus HFD-TAC (HFpEF) are highlighted in blue. I_{na}, voltage-gated sodium channel type V alpha; NCX, solute carrier family 8 (sodium/calcium exchanger; I_{NaK}, sodium/potassium-transporting ATPase subunit alpha; β1ar, adrenergic receptor beta-1; G_i guanine nucleotide-binding protein G(i) subunit alpha; AC, adenylate cyclase 1; PI3K, phosphatidylinositol-4,5-bisphosphate 3-kinase catalytic subunit gamma; DHPR, voltage-dependent calcium channel L type alpha-1C; PP2A, serine/threonine-protein phosphatase 2A catalytic subunit; RyR2 ryanodine receptor 2; CREB, cyclic AMP-responsive element-binding protein 1; ICER, cAMP response element modulator; NCX, Sodium-calcium exchanger; TPM, tropomyosin 1; I-I, protein phosphatase 1 regulatory subunit 1A; αAR, adrenergic receptor alpha-1A; AGT, angiotensinogen.

The last worthwhile comparison was between the two HFpEF models, **aged mice vs HFD TAC**. **Figure 69** shows a volcano distribution of deregulated genes between the two groups. Using over representation analysis, it was found that canonical GO terms were enriched under the umbrella of chemokine, ECM and tissue remodeling as shown in **figure 70**. KEGG pathway analysis showed that ECM protein interaction pathway and hypertrophic cardiomyopathy were significantly relevant here. ECM protein interaction pathway was further mapped to visualize a screenshot of the genes that were dysregulated as shown in **figure 71**.

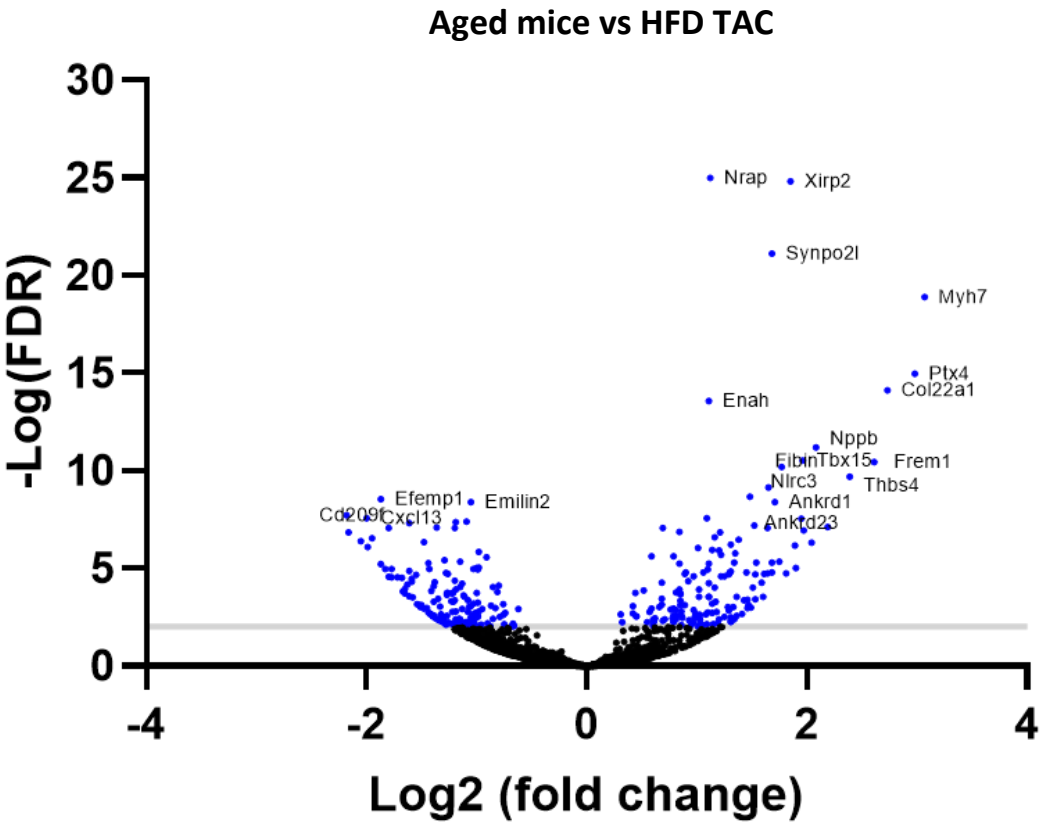

Fig. 69. Volcano plot of differentially regulated mRNAs in aging vs HFD-TAC.
The X-axis represents the log2 fold change $^{\text{ratio (aging/HFD-TAC)}}$ plotted against its significance level -log (false discovery rate-FDR). The cut off of -log (FDR)=2 at the y-axis corresponds to statistically significant deregulation. Left side represents downregulated genes and right side shows the upregulated genes in ND-TAC as compared to HFD-TAC. Some genes of highest significance are labelled.

Aged mice vs HFD TAC

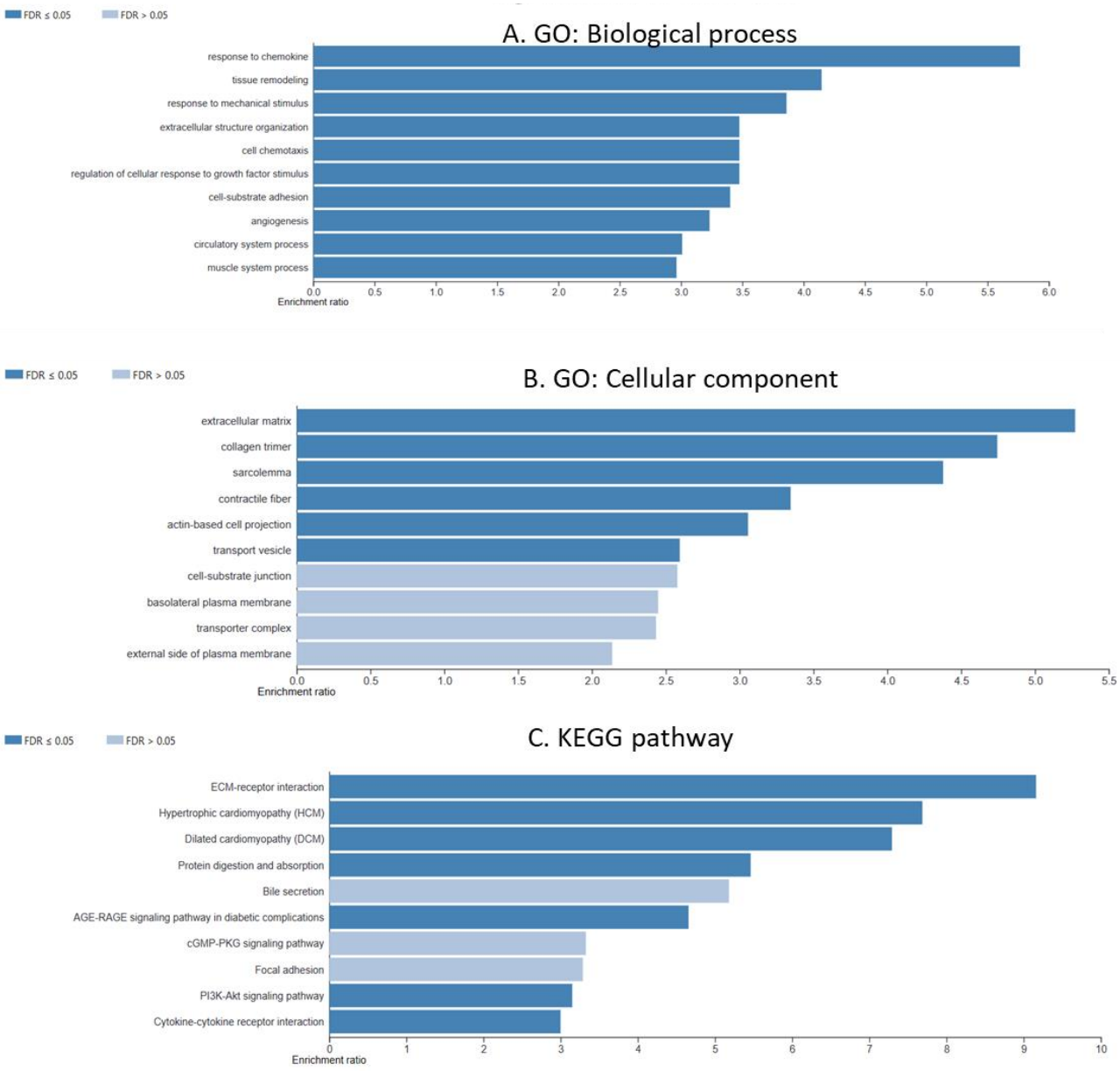

Fig. 70. Significantly over represented gene ontology terms and KEGG pathway analysis of DEGs between aging and HFD—TAC.

Bar charts show the enriched GO terms in the category of biological process (A), cellular components (B)and the list of enriched KEGG pathways (C) for significantly deregulated genes. The numbers on the chart indicate the enrichment ratio. FDR<0.05. Enrichment analysis was done using the WebGestalt platform.

Aged mice vs HFD TAC

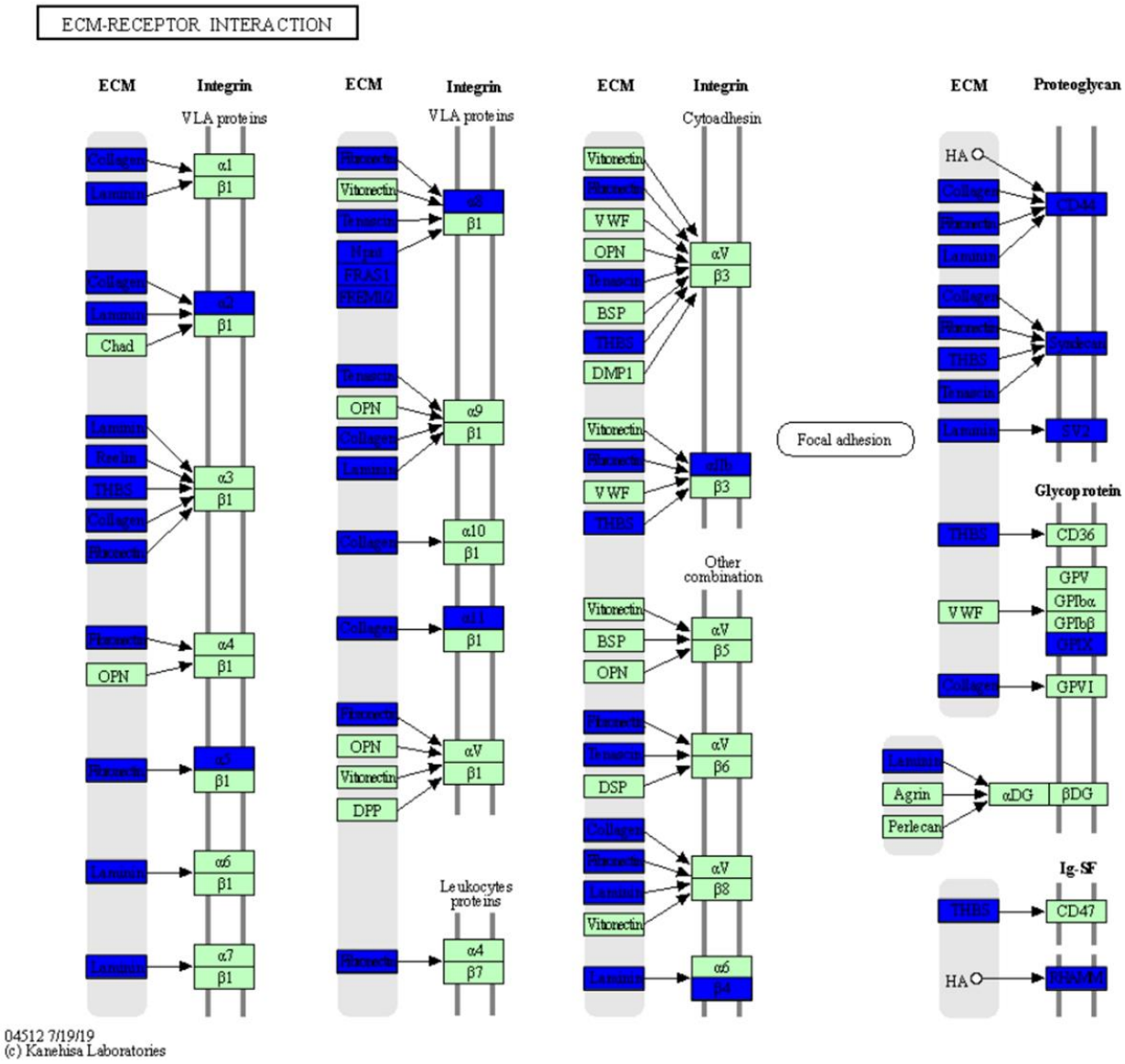

Fig. 71. Aging induced and dyslipidemia + PO HFpEF exhibit significant expression changes in genes relating to extracellular matrix receptor interaction cardiomyocytes.
Schematic view of extracellular matrix receptor interaction with key proteins associated with the KEGG pathway map (04512). Differentially expressed genes for aging induced HFpEF versus dyslipidemia + PO induced HFpEF are highlighted in blue. THBS, thrombospondin 1; α2,5,8,11, integrin alpha 2,5,8,11; β4, integrin beta 4; CD44, CD44 antigen; SV2, synaptic vesicle glycoprotein 2, GPIX, platelet glycoprotein IX; RHAMM, hyaluronan-mediated motility receptor.

Discussion

At present, HFpEF accounts for almost half of the HF cases worldwide (Oktay et al., 2013) and several factors are working in synchrony to further increase its prevalence. Increased life expectancy and aging population has given rise to a demograph that is highly susceptible to develop HFpEF (59%) as compared to young patients (46%) (Von Bibra et al., 2010). Another reason is the steady rise in cardiac and metabolic comorbidities like diabetes, obesity, metabolic syndrome and coronary artery disease. The recent past has seen advances in cardiac catheterization and imaging techniques which have proved instrumental in identifying the possibility of HF in presence of normal EF, this has further led to an increased awareness and thus higher prevalence. Morbidity and mortality associated with HFpEF and HFrEF are similar (Yancy et al., 2006) but, HFpEF suffers from a poorer prognosis because of our collective lack of its mechanistic knowledge. Clinical findings have not been reinforced with an understanding of pathological mechanisms of the syndrome. As a result, dedicated therapies aimed at positively reducing the morbidity and mortality of HFpEF have not yet been recognized (McDonagh et al., 2021). A glaring obstacle towards enhancing our understanding of HFpEF is the lack of animal models that truly capture the inherent complexity of the syndrome. HFpEF is a multifactorial and multiorgan disease which ultimately culminates in a syndrome with highly heterogenous patient populations. Tactfully capturing this heterogeneity in one pre-clinical model would require previous understanding of complex interconnected pathomechanisms. So essentially, we are at an impasse inside a vicious circle. In this dissertation we have aimed to circumvent this problem using a novel cross-comparative approach towards modeling HFpEF. A ''one-size-fits-all'' model is highly improbable and clinically unrealistic as well. We have aimed to create HFpEF models using distinct ''index events'' to drive a HFpEF like pathophysiological state in separate mouse models. These models then underwent deep characterization and stratification on clinically relevant levels in terms of HFpEF. Afterwards, the key differences and similarities were demarcated in an attempt to understand how different factors lead to a distinct avenue of pathological mechanisms leading to the shared fate of HFpEF.

Part 1: Cross-characterization of different HFpEF like states

High fat diet and western diet have been regularly used to mimic the symptoms of dyslipidemic HFpEF. However, high lipid content on its own is not sufficient to capture the pathophysiology of HFpEF and is rather more reflective of early stages of metabolic heart disease (Schilling et al., 2020). To realistically translate a HFpEF like state in mice, we used a two-hit combination of dyslipidemia induced by HFD along with a low-grade PO. PO induced by hypertensive states often leads to activation of mechanisms reminiscent of LV-DD like hypertrophy, fibrosis, ECM dysfunction, nitrosative-oxidative damage etc. (Van Heerebeek et al., 2012). A low grade PO was induced by 26G TAC surgery and when

combined with HFD, it represented theoretically a more logical and holistic presentation of HFpEF. To our knowledge, this study is the first one to use this intuitive combination. The second model was based solely on natural aging. Aging in the cardiac context is often seen as a geriatric syndrome which again has a multifactor involvement and senescence induced HF is often seen as a form of ''presbycardia''. Similar to the metabolic syndrome, a lot of distinct elements play a key role in leading to the aging driven syndrome of HFpEF. So how do these two multidimensional events show up in distinct patient populations with HFpEF? What brings these two together in terms of pathophysiology and what sets them apart? These questions are addressed in the following paragraphs.

1. High fat drives a HFpEF like state in presence of low grade pressure overload, aging reflects a distinct HFpEF like state

The models were defined to be ''HFpEF like'' or ''HFrEF like'' after an extensive characterization of systolic and diastolic function parameters measured by echocardiography, strain imaging and PV analysis. At two weeks post PO, HFD-TAC showed a preservation of EF at >50% as compared to sham while in ND-TAC it was reduced to ≤40%. The aging group also presented with a preservation of ejection fraction at >50%. FS also followed a similar pattern and was reduced in both TACs and aging group. This was further corroborated by a perturbance in r-LSR an important diastolic function parameter. While HFD group showed a significantly decreased r-LSR, only a trend was observed in ND group. Aging group showed a similar significant decrease. These results are consistent with previous reports of reduced r-LSR in models of HFpEF (Schnelle et al., 2018). PV analysis provided a much detailed look at diastolic and systolic states of the models. In HFD group, all parameters of systolic function namely- ESPVR, dp/dt_{max} and PRSW remained unchanged and were similar to the observations in aging group (except a slight increasing trend in PRSW). The ND-TAC group however showed significant increment in these systolic dysfunction parameters when compared to shams. This showed that ND group has a clearly pronounced systolic deficit which was absent in HFD-TAC and aging cohort. On the other hand, diastolic function parameters were unequivocally disturbed in HFD group with an increase in all indices- EDPVR, Tau, EDP and dp/dt_{min} in TAC as compared to shams. The aging group followed suit. The ND group exhibited a significant change in EDP and a trend towards high Tau. This indicated that in ND also, some degree of diastolic dysfunction is present which is consistent with the current clinical guidelines (Nagueh et al., 2016). This prompted us to hypothesize that the underlying mechanisms afforded by HFD must be important in shifting the HF spectrum towards a state of preserved EF when compared to ND after TAC. As previously discussed, metabolic syndrome has been reported to be a major driver of HFpEF and is often one of the most common associated comorbidity. Preservation of systolic function in HFD and not ND mice with PO further support this.

Henceforth, HFD-TAC and aging have been referred to as ''HFpEF like'' and ND-TAC as a ''HFrEF like'' state.

2. Differential hypertrophic response in dyslipidemic vs aging based HFpEF state

Hypertrophic response to PO induced by low grade TAC was found in both dietary groups as evidenced by increased LV weight, increased RWT and higher cardiomyocyte CSA as compared to controls. Both HFD and ND induced similar levels of hypertrophic response but, HFD-TAC groups showed a trend towards higher LA remodeling as well which was distinctly absent in the ND-TAC group. Patients with HFpEF have been shown to present with LA hypertrophy associated with increased wall stiffness and it has been positively correlated with higher mortality rates (Melenovsky et al., 2015). We found that both dietary models exhibited similar levels of mortality after PO, despite the evidence (albeit not significant) of LA remodeling exclusively in HFD. The levels of pro-hypertrophic natriuretic peptides also supported these findings in both dietary groups. On the other hand, in the aging based model of HFpEF, no significant hypertrophic response was observed at the organ or cellular level despite the advanced age. There was however a prominent increase in LVPWd that would indicate the initial stages of ventricular remodeling. Increased concentricity has sometimes been reported in HFpEF patients with no apparent hypertrophy and it further emphasizes the differences in HFpEF patient populations (Melenovsky et al., 2007). A look at the molecular expression of genes involved in cardiac stress response also gave some differential insights. The levels of Serca2-α RNA were significantly decreased in ND-TAC as compared to sham and aged mice as compared to young controls. This decrease was absent in HFD-TAC group, which is in contrast to previous findings (Kranstuber et al., 2012). We hypothesize that looking at advanced stages in this model may reflect the data from other studies. The pattern of expression of pro-hypertrophic natriuretic peptide ANP and BNP was also different with a clear increase in both in the HFD group, but only an increase of BNP in ND and aging group. BNP has been demonstrated to be of diagnostic and prognostic value in HF and have been shown to be higher in HFrEF vs HFpEF (Januzzi et al., 2013) but our data showed no significant differences between the two, this could be due to a relatively short period of two weeks of observation post-TAC. Whether the differential signature of natriuretic peptide activation in these two distinct HFpEF like states is of prognostic value, remains to be further explored. α-skeletal actin was increased in both dietary groups consistent with a global structural stress on the myocardium (Stilli et al., 2006) but it was unchanged within the aging group, and it could hint that other stress mechanisms might be more predominant in aging induced HFpEF.

3. Structural features of the LV myocardium show differences in steatosis and fibrosis

Structural characterization at tissue architecture level was done on the basis of steatosis and fibrosis with associated collagen content. Myocardial steatosis has been reported to occur in both HFrEF and HFpEF and is related to indices of LV remodeling (Mohmod et al., 2015). It has also been corelated with endoplasmic reticulum dysfunction and contractile deficit (Gupta et al., 2021). In the HFD group, we could observe clear accumulation of neutral lipid deposits in the ventricle with no distinction in sham vs TAC. In normal diet group reflective of HFrEF, it was absent. A plausible explanation could be that at this point in observation, the steatosis is more a function of just the HFD and not PO. Perhaps with a longer timepoint, the steatotic effects of PO could be observed. Nevertheless, increased lipid accumulation in the dyslipidemic mouse model is in line with previous reports (Mehlem et al., 2013). The aging group also showed no significant increase in lipid accumulation but, a clear increase in trend was observed. The increased content of neutral lipids in the heart is reported to reflect an increased expression of gene transcripts in the myocardium that stimulate fatty acid uptake in cardiomyocytes and triglyceride storage (Christofferson et al., 2003).

Total fibrotic area was enhanced in both dietary TAC groups as compared to their respective shams as well as the aging group compared to young controls. Perivascular fibrosis on the other hand results from an enrichment of inflammatory cells and is more prominent where predominant endothelial damage is present such as hypertensive heart disease or diabetes (López et al., 2016). Consequently, both the HFpEF models exhibited a highly significant increase in perivascular fibrosis when compared to HFrEF. This is also in correlation with higher upregulation of inflammatory cytokines in the two HFpEF states as compared to HFrEF. Untangling the two types of fibrosis is challenging because they often coexist and are quantified together but our findings stress on the importance of differentially assessing and pharmacologically targeting the two types. Studies have reported an increase in ratio of type I vs. type III collagens in both animal and human models of PO (Kasner et al., 2011). In dyslipidemic HFpEF model, collagen I/III ratio was higher and so was in aging HFpEF, the ND diet cohort however showed no such increase. It could be postulated that the combination of HFD+PO is more potent in inducing collagen switch rather than just PO alone at the early observation timepoint of two-weeks. Fibronectin (FN-1) polymerization has been implicated in increased collagen deposition and its inhibition leads to attenuation of fibrosis in mouse models of HF (Valiente-Alandi et al., 2018). We also found that all models exhibited an increase in FN-1 in line with overall increase in fibrosis.

4. Differential inflammatory profile marks dyslipidemic and aging based HFpEF like state

Furthermore, the role of inflammation was investigated in the mouse models. Progressive states of myocardial structural and function in HFpEF have been associated with a chronic low grade systemic inflammation owing to comorbid states (Mesquita et al., 2022). Experimental models have

demonstrated that enhanced production of pro-inflammatory cytokines upregulates oxidative stress, induces the differentiation of fibroblasts into pro-fibrogenic myofibroblasts, and causes ECM degradation, leading to increased myocardial stiffness and coronary microvascular dysfunction (CMD) (Paulus et al., 2013; Bairey et al., 2020). Whether this chronic meta inflammation is a general phenomenon of HFpEF or a by-product of comorbid conditions is not well understood. mRNA expression analysis of common pro-inflammatory cytokines was performed to answer some of these questions. TGF-β has been referred to as the master switch of fibrotic program induction in fibroblasts and it has been shown that inhibition of this cytokine attenuates fibrosis and improves diastolic function (unaffecting hypertrophy) in TAC based animal models of HFpEF (Kuwahara et al., 2002). In this study, we observed selective upregulation of TGF-β in HFD-TAC and aging mice only. This further reinforces the convergence of HFpEF subtypes through shared mechanisms. In ND group, it was not significantly upregulated in response to PO, this finding seems to be in line with a 2016 study by Bielecka-Dabrowa et al., who found that TGF-β1 and its downstream syndecan 4 served as biomarkers to independently distinguish HFpEF and HFrEF. IFN-γ has been shown to be elevated in adaptation to high fat diet in rodent models of long term obesity and may act through concerted effects on mitochondrial function, regulatory T cell (Treg) function and fatty acid β oxidation (Bradley et al., 2022). In our study, it was shown to be only enhanced in HFD-TAC group which may be an early adaptive response to dyslipidemic and pressure overloaded states but the two sham groups showed no difference. TNF-α was increased in HFrEF and aging based HFpEF which is concordant to previous findings (Schumacher et al., 2018). However, in contrast to what has been reported in literature (Putko et al., 2014), we found no upregulation in dyslipidemia based HFpEF. Is it an isolated difference between the two HFpEF states or not remains to be analyzed as the literature regarding such cross comparisons is scarce.

Next, interleukins involved in pro-inflammatory cascade associated with heart failure were investigated. IL-1β has been known to increase in several cardiovascular disorders and it is a well exploited therapeutic target for Anakinra (human recombinant IL-1 receptor antagonist) (Buckley et al., 2018). In our findings, IL-1β was elevated only in the HFpEF like states of HFD-TAC and aging. We did indeed see a significant increase in HFD-TAC group as compared to ND-TAC suggestive that dyslipidemic comorbid states may induce an early activation of this interleukin in the setting of HFpEF. IL-6 is another important cytokine which has been reported to have a potential as a selective biomarker in HFpEF (Albar et al., 2022). We found that it was enhanced only in the aging subtype of HFpEF states. Could it be also a selective biomarker for different HFpEF subtypes can't be extrapolated from our findings alone and would need further proof. However, we provide proof of concept that the

temporal and qualitative profile of inflammatory cytokine levels can be a putative differentiator between HFpEF and its subtypes along with HFpEF and HFrEF.

5. Endothelial dysfunction and cardiomyocyte apoptosis show distinct features in both HFpEF states

In subsequent sections we describe the effects of cytokines involved in endothelial dysfunction namely cell adhesion molecules. Previous reports have associated VCAM-1 with HFpEF incidence and not HFrEF with consistent risk rates in human patients (Patel et al., 2020). Our findings resonated with this as VCAM-1 overexpression seemed to be selectively induced in both HFpEF like states, i.e. dyslipidemia and aging and not in HFrEF. ICAM-1 showed an overall increase in all groups in comparison with their respective controls. PO has been known to induce ICAM-1 expression in mice models of TAC as early as 48 hours after surgery (Salvador et al., 2015). Our low grade TACs may have taken longer but we don't have the data from early timepoints but it might be worth further exploring to characterize different grades of PO induced by TAC. Moreover, ICAM-1has been implicated to be overexpressed in senescent cell lines in a p53 dependent manner, which correlates to our findings of enhanced expression in aging (Gorgoulis et al., 2005). PECAM-1 is reported to be a critical regulator of atherosclerosis (Stevens et al., 2008) and is shown to have pleiotropic effects on cardiovascular pathophysiology (Caligiuri et al., 2019). However, we found only an increased expression in the HFrEF group. This is in contrast to previous findings but they were reported in a cardiorenal model of HFpEF (Valero-Muñoz et al., 2021). Whether this is of prognostic value remains uncertain but it highlights again the importance of recognizing distinct cytokine profile in HFpEF subtypes.

In line with investigation of endothelial damage pathways in the models, we also looked at CD45 positive cells in ventricular sections. CD45 is one of the best markers for hematopoietic cells and is an important factor in driving endothelial-to-mesenchymal (EndMT) transition in a diverse set of cardiovascular disorders (Yamashiro et al., 2023). $CD45^+$ leukocytes have been reported to be involved in chronic pressure overload HFpEF and are tied to IL- 1β, IL6 and IL10 induced pro-inflammatory states (Liu et al., 2021). In our experiments, $CD45^+$ cells were only upregulated in the aging group and not in either dietary groups with PO. While Yamashiro et al., describe a systematic review of different PO models showing an increase in CD45 containing cell upregulation, they don't talk about low grade PO for a brief period of time which may be the differentiating factor in our models. Nonetheless, crosstalk between innate immunity and aging has been previously reported and mechanisms underlying myocardial aging have been implied as a T-cell mediated phenomenon (Ramos et al., 2017; Trial et al., 2017). Adverse fibrotic outcomes have also been positively corelated with higher $CD45^+$ cell populations in aging hearts (Cieslik et al., 2014).

Endothelial dysfunction and inflammation are highly multidimensional and it is very unlikely that only a handful of factors described above characterize them in their entirety. So, we sought to increase our repertoire of understanding by assessing the expression of NADPH oxidase- NOX2. NOX2 is a major driver of ROS induced endothelial damage (Lassègue et al., 2012). EndoMT induced by pressure overload has been linked back to NOX2 dependent mechanisms working in concert with VCAM-1 upregulation (Murdoch et al., 2014) which is further reinforced in our study. We found that NOX2 levels were enhanced after TAC in both dietary groups and not in the aging cohort. It could be probable that mechanical stress such as that induced by PO is a pre-requisite here (Akki et al., 2009), because NOX2 requires activation. NOX2 activation depends on various transduction pathways (PKC, PKD, PI3K and MAPK) which first phosphorylate one of NOX2 regulatory subunits $p47^{phox}$ (Zhang et al., 2013). While we have studied the activation of PI3 and MAPK pathways as described in further sections, we did not exclusively look at $p47^{phox}$ activation.

Class II histone deacetylases including HDAC-4 are important epigenetic modulators that can directly interact with essential transcription factors that drive hypertrophy and are often activated by ROS induced states (Backs et al., 2006). We wanted to see if HDAC-4 activation is differentially regulated since cardiac hypertrophy was a prominent distinguishing feature present in HFD induced HFpEF and not aging. It was found that HDAC-4 was highly phosphorylated in the HFD-TAC group as compared to HFD-sham, while ND group showed no such difference and neither did the aging group. It may be suggested that hypertrophy in the two-hit combination of HFD and PO has an additional involvement of HDAC-4 activation, which is not the case in regular diet + PO models.

Maintenance of programmed cell death or apoptosis is a fine balancing act in the context of HF. Apoptosis, necrosis and autophagy have been implicated in the dynamics of HFrEF (Simmonds et al., 2020). We wanted to characterize apoptosis in our HFpEF like states too. It was found that both dietary groups exhibited similar levels of cardiac apoptosis in response to PO, indicating that HFD alone does not influence ultimate cell death as assessed by TUNEL staining. Subtle effects on apoptotic pathways rendered by HFD have been previously described (Wang et al., 2019). A diabetic model of HFpEF has also been reported to have increased apoptosis (Mátyás et al., 2017). This may further assert that not just HFD but an overall state of insulin resistance as in diabetic complications may be more potent in driving myocardial cell death. In the aging group, apoptosis was observed to be even higher than HFrEF group. Cardiac-aging with abnormal diastolic function has been characterized by increased levels of programmed cell death (Lakatta et al., 2003). It might be worthwhile to look at mediators of apoptosis in these two HFpEF states to unravel hidden differences.

6. Cardiac kinases and calcium handling show a marked divergence

Cardiac kinases are just as important as the above mentioned mediators in the pathophysiology of HF and are potential targets (Vlahos et al., 2003). Kinases catalyze reversible processes of phosphorylation which either directly or indirectly control a plethora of signaling pathways in cardiomyocytes.

Also known as Protein kinase B, Akt is serine/threonine protein kinase. Akt is known to regulate a myriad of processes like cardiomyocyte hypertrophy, angiogenesis, glucose metabolism and cell death (Chaanine et al., 2011). While short term Akt activation can be lead to normal physiological hypertrophy and is cardioprotective against myocardial injury, its chronic activation can lead to pathological hypertrophy and HF (DeBosch et al., 2006). Akt signaling from endothelial cells plays important roles in maintaining vascular homeostasis (Phung et al., 2006). Akt phosphorylation at Serine 473 is mediated by mTORC2. We found that Akt phosphorylation at Ser473 was increased only in the HFD-TAC group as compared to HFD-Sham, moreover a significant difference existed between the two TAC groups. Aging model did not present with increased Akt phosphorylation which is consistent with absence of hypertrophy. The difference in Akt phosphorylation levels between the two dietary groups after PO may be attributed to dyslipidemic effects of additional stress of HFD. Akt has been shown to be an important modulator of glucose and fatty acid metabolism and since these mechanisms are altered by dyslipidemia, this may plausibly explain the selective upregulation of Akt phosphorylation in HFD despite hypertrophy being present in both dietary groups.

ERK phosphorylation has both been reported in HFrEF and HFpEF (Mishra et al., 2021). ERK1/2 has been shown to be active in early phases of pathomechanisms arising because of PO and is similarly implicated in hypertrophy and fibrosis (Kehat et al., 2010). However, in our study ERK phosphorylation levels were selectively active in HFpEF like states of HFD-TAC group and aging. We did not study the early phase so we cannot say how low grade PO might play out here. But in HFpEF there was a clear increase denoting that long term maladaptive ERK activation may be an important feature in HFpEF. It has been shown that higher ERK activation after PO is seen in contractility preserved phases of HF (Gallo et al., 2019) and the same might be happening in our HFpEF like states.

p38 kinases and c-Jun N-terminal kinases (JNKs) are a part of the MAPK signal transduction pathway and are implicated in hypertrophy and remodeling (Fischer et al., 2001). Despite the presence of hypertrophy and remodeling in both dietary groups after PO, we could not see an elevation in p38 phosphorylation. It was however increased in the aging group. p38 plays a fundamental role in skeletal muscle regeneration and given the skeletal impairment in aging, a feasible link can be established between p38 activation and senescent hearts (Romero-Becerra et al., 2020). JNKs have been similarly

implicated and we saw a similar pattern of enhanced phosphorylation only in the aging group. The literature on effects of p38 and JNK activation on different types of HFpEF models is limited but our data suggest that it may be differentiator between dyslipidemic and age induced HFpEF states at the very least and consequently therapies aimed at inhibiting their activation may provide cardioprotective benefits in this subpopulation.

Abnormal dynamics of calcium handling have been implicated in HF. Our results also indicated disturbance in maintenance of rhythm and contractility like disturbances in end diastolic pressure volume relationship and Tau. A lot is known about this aspect in context of HFrEF but there is a lack of knowledge in HFpEF scenario. Calcium handling mechanisms in the models were studied. It has been shown that Ca^{2+} cycling differs in HFpEF and HFrEF qualitatively and quantitatively (Kilfoil et al., 2020). Ca2+/calmodulin-dependent protein kinase-II (CaMKII) is known to phosphorylate ion channels, calcium handling proteins and enzymes related to chromatin modification (Anderson et al., 2011; Toischer et al., 2010). Knockdown of CAMKII delta variant has been reported to lessen pathological cardiac hypertrophy and remodeling in response to PO and its inhibition exerts cardioprotective effects by improvements on maladaptive remodeling (Zhang et al., 2003; Sossalla et al., 2010). We found that CAMKII phosphorylation was enhanced in aging hearts and not in HFrEF induced by low grade PO. In the HFD-TAC group it was increased but failed to reach significance. Our assessment at a relatively early time point of a especially low grade of TAC might be a tentative reason here. Recently it has been demonstrated that CAMKII interacts with ERK and PKA pathways to regulate titin phosphorylation which is a factor influencing passive stiffness in HF, mainly diastolic dysfunction (Hamdani et al., 2013). Our findings support this to a certain extent as the pattern of ERK activation and CAMKII phosphorylation was almost similar. CAMKII and PKA affect downstream targets such as ryanodine receptor (RyR2) and phospholamban (Plb). RyrR2 is phosphorylated at serine 2814 and Plb at threonine 17 in a CAMKII dependent manner. We found a concomitant increase in phosphorylation of both RyR2 and Plb in both HFpEF groups, i.e. HFD+PO induced and aging. Hyperphosphorylated states of RyR2, could lead to SR Ca^{2+} leak leading to ventricular arrhythmogenic effects (Landstrom et al., 2017). This could potentially be a cause of sudden cardiac death in these mouse models and needs to be further explored. An investigation of PKA dependent sites (RyR serine 2808 and Plb serine 16) showed an increased activation only in the aging group. It suggests that PKA and CAMKII cross interaction are more relevant in aging induced HFpEF states. This is also suggested by McCluskey et al., who implicate this activation with enhanced endothelial damage in aging hearts undergoing HF. However, another PKA mediated phosphorylation is at cardiac troponin (CTnI) at Serine 22/23 and we could not see a subsequent effect on this. In normal diet-TAC however, p-CTnI was significantly downregulated which further supports that PKA activity was downregulated in HFrEF like states in this

study. Taken together our data asserts the importance of heterogeneity in calcium handling and dynamics in HFpEF and HFrEF.

It was of further interest to look at the differential expression of mRNA profiles in our models to get a comprehensive overview of the coding transcriptome.

Part 2: The transcriptome of different HFpEF like states

LV sections from representative mice from each of the five groups were subjected to next-generation mRNA sequencing. A look at the variation from principal component analysis revealed that there was a clear demarcation between sham and TAC of both dietary groups. Notably the two TACs were also grouped far from each other with no overlap in the quadrants. This is important because it helps establish that based on the transcriptome, these groups are highly divergent and each represents a distinct form of HF. As per previous discussion, ND-TAC represents a state of HFrEF and HFD is reflecting a HFpEF like state at two weeks post PO. This suggests that not only at the level of cardiac physiology and the functions that we assessed, these groups are also distinct in their global cardiac mRNA profile. Interestingly, we found that the aged mouse cohort (reflective of a different HFpEF subtype) was clustered with HFD-TAC group while still having its own niche. This pattern immediately makes sense in the light of our characterization results where we observed some key differences in two subtypes but the pattern of diastolic dysfunction and its associated mechanisms were similar. Next, we made a few comparative analyses relevant to our hypothesis: HFrEF like state in ND-TAC as compared to ND-sham, Dyslipidemic HFpEF like state in HFD-TAC compared to HFD-sham, HFrEF vs HFpEF like states of ND-TAC vs HFD-TAC and ultimately the two HFpEF subtypes aging HFpEF vs dyslipidemic HFpEF. In the following sections we attempt to discuss some significant relevant genes, pathways and biological processes differentially handled in these groups.

In the HFrEF state of PO induced in the presence of a normal diet (as compared by **ND sham vs ND TAC**), there was an enrichment of over represented biological terms relating to TNF-α related signaling, dilated and hypertrophic cardiomyopathy (DCM/HCM), IL-17 related mediated process, extra cellular matrix dynamics, PI3-Akt signaling and chemokine-chemokine interactions. The major KEGG pathways represented were ECM dynamics, inflammation, leukocyte recruitment and cytokine interactions. While this gives a very broad and general overview of the PO state in TAC mice, it does support that HFrEF also has major involvement of inflammatory pathways as in HFpEF which can directly influence a dilatory and hypertrophic phenotype. This has previously also been suggested (Castillo et al., 2020; Van Linthout et al., 2017). We then took a closer look at differentially regulated genes to get a better understanding. For the sake of brevity, we describe only the top few differential

genes in each comparative group. The most upregulated genes were Xirp2 (Xin repeat-containing protein 2), Myh7 (myosin beta heavy chain), Synpo2l (synaptopodin 2 like), Ace (angiotensin-converting enzyme), Nrap (nebulin-related-anchoring protein) and Col1 (collagen 1) subtypes but these were also upregulated in a common fashion in HFD-TAC group when compared to HFD-sham. This suggests that these are constituents of a cascade that gets activated in cardiopathic models of HF in general in mice and are associated with a variety of cardiac functions (Wang et al., 2016; Clausen et al., 2021; Truszkowska et al., 2017). However, these set of genes were not upregulated in aged mice who clearly also have underlying HF. To our knowledge we are the first to describe the differential upregulation of these genes in a PO based HF model as compared to HF associated with natural aging. Other highest upregulated genes were Ankrd1 (ankyrin repeat domain 1) and Serpin (serine protease inhibitors) which have been related to dilated cardiomyopathy and ECM dynamics respectively (Bouton et al., 2021). Speaking of top downregulated genes, IL-15 is involved in protective immune response by its negative effects on cardiomyocyte death (Guo et al., 2022). Its deregulation suggests a dissimilar protective immune response between the two HF states. Similar conclusions can be drawn about another downregulated gene Alox 5 (arachidonate 5 lypoxygenase) which is involved in cardiomyocyte repair (Biswas et al., 2020).

The biological processes enriched in **HFD sham vs HFD TAC** comparison were response to nitrogen and oxygen containing compounds which is in line with the high oxidative-nitrosative states of dyslipidemia, response to lipids and response to cytokines. KEGG pathway analysis showed enrichment in MAPK, PI3-Akt, IL-17 and TNF-α related pathways. Notably, the AGE/RAGE pathway associated with diabetic complications was also enriched further enforcing the induction of highly dysmetabolic states by this two hit combination. Conversely to HFrEF group, in the HFD-sham vs HFD-TAC transcriptome, we found a completely different set of upregulated and downregulated genes. Apart from the common upregulated set as described in the paragraph above, we found some uniquely upregulated genes. PlekhA6 (Pleckstrin homology domain-containing family A member 6) was enhanced in levels which is implicated to play roles in cardiac proliferation through m6A methylation (Yang et al., 2021). If this is a typical presentation in dyslipidemic HFpEF needs to be further validated. Nlrc3 (NOD like receptor CARD domain containing 3) was also highly upregulated. It is interesting because it has been known to be linked with low density lipoprotein induced inflammasome activation in HF (Wang et al., 2021). Endothelin-3 (Edn3) was also very highly upregulated and it has been linked with cardiovascular syndromes associated with renal failure (Kao et al., 2017). Renal failure is also a potent comorbidity in HFpEF and it is very interesting to see this association pop-up in dyslipidemic HFpEF models suggesting a shared pathophysiology that may go beyond the models we have studied in this thesis. Among the uniquely downregulated genes was PVR

(poliovirus receptor gene or CD155) which is reported to play pleiotropic roles in tumor progression (Molfetta et al., 2020). Molfetta and colleagues have shown that CD155 is an IFN-γ inducible protein that attenuates T cell response in endothelial cells, since immune mechanisms are a prominent feature in HFpEF, the downregulation of this regulatory component may explain some characteristics of the dyslipidemic model (Escalante et al., 2011). Emilin 2 (Elastin Microfibril Interfacer 2) was also uniquely downregulated in dyslipidemic HFpEF, remarkably it was also downregulated in aged vs HFD-TAC comparisons, suggesting a potent role in HFpEF. It has been shown that Emilin$^{-/-}$ mice show defects in cardiac septal and right ventricular walls of the heart and an increase in TGF-β (Huang et al., 2015) which is completely concomitant with our findings of increased TGF- β in both HFpEF states. This may be a highly lucrative therapeutic target in our opinion.

In the next comparison, **young vs aged** transcriptome was analyzed. Since it is not a novel comparison, we only discuss it in terms of differences in the two HFpEF states. Biological processes associated with leukocyte dynamics were highly enriched along with muscle and tissue remodeling. KEGG pathways analysis revealed enrichment of arrhythmogenic right ventricular cardiomyopathy (ARVC), DCM/HCM, rheumatoid arthritis and complement activation. Which was not the case in dyslipidemic HFpEF. Recent studies have characterized right ventricular defects in HFpEF patients and have reported that arrhythmogenic mechanisms can be prevalent in certain pheno-groups (Mohammed et al., 2014). Among the upregulated genes were CD209 and Vgll2 (Vestigial like family member 2). Vgll2 overexpression in myocytes has been linked to reduced muscle mass and efficiency and may play key roles in age related skeletal muscle changes that can ultimately affect the heart (Honda et al., 2017). CD209 was also upregulated, this protein is reported to be positively corelated with levels of reparative fibrosis. Patients with higher infiltration of CD209 positive cell in myocardial infarct zone have been reported to have higher levels of fibrosis (Nagai et al., 2014).

This brings us to the most important comparisons of HFrEF vs HFpEF and the two HFpEF subtypes. In two types of distinct HF, the biological processes that were overrepresented were related the most to actin and myosin dynamics, which may putatively explain the broad range differences in systolic and diastolic parameters. In **ND TAC vs HFD TAC**, cardiomyocyte differentiation, skeletal muscle process and differentiation along with second messenger signaling were also enriched. Consequently the cellular component was enriched in sarcolemma, ECM, contractile fiber, microtubule and spindle. T-tubule related microdefects have been corelated with HFpEF previously (Frisk et al., 2021). KEGG pathway analysis revealed representation of oocyte maturation mediated by progesterone and interestingly, adrenergic signaling in cardiomyocytes. Adrenergic signaling and its defects are important mediators in chronotropic incompetence, we looked at adrenergic signaling pathway in detail and found changes in key genes which may be potential therapeutic targets in this selectively

dysregulated pathway between HFrEF and HFpEF like states. While some literature is available on such differences (Kilfoil et al., 2020; Lohse et al., 2003) our study provides a repertoire of previously unknown and selective targets. Deregulated genes with the highest significance are now discussed. Igfbp6 (insulin-like growth factor II binding protein 6) was upregulated in HFD-TAC. It is known that prolonged states of hypoxia can increase its expression in vascular endothelial cells (Zhang et al., 2012) and its mRNA expression was increased after explantation of a left ventricular assist device (Barton et al., 2005). This suggests that this gene may be involved in homeostasis of repair and injury. Pentraxin 4 (Ptx4) was also highly upregulated and while a lot of literature is available on the role of pentraxin 3 in HF, Ptx4 has not received due attention. We suggest that it is worth investigating because of its differential expression between the two HF states. Tenemodulin (Tnmd) was also upregulated and it is of importance because its genetic variations have been implicated in high risk of type 2 diabetes, central obesity, and impaired glucose metabolism. Its levels have also been correlated with levels of serum inflammatory markers (Tolppanen et al., 2008). We feel that this gene may have a therapeutic and biomarker potential exclusively in chronic low-grade inflammatory states of dyslipidemic HFpEF. Among the uniquely downregulated genes was Rap1Gap (regulating GTPase-activating-protein) which is known to mediate angiotensin-II induced cardiomyocyte hypertrophy through its inhibitory effects on autophagy and oxidative damage (Gao et al., 2021). We provide here a novel evidence that this important cardioprotective protein is highly downregulated between HFrEF and dyslipidemic HFpEF and could be a lucrative therapeutic target. In a similar manner, Myocardin (Myocd) was also reduced which is known to be involved in maintenance of cardiomyocyte structure and sarcomeric organization, and its ablation is linked to rapidly progressing HF (Huang et al., 2009).

The two HFpEF subtypes were compared next. Between **aging vs dyslipidemic HFpEF (HFD TAC)**, highly overrepresented biological processes were involved in chemokine signaling, chemotaxis, tissue remodeling, ECM structure, growth factor signaling, cell adhesion, angiogenesis and circulatory processes. Consequently, the cellular processes reflected this as they were enriched with ECM, contractile fibers and notably, transport vesicles. KEGG pathway terms showed HCM/DCM, protein digestion, ECM receptor interaction, AGE/RAGE signaling in diabetes, PI3-Akt and cytokine-cytokine interaction. The most significantly represented pathway was the ECM receptor interaction and several elements within it were deregulated including: collagen, laminin, reelin, fibronectin, tenascin, syndecan and thrombospondin to name a few. This suggests that the two index-events of dyslipidemia + PO and aging may lead to distinct alteration of the ECM dynamics. In this regard, the common set of Xirp2, Nrap, Synpo2l, Myh7 and Col1 subtypes were upregulated here as well. Pentraxin4 and Nppb were upregulated. In terms of unique representation, we found a few candidates. Enah (enabled homolog) is a structural sarcomeric component and its overexpression is linked to enhancement of HF

after cardiac injury in mice (Belmonte et al., 2013). This can be corelated to the comparison of HFD+ PO related explicit cardiac injury vs natural aging. Another candidate was Tbx15 (T box 15) which is interestingly known to be a master trans regulator of abdominal obesity genes (Pan et al., 2021). A study has suggested that complementary activation of Tbx15 enhanced glycolytic metabolism in concurrence with the inhibition of PPAR signaling leading to exacerbated metabolic effects associated with DCM (Burke et al., 2016). Due to its strategic placement, it may be a good therapeutic target in dysmetabolic subtypes of HFpEF. Highly downregulated genes that were unique to this set included the newly discovered Efemp1 (ECM protein fibulin 3) which has been corelated to be concomitant with diastolic function indices of E/e' and is a strong predicator of HF hospitalizations (Hiromi et al., 2022). It is reported to be a matrix metalloprotein inhibitor and is implicated in angiogenesis (Zhang et al., 2009). CD209 is implicated in reparative fibrosis associated with adaptive remodeling in HF, its downregulation between the two HFpEF subtypes may suggest differences in not only activation of fibrosis but also inhibition of reparative fibrosis from turning pathologic in nature (Nagai et al., 2014).

To summarize, transcriptomic analysis identified several genes of known and unknown functions implicated in HFpEF vs HFrEF and within the two HFpEF subtypes suggesting that these HF states are mechanistically different pheno-groups and warrant a tailored approach towards disease modeling and therapy.

Limitations:

Even though this cross-comparative approach provided a lot of information on the differential pathomechanisms of these models, it is important to talk about potential caveats in the study.

1. HF is highly dynamic and whether HFpEF and HFrEF are distinct or progressive states of the same HF spectrum is still hotly debated in the medical community. What we have tried to capture with our models is a snapshot of characteristics that resemble HFrEF or HFpEF like states and not a fixed end point but a rather dynamic phenotype.
2. We have characterized the models after a relatively short term after PO compared to other studies. It may be worthwhile to explore a long term effects on these animals.
3. HF in mice is not like humans which develops "insidiously over several years". HF in murine models tend to quickly proceed to advanced stages reflecting HFrEF, this may affect extrapolation of our findings to long term effects.
4. It would have been beneficial to characterize the aspect of exercise stress test in HFpEF models because exercise intolerance is an important cornerstone in its pathophysiology. Due to the limited scope of the dissertation project, this aspect could not be investigated.
5. Validation of important targets of transcriptomics data could not be done due to time constraints.

Conclusions and outlook:

In this study we have adopted a novel cross- comparative approach towards demystifying the mechanistic differences in HFpEF subtypes through dedicated mouse models. We also report the use of an intuitive two-hit combination of dyslipidemia and low grade pressure overload to model metabolic syndrome in HFpEF. Our data collectively describes why some HFpEF (and its subtypes) and HFrEF share pathological characteristics and what is unique between them. Collectively, our results from characterization experiments suggest that the two HFpEF like states driven by distinct etiologies- ''metabolic'' and ''geriatric''; differ on various levels of cardiac structure and function amongst each other and with HFrEF. Dyslipidemia+ low grade pressure overload gave rise to an overall hypertrophic, highly inflammatory, steatotic, fibrotic, apoptotic phenotype with some calcium kinetics dysfunction. LA hypertrophy and LV concentric hypertrophy were evident here. Moreover, we could provide evidence of a shift in HF spectrum towards preservation of ejection fraction with the combination of high fat diet and low grade pressure overload, further reinforcing the implication of dyslipidemic metabolic effects in HFpEF. In contrast, aging induced HFpEF exhibited a non-hypertrophic, non-steatotic, highly fibrotic apoptotic phenotype with highly pronounced differences in calcium handling. However, it showed no evidence for LV and LA remodeling.

Moreover, differential analysis of the transcriptome generated through this study will continue to provide potential biomarkers and therapeutic targets between different HFpEF subtypes for further validation. For future work, sex specific differences in these mechanisms could be investigated by including male models as well. Another important avenue worth exploring would be to try and reverse these deleterious effects by reversing PO or through dietary improvements to ''cure'' the HFpEF phenotype. A cross comparative approach like this nonetheless gives us an opportunity to customize disease modeling for a highly variable syndrome like HFpEF into distinct tailor-made models. These models can then be correlated with HFpEF subtypes in the clinic and be used to test personalized therapeutic approaches, which would be the ultimate goal of these endeavors.

References:

Abraham WT, Lindenfeld J, Ponikowski P, Agostoni P, Butler J, Desai AS, Filippatos G, Gniot J, Fu M, Gullestad L, Howlett JG, Nicholls SJ, Redon J, Schenkenberger I, Silva-Cardoso J, Störk S, Krzysztof Wranicz J, Savarese G, Brueckmann M, Jamal W, Nordaby M, Peil B, Ritter I, Ustyugova A, Zeller C, Salsali A, Anker SD. Effect of empagliflozin on exercise ability and symptoms in heart failure patients with reduced and preserved ejection fraction, with and without type 2 diabetes. Eur. J. Heart. Fail. 42, 700-710 (2021).

Agrawal V, Fortune N, Yu S, Fuentes J, Shi F, Nichols D, Gleaves L, Poovey E, Wang TJ, Brittain EL, Collins S, West JD, Hemnes AR. Natriuretic peptide receptor C contributes to disproportionate right ventricular hypertrophy in a rodent model of obesity-induced heart failure with preserved ejection fraction with pulmonary hypertension. Pulm. Circ. 9, 1–10 (2019).

Akiyama E, Sugiyama S, Matsuzawa Y, Konishi M, Suzuki H, Nozaki T, Ohba K, Matsubara J, Maeda H, Horibata Y, Sakamoto K, Sugamura K, Yamamuro M, Sumida H, Kaikita K, Iwashita S, Matsui K, Kimura K, Umemura S, Ogawa H. Incremental prognostic significance of peripheral endothelial dysfunction in patients with heart failure with normal left ventricular ejection fraction. J. Am. Coll. Cardiol. 60, 1778–1786 (2012).

Akki, A., Zhang, M., Murdoch, C., Brewer, A., Shah, A. M. NADPH oxidase signaling and cardiac myocyte function. J. Mol. Cell. Cardiol. 47, 15–22 (2009).

Albar Z, Albakri M, Hajjari J, Karnib M, Janus SE, Al-Kindi SG. Inflammatory Markers and Risk of Heart Failure With Reduced to Preserved Ejection Fraction. Am. J. Cardiol. 167, 68–75 (2022).

Anderson, M. E., Brown, J. H., Bers, D. M. CaMKII in myocardial hypertrophy and heart failure. J. Mol. Cell. Cardiol. 51, 468–473 (2011).

Andrews, S. Babraham Bioinformatics - FastQC A Quality Control tool for High Throughput Sequence Data. Soil 5 at https://www.bioinformatics.babraham.ac.uk/projects/fastqc/ (2010).

Arcopinto, M., Valente, V., Giardino, F., Marra, A. M., Cittadini, A. What have we learned so far from the sex/gender issue in heart failure? An overview of current evidence. Intern. Emerg. Med. 17, 1589–1598 (2022).

Armstrong AC, Gjesdal O, Almeida A, Nacif M, Wu C, Bluemke DA, Brumback L, Lima JA. Left ventricular mass and hypertrophy by echocardiography and cardiac magnetic resonance: The Multi-Ethnic study of atherosclerosis. Echocardiography 31, 12–20 (2014).

Aurich AC, Niemann B, Pan R, Gruenler S, Issa H, Silber RE, Rohrbach S. Age-dependent effects of high fat-diet on murine left ventricles: Role of palmitate. Basic Res. Cardiol. 108, 5–10 (2013).

Backs, J., Song, K., Bezprozvannaya, S., Chang, S., Olson, E. N. CaM kinase II selectively signals to histone deacetylase 4 during cardiomyocyte hypertrophy. J. Clin. Invest. 116, 1853–1864 (2006).

Bairey Merz CN, Zamani SK, Samuel TJ, Wei J, Thomson LEJ, Tamarappoo B, Sharif B, Nelson MD. Left atrial stiffness in women with ischemia and no obstructive coronary artery disease: Novel insight from left atrial feature tracking. Clin. Cardiol. 43, 986-992 (2020).

Barry, W. H., Bridge, J. H. B. Intracellular calcium homeostasis in cardiac myocytes. Circulation 87, 1806–1815 (1993).

Barton PJ, Felkin LE, Birks EJ, Cullen ME, Banner NR, Grindle S, Hall JL, Miller LW, Yacoub MH. Myocardial insulin-like growth factor-I gene expression during recovery from heart failure after combined left ventricular assist device and clenbuterol therapy. Circulation 112, 146–150 (2005).

Beale AL, Nanayakkara S, Segan L, Mariani JA, Maeder MT, van Empel V, Vizi D, Evans S, Lam CSP, Kaye DM. Sex Differences in Heart Failure With Preserved Ejection Fraction Pathophysiology: A Detailed Invasive Hemodynamic and Echocardiographic Analysis. JACC Heart. Fail. 7, 239–249 (2019).

Belmonte, S. L., Ram, R., Mickelsen, D. M., Gertler, F. B., Blaxall, B. C. Cardiac overexpression of Mammalian enabled (Mena) exacerbates heart failure in mice. Am. J. Physiol. Heart. Circ. Physiol. 305, H875-84 (2013).

Bhan A, Sirker A, Zhang J, Protti A, Catibog N, Driver W, Botnar R, Monaghan MJ, Shah AM. High-frequency speckle tracking echocardiography in the assessment of left ventricular function and remodeling after murine myocardial infarction. Am. J. Physiol. Heart. Circ. Physiol. 306, H1371-83 (2014).

Bhatt DL, Szarek M, Steg PG, Cannon CP, Leiter LA, McGuire DK, Lewis JB, Riddle MC, Voors AA, Metra M, Lund LH, Komajda M, Testani JM, Wilcox CS, Ponikowski P, Lopes RD, Verma S, Lapuerta P, Pitt B. Sotagliflozin in Patients with Diabetes and Recent Worsening Heart Failure. N. Engl. J. Med. 384, 117–128 (2021).

Bielecka-Dabrowa A, Sakowicz A, Misztal M, von Haehling S, Ahmed A, Pietrucha T, Rysz J, Banach M. Differences in biochemical and genetic biomarkers in patients with heart failure of various etiologies. Int. J. Cardiol. 221, 1073–1080 (2016).

Biswas D, Tozer K, Dao KT, Perez LJ, Mercer A, Brown A, Hossain I, Yip AM, Aguiar C, Motawea H, Brunt KR, Shea J, Legare JF, Hassan A, Kienesberger PC, Pulinilkunnil T. Adverse Outcomes in Obese Cardiac Surgery Patients Correlates With Altered Branched-Chain Amino Acid Catabolism in Adipose Tissue and Heart. Front. Endocrinol. (Lausanne). 11, 534–538 (2020).

Borbély A, van der Velden J, Papp Z, Bronzwaer JG, Edes I, Stienen GJ, Paulus WJ. Cardiomyocyte stiffness in diastolic heart failure. Circulation 111, 774–781 (2005).

Borlaug BA, Anstrom KJ, Lewis GD, Shah SJ, Levine JA, Koepp GA, Givertz MM, Felker GM, LeWinter MM, Mann DL, Margulies KB, Smith AL, Tang WHW, Whellan DJ, Chen HH, Davila-Roman VG, McNulty S, Desvigne-Nickens P, Hernandez AF, Braunwald E, Redfield MM. Effect of Inorganic Nitrite vs Placebo on Exercise Capacity Among Patients With Heart Failure With Preserved Ejection Fraction: The INDIE-HFpEF Randomized Clinical Trial. JAMA - J. Am. Med. Assoc. 320, 1764–1773 (2018).

Borlaug BA, Kass DA. Invasive hemodynamic assessment in heart failure. Cardiol. Clin. 29, 269-80 (2011).

Borlaug BA, Kass DA. Ventricular-vascular interaction in heart failure. Heart. Fail. Clin. 4, 23–36 (2008).

Borlaug BA, Melenovsky V, Russell SD, Kessler K, Pacak K, Becker LC, Kass DA. Impaired chronotropic and vasodilator reserves limit exercise capacity in patients with heart failure and a preserved ejection fraction. Circulation 114, 2138–2147 (2006).

Borlaug BA, Olson TP, Lam CS, Flood KS, Lerman A, Johnson BD, Redfield MM. Global cardiovascular reserve dysfunction in heart failure with preserved ejection fraction. J. Am. Coll. Cardiol. 56, 845–854 (2010).

Borlaug, B. A. The pathophysiology of heart failure with preserved ejection fraction. Nat. Rev. Cardiol. 11, 507–515 (2014).

Bouton, M. C., Corral, J., Lucas, A. R. Editorial: The Serpin Family in the Cardiovascular System. Front. Cardiovasc. Med. 8, 490 (2021).

Bozkurt B, Coats AJS, Tsutsui H, Abdelhamid CM, Adamopoulos S, Albert N, Anker SD, Atherton J, Böhm M, Butler J, Drazner MH, Michael Felker G, Filippatos G, Fiuzat M, Fonarow GC, Gomez-Mesa JE, Heidenreich P, Imamura T, Jankowska EA, Januzzi J, Khazanie P, Kinugawa K, Lam CSP, Matsue Y, Metra M, Ohtani T, Francesco Piepoli M, Ponikowski P, Rosano GMC, Sakata Y, Seferović P, Starling RC, Teerlink JR, Vardeny O, Yamamoto K, Yancy C, Zhang J, Zieroth S. Universal definition and classification of heart failure: a report of the Heart Failure Society of America, Heart Failure Association of the European Society of Cardiology, Japanese Heart Failure Society and Writing Committee of the Universal Definition. Eur. J. Heart. fail. 23, 352–380 (2021).

Bradley D, Smith AJ, Blaszczak A, Shantaram D, Bergin SM, Jalilvand A, Wright V, Wyne KL, Dewal RS, Baer LA, Wright KR, Stanford KI, Needleman B, Brethauer S, Noria S, Renton D, Joseph JJ, Lovett-Racke A, Liu J, Hsueh WA. Interferon gamma mediates the reduction of adipose tissue regulatory T cells in human obesity. Nat. Commun. 13, 5606 (2022).

Bridge, J. H. B., Smolley, J. R., Spitzer, K. W. The Relationship Between Charge Movements Associated with I Ca and I Na-Ca in Cardiac Myocyte. Science 248, 376–378 (1990).

Bristow MR, Saxon LA, Feldman AM, Mei C, Anderson SA, DeMets DL. Lessons Learned and Insights Gained in the Design, Analysis, and Outcomes of the COMPANION Trial. JACC Heart. Fail. 7, 521-535 (2016).

Broderick TL, Jankowski M, Wang D, Danalache BA, Parrott CR, Gutkowska J. Downregulation in GATA4 and Downstream Structural and Contractile Genes in the db/db Mouse Heart. ISRN Endocrinol. 2012, 1–12 (2012).

Brubaker PH, Joo KC, Stewart KP, Fray B, Moore B, Kitzman DW. Chronotropic incompetence and its contribution to exercise intolerance in older heart failure patients. J. Cardiopulm. Rehabil. 26, 86–89 (2006).

Buckley, L. F., Abbate, A. Interleukin-1 blockade in cardiovascular diseases: A clinical update. Eur. J. Heart Fail. 39, 2063–2069 (2018).

Burke MA, Chang S, Wakimoto H, Gorham JM, Conner DA, Christodoulou DC, Parfenov MG, DePalma SR, Eminaga S, Konno T, Seidman JG, Seidman CE. Molecular profiling of dilated cardiomyopathy that progresses to heart failure. JCI Insight 1, 898–907 (2016).

Caligiuri, G. Mechanotransduction, immunoregulation, and metabolic functions of CD31 in cardiovascular pathophysiology. Cardiovasc. Res. 115, 1425–1434 (2019).

Castillo, E. C., Vázquez-Garza, E., Yee-Trejo, D., García-Rivas, G., Torre-Amione, G. What Is the Role of the Inflammation in the Pathogenesis of Heart Failure? Curr. Cardiol. Rep. 22, 139–148 (2020).

Cavalera, M., Wang, J., Frangogiannis, N. G. Obesity, metabolic dysfunction, and cardiac fibrosis: Pathophysiological pathways, molecular mechanisms, and therapeutic opportunities. Transl. Res. 164, 323–335 (2014).

Chaanine, A. H., Hajjar, R. J. AKT signalling in the failing heart. Eur. J. Heart. Fail. 13, 825–829 (2011).

Che Y, Wang ZP, Yuan Y, Zhang N, Jin YG, Wan CX, Tang QZ. Role of autophagy in a model of obesity: A long-term high fat diet induces cardiac dysfunction. Mol. Med. Rep. 18, 3251–3261 (2018).

Chirinos JA, Bhattacharya P, Kumar A, Proto E, Konda P, Segers P, Akers SR, Townsend RR, Zamani P. Impact of diabetes mellitus on ventricular structure, arterial stiffness, and pulsatile hemodynamics in heart failure with preserved ejection fraction. J. Am. Heart. Assoc. 8, 457–477 (2019).

Christoffersen C, Bollano E, Lindegaard ML, Bartels ED, Goetze JP, Andersen CB, Nielsen LB. Cardiac lipid accumulation associated with diastolic dysfunction in obese mice. Endocrinology 144, 3483–3490 (2003).

Cieslik, K. A., Trial, J. A., Crawford, J. R., Taffet, G. E., Entman, M. L. Adverse fibrosis in the aging heart depends on signaling between myeloid and mesenchymal cells; role of inflammatory fibroblasts. J. Mol. Cell. Cardiol. 70, 56–63 (2014).

Clausen, A. G., Vad, O. B., Andersen, J. H., Olesen, M. S. Loss-of-Function Variants in the SYNPO2L Gene Are Associated With Atrial Fibrillation. Front. Cardiovasc. Med. 8, 667–674 (2021).

Clément K. Genetics of human obesity. C. R. Biol. 329, 608-622 (2006).

Clemenza, F., Citarrella, R., Patti, A., Rizzo, M. Obesity and HFpEF. J. Clin. Med. 11, 3858 (2022).

Dauterman K, Pak PH, Maughan WL, Nussbacher A, Ariê S, Liu CP, Kass DA. Contribution of external forces to left ventricular diastolic pressure: Implications for the clinical use of the starling law. Ann. Intern. Med. 122, 737–742 (1995).

Dávila-Román VG, Vedala G, Herrero P, de las Fuentes L, Rogers JG, Kelly DP, Gropler RJ. Altered myocardial fatty acid and glucose metabolism in idiopathic dilated cardiomyopathy. J. Am. Coll. Cardiol. 40, 271–277 (2002).

de Boer RA, De Keulenaer G, Bauersachs J, Brutsaert D, Cleland JG, Diez J, Du XJ, Ford P, Heinzel FR, Lipson KE, McDonagh T, Lopez-Andres N, Lunde IG, Lyon AR, Pollesello P, Prasad SK, Tocchetti CG, Mayr M, Sluijter JPG, Thum T, Tschöpe C, Zannad F, Zimmermann WH, Ruschitzka F, Filippatos G, Lindsey ML, Maack C, Heymans S. Towards better definition, quantification and treatment of fibrosis in heart failure. A scientific roadmap by the Committee of Translational Research of the Heart Failure Association (HFA) of the European Society of Cardiology. Eur. J. Heart. Fail. 21, 272–285 (2019).

DeBosch B, Treskov I, Lupu TS, Weinheimer C, Kovacs A, Courtois M, Muslin AJ. Akt1 is required for physiological cardiac growth. Circulation 113, 2097–2104 (2006).

Deng Y, Xie M, Li Q, Xu X, Ou W, Zhang Y, Xiao H, Yu H, Zheng Y, Liang Y, Jiang C, Chen G, Du D, Zheng W, Wang S, Gong M, Chen Y, Tian R, Li T. Targeting Mitochondria-Inflammation Circuit by β-Hydroxybutyrate Mitigates HFpEF. Circ. Res. 128, 232–245 (2021).

Djoussé L, Matsumoto C, Petrone A, Weir NL, Tsai MY, Gaziano JM. Plasma galectin 3 and heart failure risk in the Physicians' Health Study. Eur. J. Heart. Fail. 16, 350-354 (2014).

Dobin A, Davis CA, Schlesinger F, Drenkow J, Zaleski C, Jha S, Batut P, Chaisson M, Gingeras TR. STAR: Ultrafast universal RNA-seq aligner. Bioinformatics 29, 15–21 (2013).

Doi R, Masuyama T, Yamamoto K, Doi Y, Mano T, Sakata Y, Ono K, Kuzuya T, Hirota S, Koyama T, Miwa T, Hori M. Development of different phenotypes of hypertensive heart failure: Systolic versus diastolic failure in Dahl salt-sensitive rats. J. Hypertens. 18, 111–120 (2000).

Donaldson C, Palmer BM, Zile M, Maughan DW, Ikonomidis JS, Granzier H, Meyer M, VanBuren P, LeWinter MM. Myosin cross-bridge dynamics in patients with hypertension and concentric left ventricular remodeling. Circ. Heart. Fail. 5, 803–811 (2012).

Dunlay, S. M., Roger, V. L., Redfield, M. M. Epidemiology of heart failure with preserved ejection fraction. Nat. Rev. Cardiol. 14, 591–602 (2017).

Durinck, S., Spellman, P. T., Birney, E., Huber, W. Mapping identifiers for the integration of genomic datasets with the R/ Bioconductor package biomaRt. Nat. Protoc. 4, 1184–1191 (2009).

Eaton CB, Pettinger M, Rossouw J, Martin LW, Foraker R, Quddus A, Liu S, Wampler NS, Hank Wu WC, Manson JE, Margolis K, Johnson KC, Allison M, Corbie-Smith G, Rosamond W, Breathett K, Klein L. Risk Factors for Incident Hospitalized Heart Failure with Preserved Versus Reduced Ejection Fraction in a Multiracial Cohort of Postmenopausal Women. Circ. Heart. Fail. 9, 883–893 (2016).

Eichhorn, E. J., Bristow, M. R. Medical therapy can improve the biological properties of the chronically failing heart: A new era in the treatment of heart failure. Circulation 94, 2285–2296 (1996).

Ennezat PV, Lefetz Y, Maréchaux S, Six-Carpentier M, Deklunder G, Montaigne D, Bauchart JJ, Mounier-Véhier C, Jude B, Nevière R, Bauters C, Asseman P, de Groote P, Lejemtel TH. Left Ventricular Abnormal Response During Dynamic Exercise in Patients With Heart Failure and Preserved Left Ventricular Ejection Fraction at Rest. J. Card. Fail. 14, 475–480 (2008).

Escalante, N. K., Von Rossum, A., Lee, M., Choy, J. C. CD155 on human vascular endothelial cells attenuates the acquisition of effector functions in CD8 T cells. Arterioscler. Thromb. Vasc. Biol. 31, 1177–1184 (2011).

Fan LM, Cahill-Smith S, Geng L, Du J, Brooks G, Li JM. Aging-associated metabolic disorder induces Nox2 activation and oxidative damage of endothelial function. Free. Radic. Biol. Med. 108, 940–951 (2017).

Ferrannini, E., Mark, M., Mayoux, E. CV protection in the EMPA-REG OUTCOME trial: A thrifty substrate hypothesis. Diab. Care. 39, 1108–1114 (2016).

Ferrari R, Böhm M, Cleland JG, Paulus WJ, Pieske B, Rapezzi C, Tavazzi L. Heart failure with preserved ejection fraction: Uncertainties and dilemmas. Eur. J. Heart. Fail. 17, 665–671 (2015).

Fischer TA, Ludwig S, Flory E, Gambaryan S, Singh K, Finn P, Pfeffer MA, Kelly RA, Pfeffer JM. Activation of cardiac c-Jun NH2-terminal kinases and p38-mitogen-activated protein kinases with abrupt changes in hemodynamic load. Hypertension 37, 1222–1228 (2001).

Flurkey, C. The mouse in biomedical research. Elsevier 1–313 (Amsterdam; Boston, 2007).

Frisk, M., Le, C., Shen, X. Etiology-Dependent Impairment of Diastolic Cardiomyocyte Calcium Homeostasis in Heart Failure With Preserved Ejection Fraction. J. Am. Coll. Cardiol. 77, 405–419 (2021).

Gallo, S., Vitacolonna, A., Bonzano, A., Comoglio, P., Crepaldi, T. ERK: A key player in the pathophysiology of cardiac hypertrophy. Int. J. Mol. Sci. 20, 2164–2170 (2019).

Gandhi SK, Powers JC, Nomeir AM, Fowle K, Kitzman DW, Rankin KM, Little WC. The Pathogenesis of Acute Pulmonary Edema Associated with Hypertension. N. Engl. J. Med. 344, 17–22 (2001).

Gao Y, Bai X, Lu J, Zhang L, Yan X, Huang X, Dai H, Wang Y, Hou L, Wang S, Tian A, Li J. Prognostic Value of Multiple Circulating Biomarkers for 2-Year Death in Acute Heart Failure With Preserved Ejection Fraction. Front. Cardiovasc. Med. 8, 282–295 (2021).

Gao Y, Zhao D, Xie WZ, Meng T, Xu C, Liu Y, Zhang P, Bi X, Zhao Z. Rap1GAP Mediates Angiotensin II-Induced Cardiomyocyte Hypertrophy by Inhibiting Autophagy and Increasing Oxidative Stress. Oxid. Med. Cell. Longev. 2021, 27–29 (2021).

Garnier A, Fortin D, Deloménie C, Momken I, Veksler V, Ventura-Clapier R. Depressed mitochondrial transcription factors and oxidative capacity in rat failing cardiac and skeletal muscles. J. Physiol. 551, 491–501 (2003).

Gorgoulis VG, Pratsinis H, Zacharatos P, Demoliou C, Sigala F, Asimacopoulos PJ, Papavassiliou AG, Kletsas D. p53-Dependent ICAM-1 overexpression in senescent human cells identified in atherosclerotic lesions. Lab. Investig. 85, 502–511 (2005).

Grützner A, Garcia-Manyes S, Kötter S, Badilla CL, Fernandez JM, Linke WA. Modulation of titin-based stiffness by disulfide bonding in the cardiac titin N2-B unique sequence. Biophys. J. 97, 825–834 (2009).

Guo Y, Mei Z, Li D, Banerjee A, Khalil MA, Burke A, Ritter J, Lau C, Kreisel D, Gelman AE, Jacobsen E, Luzina IG, Atamas SP, Krupnick AS. Ischemia reperfusion injury facilitates lung allograft acceptance through IL-33-mediated activation of donor-derived IL-5 producing group 2 innate lymphoid cells. Am. J. Transplant. 22, 1963-1975 (2022).

Gupta R, Ranchal P, Mahajan S, Pattarkine R, Patibandla S, Fallon JT, Lanier GM. Lipid inclusions in cardiac myocytes-A rare case of cardiolipotoxicity. Future. Cardiol. 17, 293–299 (2021).

Hahn VS, Yanek LR, Vaishnav J, Ying W, Vaidya D, Lee YZJ, Riley SJ, Subramanya V, Brown EE, Hopkins CD, Ononogbu S, Perzel Mandell K, Halushka MK, Steenbergen C Jr, Rosenberg AZ, Tedford RJ, Judge DP, Shah SJ, Russell SD, Kass DA, Sharma K. Endomyocardial Biopsy Characterization of Heart Failure With Preserved Ejection Fraction and Prevalence of Cardiac Amyloidosis. JACC Heart. Fail. 8, 712–724 (2020).

Hamdani, N., Franssen, C. & Lourenzo, A. Myocardial titin hypophosphorylation importantly contributes to heart failure with preserved ejection fraction in a rat metabolic risk model. Circ. Heart. Fail. 6, 1239–1249 (2013).

Hamdani, N., Krysiak, J., Kreusser, M. M., Neef, S. Hamdani N, Krysiak J, Kreusser MM, et al. Crucial role for Ca2(+) /calmodulin-dependent protein kinase-II in regulating diastolic stress of normal and failing hearts via titin phosphorylation. Circ. Res. 112, 664–674 (2013).

Harvey AP, Robinson E, Edgar KS, McMullan R, O'Neill KM, Alderdice M, Amirkhah R, Dunne PD, McDermott BJ, Grieve DJ. Downregulation of PPARA during experimental left ventricular hypertrophy is critically dependent on NOX2 nadph oxidase signalling. Int. J. Mol. Sci. 21, 1–21 (2020).

Haykowsky MJ, Brubaker PH, John JM, Stewart KP, Morgan TM, Kitzman DW. Determinants of exercise intolerance in elderly heart failure patients with preserved ejection fraction. J. Am. Coll. Cardiol. 58, 265–274 (2011).

Hiromi W.L. Koh, Anna Pilbrow, Sock Hwee Tan, Qing Zhao, Peter I. Benke, Bo Burla, Federico Torta, John W. Pickering, Richard Troughton, Christopher Pemberton, Wern-Miin Soo, Lieng Hsi Ling, Robert N. Doughty, Hyungwon Choi, Markus R. Wenk, A. Mark Richards, Mark Y. Chan. Plasma multi-omic and

cardiac imaging network signatures predict poor long-term outcomes after acute myocardial infarction. medRxiv 10, 682–694 (2022).

Ho JE, Lyass A, Lee DS, Vasan RS, Kannel WB, Larson MG, Levy D. Predictors of new-onset heart failure differences in preserved versus reduced ejection fraction. Circ. Heart. Fail. 6, 279–286 (2013).

Honda M, Hidaka K, Fukada SI, Sugawa R, Shirai M, Ikawa M, Morisaki T. Vestigial-like 2 contributes to normal muscle fiber type distribution in mice. Sci. Rep. 7, 7168 (2017).

Hu P, Zhang D, Swenson L, Chakrabarti G, Abel ED, Litwin SE. Minimally invasive aortic banding in mice: Effects of altered cardiomyocyte insulin signaling during pressure overload. Am. J. Physiol. 285, (2003).

Huang J, Min Lu M, Cheng L, Yuan LJ, Zhu X, Stout AL, Chen M, Li J, Parmacek MS. Myocardin is required for cardiomyocyte survival and maintenance of heart function. Proc. Natl. Acad. Sci. U. S. A. 106, 18734–18739 (2009).

Huang M, Sannaningaiah D, Zhao N, Gong Y, Grondolsky J, Hoover-Plow J. EMILIN2 regulates platelet activation, thrombus formation, and clot retraction. PLoS One 10, 284–292 (2015).

Hundley WG, Kitzman DW, Morgan TM, Hamilton CA, Darty SN, Stewart KP, Herrington DM, Link KM, Little WC. Cardiac cycle-dependent changes in aortic area and distensibility are reduced in older patients with isolated diastolic heart failure and correlate with exercise intolerance. J. Am. Coll. Cardiol. 38, 796–802 (2001).

Januzzi, J. L. Natriuretic peptides, ejection fraction, and prognosis: Parsing the phenotypes of heart failure. J. Am. Coll. Cardiol. 61, 1507–1509 (2013).

Jeong MY, Lin YH, Wennersten SA, Demos-Davies KM, Cavasin MA, Mahaffey JH, Monzani V, Saripalli C, Mascagni P, Reece TB, Ambardekar AV, Granzier HL, Dinarello CA, McKinsey TA. Histone deacetylase activity governs diastolic dysfunction through a nongenomic mechanism. Sci. Transl. Med. 10, 144–154 (2018).

Johnston SL, Souter DM, Tolkamp BJ, Gordon IJ, Illius AW, Kyriazakis I, Speakman JR. Intake compensates for resting metabolic rate variation in female C57BL/6J mice fed high-fat diets. Obesity 15, 600–606 (2007).

Juillière Y, Venner C, Filippetti L, Popovic B, Huttin O, Selton-Suty C. Heart failure with preserved ejection fraction: A systemic disease linked to multiple comorbidities, targeting new therapeutic options. Arch. Cardiovasc. Dis. 111, 766–781 (2018).

Kalogeropoulos AP, Martin RP. Visual assessment of left ventricular function in the era of high definition: the machine and the eye of the beholder. J. Am. Soc. Echocardiogr. 23, 265-266 (2010).

Kaludercic N, Takimoto E, Nagayama T, Feng N, Lai EW, Bedja D, Chen K, Gabrielson KL, Blakely RD, Shih JC, Pacak K, Kass DA, Di Lisa F, Paolocci N. Monoamine oxidase A mediated enhanced catabolism of norepinephrine contributes to adverse remodeling and pump failure in hearts with pressure overload. Circ. Res. 106, 193–202 (2010).

Kao CC, Cheng SY, Wu MY, Chien SC, Lu HF, Hsu YW, Zhang YF, Wu MS, Chang WC. Associations of genetic variants of endothelin with cardiovascular complications in patients with renal failure. BMC Nephrol. 18, 291–298 (2017).

Karwi, Q. G., Uddin, G. M., Ho, K. L., Lopaschuk, G. D. Loss of Metabolic Flexibility in the Failing Heart. Front. Cardiovasc. Med. 6, 68–79 (2018).

Kasner M, Westermann D, Lopez B, Gaub R, Escher F, Kühl U, Schultheiss HP, Tschöpe C. Diastolic tissue doppler indexes correlate with the degree of collagen expression and cross-linking in heart failure and normal ejection fraction. J. Am. Coll. Cardiol. 57, 977–985 (2011).

Kehat, I., Molkentin, J. D. Extracellular signal-regulated kinase 1/2 (ERK1/2) signaling in cardiac hypertrophy. Ann. N. Y. Acad. Sci. 1188, 96–102 (2010).

Khan MS, Fonarow GC, Khan H, Greene SJ, Anker SD, Gheorghiade M, Butler J. Renin–angiotensin blockade in heart failure with preserved ejection fraction: a systematic review and meta-analysis. ESC Heart. Fail. 4, 402–408 (2017).

Kilfoil PJ, Lotteau S, Zhang R, Yue X, Aynaszyan S, Solymani RE, Cingolani E, Marbán E, Goldhaber JI. Distinct features of calcium handling and β-adrenergic sensitivity in heart failure with preserved versus reduced ejection fraction. J. Physiol. 598, 5091–5108 (2020).

Klein, S. L., Flanagan, K. L. Sex differences in immune responses. Nat. Rev. Immun. 16, 626–638 (2016).

Kranstuber AL, Del Rio C, Biesiadecki BJ, Hamlin RL, Ottobre J, Gyorke S, Lacombe VA. Advanced glycation end product cross-link breaker attenuates diabetes-induced cardiac dysfunction by improving sarcoplasmic reticulum calcium handling. Front. Physiol. 3, 292–300 (2012).

Kravtsov, G. M., Kam, K. W. L., Liu, J., Wu, S., Wong, T. M. Altered Ca2+ handling by ryanodine receptor and Na +-Ca2+ exchange in the heart from ovariectomized rats: Role of protein kinase A. Am. J. Physiol. 292, C1625-35 (2007).

Kuo JY, Jin X, Sun JY, Chang SH, Chi PC, Sung KT, Mok GSP, Yun CH, Chang SC, Chung FP, Yu CH, Wu TH, Hung CL, Yeh HI, Lam CSP. Insights on Distinct Left Atrial Remodeling Between Atrial Fibrillation and Heart Failure With Preserved Ejection Fraction. Front. Cardiovasc. Med. 9, 85736 (2022).

Kuwahara F, Kai H, Tokuda K, Kai M, Takeshita A, Egashira K, Imaizumi T. Transforming growth factor-β function blocking prevents myocardial fibrosis and diastolic dysfunction in pressure-overloaded rats. Circulation 106, 130–135 (2002).

Lakatta, E. G., Levy, D. Arterial and cardiac aging: Major shareholders in cardiovascular disease enterprises: Part II: The aging heart in health: Links to heart disease. Circulation 107, 346–354 (2003).

Lam, C. S. P and Solomon, S. D. Classification of Heart Failure According to Ejection Fraction: JACC Review Topic of the Week. J. Am. Coll. Cardiol. 77, 3217–3225 (2021).

Landstrom, A. P., Dobrev, D., Wehrens, X. H. T. Calcium Signaling and Cardiac Arrhythmias. Circ. Res. 120, 1969–1993 (2017).

Lassègue, B., San Martín, A., Griendling, K. K. Biochemistry, physiology, and pathophysiology of NADPH oxidases in the cardiovascular system. Circ. Res. 110, 1364–1390 (2012).

Lau ES, Cunningham T, Hardin KM, Liu E, Malhotra R, Nayor M, Lewis GD, Ho JE. Sex Differences in Cardiometabolic Traits and Determinants of Exercise Capacity in Heart Failure with Preserved Ejection Fraction. JAMA Cardiol. 5, 30–37 (2020).

Lauzier B, Vaillant F, Merlen C, Gélinas R, Bouchard B, Rivard ME, Labarthe F, Dolinsky VW, Dyck JR, Allen BG, Chatham JC, Des Rosiers C. Metabolic effects of glutamine on the heart: Anaplerosis versus the hexosamine biosynthetic pathway. J. Mol. Cell. Cardiol. 55, 92–100 (2013).

Lee DS, Gona P, Vasan RS, Larson MG, Benjamin EJ, Wang TJ, Tu JV, Levy D. Relation of disease pathogenesis and risk factors to heart failure with preserved or reduced ejection fraction: Insights from the framingham heart study of the national heart, lung, and blood institute. Circulation 119, 3070–3077 (2009).

LeWinter, M. M., Granzier, H. L. Titin is a major human disease gene. Circulation 127, 938–944 (2013).

Liao, Y., Smyth, G. K., Shi, W. FeatureCounts: An efficient general purpose program for assigning sequence reads to genomic features. Bioinformatics 30, 923–930 (2014).

Liu, X., Shi, G. P., Guo, J. Innate Immune Cells in Pressure Overload-Induced Cardiac Hypertrophy and Remodeling. Front. Cell. Dev. Biol. 9, 666–679 (2021).

Loffredo FS, Steinhauser ML, Jay SM, Gannon J, Pancoast JR, Yalamanchi P, Sinha M, Dall'Osso C, Khong D, Shadrach JL, Miller CM, Singer BS, Stewart A, Psychogios N, Gerszten RE, Hartigan AJ, Kim MJ, Serwold T, Wagers AJ, Lee RT. Growth differentiation factor 11 is a circulating factor that reverses age-related cardiac hypertrophy. Cell 153, 828–839 (2013).

Lohse MJ, Engelhardt S, Eschenhagen T. What is the role of beta-adrenergic signaling in heart failure? Circ. Res. 93, 896-906 (2003).

López B, Ravassa S, González A, Zubillaga E, Bonavila C, Bergés M, Echegaray K, Beaumont J, Moreno MU, San José G, Larman M, Querejeta R, Díez J. Myocardial collagen cross-linking is associated with heart failure hospitalization in patients with hypertensive heart failure. J. Am. Coll. Cardiol. 67, 251–260 (2016).

Louch, W. E., Stokke, M. K., Sjaastad, I., Christensen, G., Sejersted, O. M. No rest for the weary: Diastolic calcium homeostasis in the normal and failing myocardium. Physiology 27, 308–323 (2012).

Love MI, Huber W, Anders S. Moderated estimation of fold change and dispersion for RNA-seq data with DESeq2. Genome Biol. 15, 550-560 (2014).

Lund, L. H., Oldgren, J., James, S. Registry-Based Pragmatic Trials in Heart Failure: Current Experience and Future Directions. Curr. Heart. Fail. Rep. 14, 59–70 (2017).

Mahmod M, Pal N, Rayner J, Holloway C, Raman B, Dass S, Levelt E, Ariga R, Ferreira V, Banerjee R, Schneider JE, Rodgers C, Francis JM, Karamitsos TD, Frenneaux M, Ashrafian H, Neubauer S, Rider O. The interplay between metabolic alterations, diastolic strain rate and exercise capacity in mild heart failure with preserved ejection fraction: A cardiovascular magnetic resonance study. J. Cardiovasc. Magn. Reson. 20, 88–98 (2018).

Mátyás C, Németh BT, Oláh A, Török M, Ruppert M, Kellermayer D, Barta BA, Szabó G, Kökény G, Horváth EM, Bódi B, Papp Z, Merkely B, Radovits T. Prevention of the development of heart failure with preserved ejection fraction by the phosphodiesterase-5A inhibitor vardenafil in rats with type 2 diabetes. Eur. J. Heart. Fail. 19, 326–336 (2017).

McCluskey, C., Mooney, L., Paul, A., Currie, S. Compromised cardiovascular function in aged rats corresponds with increased expression and activity of calcium/calmodulin dependent protein kinase IIδ in aortic endothelium. Vascul. Pharmacol. 118, 118–119 (2019).

McDonagh TA, Metra M, Adamo M, Gardner RS, Baumbach A, Böhm M, Burri H, Butler J, Čelutkienė J, Chioncel O, Cleland JGF, Coats AJS, Crespo-Leiro MG, Farmakis D, Gilard M, Heymans S, Hoes AW, Jaarsma T, Jankowska EA, Lainscak M, Lam CSP, Lyon AR, McMurray JJV, Mebazaa A, Mindham R, Muneretto C, Francesco Piepoli M, Price S, Rosano GMC, Ruschitzka F, Kathrine Skibelund A. 2021 ESC

Guidelines for the diagnosis and treatment of acute and chronic heart failure. Eur. J. Heart Fail. 42, 3599–3726 at (2021).

McHugh K, DeVore AD, Wu J, Matsouaka RA, Fonarow GC, Heidenreich PA, Yancy CW, Green JB, Altman N, Hernandez AF. Heart Failure With Preserved Ejection Fraction and Diabetes: JACC State-of-the-Art Review. J. Am. Coll. Cardiol.73, 602–611 (2019).

McMurray JJ, Carson PE, Komajda M, McKelvie R, Zile MR, Ptaszynska A, Staiger C, Donovan JM, Massie BM. Heart failure with preserved ejection fraction: Clinical characteristics of 4133 patients enrolled in the I-PRESERVE trial. Eur. J. Heart Fail. 10, 149–156 (2008).

Mehlem, A., Hagberg, C. E., Muhl, L., Eriksson, U., Falkevall, A. Imaging of neutral lipids by oil red O for analyzing the metabolic status in health and disease. Nat. Protoc. 8, 1149–1154 (2013).

Mele, D., Nardozza, M., Ferrari, R. Left ventricular ejection fraction and heart failure: an indissoluble marriage? Eur. J. Heart. Fail. 20, 427–430 (2018).

Melenovsky V, Borlaug BA, Rosen B, Hay I, Ferruci L, Morell CH, Lakatta EG, Najjar SS, Kass DA. Cardiovascular Features of Heart Failure With Preserved Ejection Fraction Versus Nonfailing Hypertensive Left Ventricular Hypertrophy in the Urban Baltimore Community. The Role of Atrial Remodeling/Dysfunction. J. Am. Coll. Cardiol. 49, 198–207 (2007).

Melenovsky V, Hwang SJ, Redfield MM, Zakeri R, Lin G, Borlaug BA. Left atrial remodeling and function in advanced heart failure with preserved or reduced ejection fraction. Circ. Heart. Fail. 8, 295–303 (2015).

Meng Q, Lai YC, Kelly NJ, Bueno M, Baust JJ, Bachman TN, Goncharov D, Vanderpool RR, Radder JE, Hu J, Goncharova E, Morris AM, Mora AL, Shapiro SD, Gladwin MT. Development of a mouse model of metabolic syndrome, pulmonary hypertension, and heart failure with preserved ejection fraction. Am. J. Respir. Cell. Mol. Biol. 56, 497–505 (2017).

Mesquita T, Zhang R, Cho JH, Zhang R, Lin YN, Sanchez L, Goldhaber JI, Yu JK, Liang JA, Liu W, Trayanova NA, Cingolani E. Mechanisms of Sinoatrial Node Dysfunction in Heart Failure With Preserved Ejection Fraction. Circulation 145, 45-60 (2022).

Miranda-Silva D, Wüst RCI, Conceição G, Gonçalves-Rodrigues P, Gonçalves N, Gonçalves A, Kuster DWD, Leite-Moreira AF, van der Velden J, de Sousa Beleza JM, Magalhães J, Stienen GJM, Falcão-Pires I. Disturbed cardiac mitochondrial and cytosolic calcium handling in a metabolic risk-related rat model of heart failure with preserved ejection fraction. Acta Physiol. 228, 378–286 (2020).

Mishra, S., Kass, D. A. Cellular and molecular pathobiology of heart failure with preserved ejection fraction. Nat. Rev. Cardiol. 18, 400–423 (2021).

Mohammed SF, Hussain I, AbouEzzeddine OF, Takahama H, Kwon SH, Forfia P, Roger VL, Redfield MM. Right ventricular function in heart failure with preserved ejection fraction: A community-based study. Circulation 130, 2310–2320 (2014).

Mohammed SF, Storlie JR, Oehler EA, Bowen LA, Korinek J, Lam CS, Simari RD, Burnett JC Jr, Redfield MM. Variable phenotype in murine transverse aortic constriction. Cardiovasc. Pathol. 21, 188–198 (2012).

Molfetta R, Zitti B, Lecce M, Milito ND, Stabile H, Fionda C, Cippitelli M, Gismondi A, Santoni A, Paolini R. Cd155: A multi-functional molecule in tumor progression. Int. J. Mol. Sci. 21, 922–929 (2020).

Mottillo S, Filion KB, Genest J, Joseph L, Pilote L, Poirier P, Rinfret S, Schiffrin EL, Eisenberg MJ. The metabolic syndrome and cardiovascular risk: A systematic review and meta-analysis. J. Am. Coll. Cardiol. 56, 1113–1132 (2010).

Murdoch CE, Chaubey S, Zeng L, Yu B, Ivetic A, Walker SJ, Vanhoutte D, Heymans S, Grieve DJ, Cave AC, Brewer AC, Zhang M, Shah AM. Endothelial NADPH oxidase-2 promotes interstitial cardiac fibrosis and diastolic dysfunction through proinflammatory effects and endothelial- mesenchymal transition. J. Am. Coll. Cardiol. 63, 2734–2741 (2014).

Murray AJ, Cole MA, Lygate CA, Carr CA, Stuckey DJ, Little SE, Neubauer S, Clarke K. Increased mitochondrial uncoupling proteins, respiratory uncoupling and decreased efficiency in the chronically infarcted rat heart. J. Mol. Cell. Cardiol. 44, 694–700 (2008).

Nagai T, Honda S, Sugano Y, Matsuyama TA, Ohta-Ogo K, Asaumi Y, Ikeda Y, Kusano K, Ishihara M, Yasuda S, Ogawa H, Ishibashi-Ueda H, Anzai T. Decreased myocardial dendritic cells is associated with impaired reparative fibrosis and development of cardiac rupture after myocardial infarction in humans. J. Am. Heart. Assoc. 3, 839–844 (2014).

Nagueh SF, Smiseth OA, Appleton CP, Byrd BF 3rd, Dokainish H, Edvardsen T, Flachskampf FA, Gillebert TC, Klein AL, Lancellotti P, Marino P, Oh JK, Alexandru Popescu B, Waggoner AD.Recommendations for the evaluation of left ventricular diastolic function by echocardiography: An update from the American society of echocardiography and the European association of cardiovascular imaging. Eur. J. Heart Fail. Cardiovasc. Imaging 17, 1321–1360 (2016).

Nakamura, M., Sadoshima, J. Mechanisms of physiological and pathological cardiac hypertrophy. Nat. Rev. Cardiol. 15, 387–407 (2018).

Newman, J. C., Verdin, E. Ketone bodies as signaling metabolites. Trends Endocrinol. Metab. 25, 42–52 (2014).

Noordali, H., Loudon, B. L., Frenneaux, M. P. & Madhani, M. Cardiac metabolism — A promising therapeutic target for heart failure. Pharmacol. Therap. 182, 95–114 (2018).

Oktay, A. A., Rich, J. D., Shah, S. J. The emerging epidemic of heart failure with preserved ejection fraction. Curr. Heart. Fail. Rep. 10, 401–410 (2013).

Owan TE, Hodge DO, Herges RM, Jacobsen SJ, Roger VL, Redfield MM. Trends in Prevalence and Outcome of Heart Failure with Preserved Ejection Fraction. N. Engl. J. Med. 355, 251–259 (2006).

Pacher, P., Nagayama, T., Mukhopadhyay, P., Bátkai, S., Kass, D. A. Measurement of cardiac function using pressure-volume conductance catheter technique in mice and rats. Nat. Protoc. 3, 1422–1434 (2008).

Pan DZ, Miao Z, Comenho C, Rajkumar S, Koka A, Lee SHT, Alvarez M, Kaminska D, Ko A, Sinsheimer JS, Mohlke KL, Mancuso N, Muñoz-Hernandez LL, Herrera-Hernandez M, Tusié-Luna MT, Aguilar-Salinas C, Pietiläinen KH, Pihlajamäki J, Laakso M, Garske KM, Pajukanta P. Correction to: Identification of TBX15 as an adipose master trans regulator of abdominal obesity genes. Genome Med. 13, 123–141 (2021).

Panchal SK, Poudyal H, Iyer A, Nazer R, Alam MA, Diwan V, Kauter K, Sernia C, Campbell F, Ward L, Gobe G, Fenning A, Brown L. High-carbohydrate high-fat diet-induced metabolic syndrome and cardiovascular remodeling in rats. J. Cardiovasc. Pharmacol. 57, 51–64 (2011).

Parks, R. J., Ray, G., Bienvenu, L. A., Rose, R. A., Howlett, S. E. Sex differences in SR Ca2+ release in murine ventricular myocytes are regulated by the cAMP/PKA pathway. J. Mol. Cell. Cardiol. 75, 162–173 (2014).

Patel RB, Colangelo LA, Bielinski SJ, Larson NB, Ding J, Allen NB, Michos ED, Shah SJ, Lloyd-Jones DM. Circulating vascular cell adhesion molecule-1 and incident heart failure: The multi-ethnic study of atherosclerosis (MESA). J. Am. Heart Assoc. 9, 390–394 (2020).

Paulus, W. J., Tschöpe, C. A novel paradigm for heart failure with preserved ejection fraction: Comorbidities drive myocardial dysfunction and remodeling through coronary microvascular endothelial inflammation. J. Am. Coll. Cardiol. 62, 263–271 (2013).

Peng H, Yang XP, Carretero OA, Nakagawa P, D'Ambrosio M, Leung P, Xu J, Peterson EL, González GE, Harding P, Rhaleb NE. Angiotensin II-induced dilated cardiomyopathy in Balb/c but not C57BL/6J mice. Exp. Physiol. 96, 756–764 (2011).

Perrone-Filardi P, Savarese G, Scarano M, Cavazzina R, Trimarco B, Minneci S, Maggioni AP, Tavazzi L, Tognoni G, Marchioli R. Prognostic impact of metabolic syndrome in patients with chronic heart failure: Data from GISSI-HF trial. Int. J. Cardiol. 178, 85–90 (2015).

Peterson LR, Soto PF, Herrero P, Mohammed BS, Avidan MS, Schechtman KB, Dence C, Gropler RJ. Impact of Gender on the Myocardial Metabolic Response to Obesity. JACC Cardiovasc. Imaging 1, 424–433 (2008).

Phan TT, Abozguia K, Nallur Shivu G, Mahadevan G, Ahmed I, Williams L, Dwivedi G, Patel K, Steendijk P, Ashrafian H, Henning A, Frenneaux M. Heart Failure With Preserved Ejection Fraction Is Characterized by Dynamic Impairment of Active Relaxation and Contraction of the Left Ventricle on Exercise and Associated With Myocardial Energy Deficiency. J. Am. Coll. Cardiol. 54, 402–409 (2009).

Phung TL, Ziv K, Dabydeen D, Eyiah-Mensah G, Riveros M, Perruzzi C, Sun J, Monahan-Earley RA, Shiojima I, Nagy JA, Lin MI, Walsh K, Dvorak AM, Briscoe DM, Neeman M, Sessa WC, Dvorak HF, Benjamin LE. Pathological angiogenesis is induced by sustained Akt signaling and inhibited by rapamycin. Cancer Cell 10, 159–170 (2006).

Piek A, Koonen DPY, Schouten EM, Lindtstedt EL, Michaëlsson E, de Boer RA, Silljé HHW. Pharmacological myeloperoxidase (MPO) inhibition in an obese/hypertensive mouse model attenuates obesity and liver damage, but not cardiac remodeling. Sci. Rep. 9, 765–771 (2019).

Pieske B, Maggioni AP, Lam CSP, Pieske-Kraigher E, Filippatos G, Butler J, Ponikowski P, Shah SJ, Solomon SD, Scalise AV, Mueller K, Roessig L, Gheorghiade M. Vericiguat in patients with worsening chronic heart failure and preserved ejection fraction: Results of the SOluble guanylate Cyclase stimulatoR in heArT failurE patientS with PRESERVED EF (SOCRATES-PRESERVED) study. Eur. J. Heart Fail. 38, 1119–1127 (2017).

Pitt B, Pfeffer MA, Assmann SF, Boineau R, Anand IS, Claggett B, Clausell N, Desai AS, Diaz R, Fleg JL, Gordeev I, Harty B, Heitner JF, Kenwood CT, Lewis EF, O'Meara E, Probstfield JL, Shaburishvili T, Shah SJ, Solomon SD, Sweitzer NK, Yang S, McKinlay SM; TOPCAT Investigators. Spironolactone for heart failure with preserved ejection fraction. N. Engl. J. Med. 10, 1383-1392 (2014).

Pugliese NR, Fabiani I, Santini C, Rovai I, Pedrinelli R, Natali A, Dini FL. Value of combined cardiopulmonary and echocardiography stress test to characterize the haemodynamic and metabolic responses of patients with heart failure and mid-range ejection fraction. Eur. J. Heart Fail. Cardiovasc. Imaging 20, 828–836 (2019).

Putko BN, Wang Z, Lo J, Anderson T, Becher H, Dyck JR, Kassiri Z, Oudit GY; Alberta HEART Investigators. Circulating levels of tumor necrosis factor-alpha receptor 2 are increased in heart failure with preserved ejection fraction relative to heart failure with reduced ejection fraction: Evidence for a divergence in pathophysiology. PLoS One 9, 495–501 (2014).

Ramos GC, van den Berg A, Nunes-Silva V, Weirather J, Peters L, Burkard M, Friedrich M, Pinnecker J, Abeßer M, Heinze KG, Schuh K, Beyersdorf N, Kerkau T, Demengeot J, Frantz S, Hofmann U. Myocardial aging as a T-cell-mediated phenomenon. Proc. Natl. Acad. Sci. U. S. A. 114, E2420–E2429 (2017).

Ravassa S, Trippel T, Bach D, Bachran D, González A, López B, Wachter R, Hasenfuss G, Delles C, Dominiczak AF, Pieske B, Díez J, Edelmann F. Biomarker-based phenotyping of myocardial fibrosis identifies patients with heart failure with preserved ejection fraction resistant to the beneficial effects of spironolactone: results from the Aldo-DHF trial. Eur. J. Heart. Fail. 20, 1290–1299 (2018).

Rich, M., Kitzman, D. Heart failure in octogenarians: A fundamentally different disease. Am. J. Geriatr. Cardiol. 9, 97–104 (2000).

Roh JD, Houstis N, Yu A, Chang B, Yeri A, Li H, Hobson R, Lerchenmüller C, Vujic A, Chaudhari V, Damilano F, Platt C, Zlotoff D, Lee RT, Shah R, Jerosch-Herold M, Rosenzweig A. Exercise training reverses cardiac aging phenotypes associated with heart failure with preserved ejection fraction in male mice. Aging Cell 19, 159–163 (2020).

Romero-Becerra, R., Santamans, A. M., Folgueira, C., Sabio, G. P38 mapk pathway in the heart: New insights in health and disease. Int. J. Mol. Sci. 21, 1–19 (2020).

Rosca MG, Vazquez EJ, Kerner J, Parland W, Chandler MP, Stanley W, Sabbah HN, Hoppel CL. Cardiac mitochondria in heart failure: Decrease in respirasomes and oxidative phosphorylation. Cardiovasc. Res. 80, 30–39 (2008).

Rose, B. A., Force, T., Wang, Y. Mitogen-activated protein kinase signaling in the heart: Angels versus demons in a heart-breaking tale. Physiol. Rev. 90, 1507–1546 (2010).

Salinero, A. E., Anderson, B. M., Zuloaga, K. L. Sex differences in the metabolic effects of diet-induced obesity vary by age of onset. Int. J. Obes. 42, 1088–1091 (2018).

Salvador AM, Nevers T, Velázquez F, Aronovitz M, Wang B, Abadía Molina A, Jaffe IZ, Karas RH, Blanton RM, Alcaide P. Intercellular adhesion molecule 1 regulates left ventricular leukocyte infiltration, cardiac remodeling, and function in pressure overload-induced heart failure. J. Am. Heart Assoc. 5, 126–132 (2015).

Sanders-van Wijk S, Tromp J, Beussink-Nelson L, Hage C, Svedlund S, Saraste A, Swat SA, Sanchez C, Njoroge J, Tan RS, Fermer ML, Gan LM, Lund LH, Lam CSP, Shah SJ. Proteomic Evaluation of the Comorbidity-Inflammation Paradigm in Heart Failure With Preserved Ejection Fraction Results From the PROMIS-HFpEF Study. Circulation 142, 2029–2044 (2020).

Santos, C. X. C., Raza, S., Shah, A. M. Redox signaling in the cardiomyocyte: From physiology to failure. Int. J. Biochem. Cell Biol. 74, 145–151 (2016).

Savarese G, Becher PM, Lund LH, Seferovic P, Rosano GMC, Coats AJS. Global burden of heart failure: a comprehensive and updated review of epidemiology. Cardiovasc. Res. 118, 3272–3287 (2023).

Scantlebury, D. C., Borlaug, B. A. Why are women more likely than men to develop heart failure with preserved ejection fraction? Curr. Opin. Cardiol. 26, 562–568 (2011).

Schiattarella GG, Altamirano F, Tong D, French KM, Villalobos E, Kim SY, Luo X, Jiang N, May HI, Wang ZV, Hill TM, Mammen PPA, Huang J, Lee DI, Hahn VS, Sharma K, Kass DA, Lavandero S, Gillette TG, Hill JA. Nitrosative stress drives heart failure with preserved ejection fraction. Nature 568, 351–356 (2019).

Schilling, J. D. Trimming the Fat in HFpEF: Learning How to Target the Metabolic Disease Phenotype. JACC: Basic. Transl. Sci. 5, 928–930 (2020).

Schnelle M, Catibog N, Zhang M, Nabeebaccus AA, Anderson G, Richards DA, Sawyer G, Zhang X, Toischer K, Hasenfuss G, Monaghan MJ, Shah AM. Echocardiographic evaluation of diastolic function in mouse models of heart disease. J. Mol. Cell. Cardiol. 114, 20–28 (2018).

Schumacher, S. M., Naga Prasad, S. V. Tumor Necrosis Factor-α in Heart Failure: an Updated Review. Curr. Cardiol. Rep. 20, 117–123 (2018).

Segers, V. F. M., Brutsaert, D. L., De Keulenaer, G. W. Cardiac remodeling: Endothelial cells have more to say than just NO. Front. Physiol. 11, 382–394 (2018).

Selby, D. E., Palmer, B. M., Lewinter, M. M., Meyer, M. Tachycardia-induced diastolic dysfunction and resting tone in myocardium from patients with a normal ejection fraction. J. Am. Coll. Cardiol. 58, 147–154 (2011).

Shah KS, Xu H, Matsouaka RA, Bhatt DL, Heidenreich PA, Hernandez AF, Devore AD, Yancy CW, Fonarow GC. Heart Failure With Preserved, Borderline, and Reduced Ejection Fraction: 5-Year Outcomes. J. Am. Coll. Cardiol. 70, 2476–2486 (2017).

Shah, S. J., Katz, D. H., Deo, R. C. Phenotypic Spectrum of Heart Failure with Preserved Ejection Fraction. Heart. Fail. Clin. 10, 407–418 (2014).

Shanaki, M., Omidifar, A., Shabani, P., Toolabi, K. Association between HDACs and pro-inflammatory cytokine gene expressions in obesity. Arch. Physiol. Biochem. 128, 880–886 (2022).

Sheeran, F. L., Pepe, S. Energy deficiency in the failing heart: Linking increased reactive oxygen species and disruption of oxidative phosphorylation rate. Biochim Biophys Acta - Bioenergetics 1757, 543–552 (2006).

Simmonds, S. J., Cuijpers, I., Heymans, S., Jones, E. A. V. Cellular and Molecular Differences between HFpEF and HFrEF: A Step Ahead in an Improved Pathological Understanding. Cells 9, 242–250 (2020).

Solomon SD, Claggett B, Lewis EF, Desai A, Anand I, Sweitzer NK, O'Meara E, Shah SJ, McKinlay S, Fleg JL, Sopko G, Pitt B, Pfeffer MA. Influence of ejection fraction on outcomes and efficacy of spironolactone in patients with heart failure with preserved ejection fraction. Eur. J. Heart Fail. 37, 455–462 (2016).

Song M, Mihara K, Chen Y, Scorrano L, Dorn GW 2nd. W. Mitochondrial fission and fusion factors reciprocally orchestrate mitophagic culling in mouse hearts and cultured fibroblasts. Cell. Metab. 21, 273–286 (2015).

Sossalla S, Fluschnik N, Schotola H, Ort KR, Neef S, Schulte T, Wittköpper K, Renner A, Schmitto JD, Gummert J, El-Armouche A, Hasenfuss G, Maier LS. Inhibition of elevated Ca2+/calmodulin-dependent protein kinase II improves contractility in human failing myocardium. Circ. Res. 107, 1150–1161 (2010).

Stephen, S. A. Unwanted effects of propranolol. Am. J. Cardiol. 18, 463–472 (1966).

Stevens HY, Melchior B, Bell KS, Yun S, Yeh JC, Frangos JA. PECAM-1 is a critical mediator of atherosclerosis. DMM Dis. Model. Mech. 1, 175–181 (2008).

Stilli D, Bocchi L, Berni R, Zaniboni M, Cacciani F, Chaponnier C, Musso E, Gabbiani G, Clément S. Correlation of α-skeletal actin expression, ventricular fibrosis and heart function with the degree of pressure overload cardiac hypertrophy in rats. Exp. Physiol. 91, 571–580 (2006).

Streng KW, Nauta JF, Hillege HL, Anker SD, Cleland JG, Dickstein K, Filippatos G, Lang CC, Metra M, Ng LL, Ponikowski P, Samani NJ, van Veldhuisen DJ, Zwinderman AH, Zannad F, Damman K, van der Meer P, Voors AA. Non-cardiac comorbidities in heart failure with reduced, mid-range and preserved ejection fraction. Int. J. Cardiol. 15, 132–139 (2018).

Tan YT, Wenzelburger F, Lee E, Heatlie G, Leyva F, Patel K, Frenneaux M, Sanderson JE. The Pathophysiology of Heart Failure With Normal Ejection Fraction. Exercise Echocardiography Reveals Complex Abnormalities of Both Systolic and Diastolic Ventricular Function Involving Torsion, Untwist, and Longitudinal Motion. J. Am. Coll. Cardiol. 54, 36–46 (2009).

Tanabe M, Lamia B, Tanaka H, Schwartzman D, Pinsky MR, Gorcsan J 3rd. Echocardiographic Speckle Tracking Radial Strain Imaging to Assess Ventricular Dyssynchrony in a Pacing Model of Resynchronization Therapy. J. Am. Soc. Echocardiogr. 21, 1382–1388 (2008).

Toischer K, Rokita AG, Unsöld B, Zhu W, Kararigas G, Sossalla S, Reuter SP, Becker A, Teucher N, Seidler T, Grebe C, Preuss L, Gupta SN, Schmidt K, Lehnart SE, Krüger M, Linke WA, Backs J, Regitz-Zagrosek V, Schäfer K, Field LJ, Maier LS, Hasenfuss G. Differential cardiac remodeling in preload versus afterload. Circulation 122, 993–1003 (2010).

Tolppanen AM, Pulkkinen L, Herder C, Koenig W, Kolehmainen M, Lindström J, Tuomilehto J, Uusitupa M; Finnish Diabetes Prevention Study Group. The genetic variation of the tenomodulin gene (TNMD) is associated with serum levels of systemic immune mediators - The Finnish Diabetes Prevention Study. Genet. Med. 10, 536–544 (2008).

Tong D, Schiattarella GG, Jiang N, May HI, Lavandero S, Gillette TG, Hill JA. Female Sex Is Protective in a Preclinical Model of Heart Failure with Preserved Ejection Fraction. Circulation 140, 1769–1771 (2019).

Trial, J. A., Heredia, C. P., Taffet, G. E., Entman, M. L., Cieslik, K. A. Dissecting the role of myeloid and mesenchymal fibroblasts in age-dependent cardiac fibrosis. Basic Res. Cardiol. 112, 34–40 (2017).

Truszkowska GT, Bilińska ZT, Muchowicz A, Pollak A, Biernacka A, Kozar-Kamińska K, Stawiński P, Gasperowicz P, Kosińska J, Zieliński T, Płoski R. Homozygous truncating mutation in NRAP gene identified by whole exome sequencing in a patient with dilated cardiomyopathy. Sci. Rep. 7, 82–96 (2017).

Tsao CW, Lyass A, Enserro D, Larson MG, Ho JE, Kizer JR, Gottdiener JS, Psaty BM, Vasan RS. Temporal Trends in the Incidence of and Mortality Associated With Heart Failure With Preserved and Reduced Ejection Fraction. JACC Heart. Fail. 6, 678–685 (2018).

Upadhya B, Kitzman DW. Heart failure with preserved ejection fraction: New approaches to diagnosis and management. Clin. Cardiol. 43, 145–155 (2020).

Valero-Muñoz M, Oh A, Faudoa E, Bretón-Romero R, El Adili F, Bujor A, Sam F. Endothelial-Mesenchymal Transition in Heart Failure with a Preserved Ejection Fraction: Insights into the Cardiorenal Syndrome. Circ. Heart. Fail. 14, E008372 (2021).

Valiente-Alandi I, Potter SJ, Salvador AM, Schafer AE, Schips T, Carrillo-Salinas F, Gibson AM, Nieman ML, Perkins C, Sargent MA, Huo J, Lorenz JN, DeFalco T, Molkentin JD, Alcaide P, Blaxall BC. Inhibiting fibronectin attenuates fibrosis and improves cardiac function in a model of heart failure. Circulation 138, 1236–1252 (2018).

Van Aelst LNL, Arrigo M, Placido R, Akiyama E, Girerd N, Zannad F, Manivet P, Rossignol P, Badoz M, Sadoune M, Launay JM, Gayat E, Lam CSP, Cohen-Solal A, Mebazaa A, Seronde MF. Acutely decompensated heart failure with preserved and reduced ejection fraction present with comparable haemodynamic congestion. Eur. J. Heart Fail. 20, 738–747 (2018).

van den Borne SW, Diez J, Blankesteijn WM, Verjans J, Hofstra L, Narula J. Myocardial remodeling after infarction: the role of myofibroblasts. Nat. Rev. Cardiol. 7, 30-37 (2010).

van Ham WB, Kessler EL, Oerlemans MIFJ, Handoko ML, Sluijter JPG, van Veen TAB, den Ruijter HM, de Jager SCA. Clinical Phenotypes of Heart Failure With Preserved Ejection Fraction to Select Preclinical Animal Models. JACC: Basic Transl. Sci. 7, 844-857 (2022).

van Heerebeek L, Franssen CP, Hamdani N, Verheugt FW, Somsen GA, Paulus WJ. Molecular and cellular basis for diastolic dysfunction. Curr. Heart Fail. Rep. 9, 293–302 (2012).

van Heerebeek L, Hamdani N, Handoko ML, Falcao-Pires I, Musters RJ, Kupreishvili K, Ijsselmuiden AJ, Schalkwijk CG, Bronzwaer JG, Diamant M, Borbély A, van der Velden J, Stienen GJ, Laarman GJ, Niessen HW, Paulus WJ. Diastolic stiffness of the failing diabetic heart: Importance of fibrosis, advanced glycation end products, and myocyte resting tension. Circulation 117, 43–51 (2008).

Van Linthout S, Hamdani N, Miteva K, Koschel A, Müller I, Pinzur L, Aberman Z, Pappritz K, Linke WA, Tschöpe C. Placenta-Derived Adherent Stromal Cells Improve Diabetes Mellitus-Associated Left Ventricular Diastolic Performance. Stem. Cells Transl. Med. 6, 2135-2145 (2017).

Vlahos, C. J., McDowell, S. A., Clerk, A. Kinases as therapeutic targets for heart failure. Nat. Rev. Drug Disc. 2, 99–113 (2003).

Von Bibra, H., St John Sutton, M. Diastolic dysfunction in diabetes and the metabolic syndrome: Promising potential for diagnosis and prognosis. Diabetologia 53, 1033–1045 (2010).

Wachter R, Schmidt-Schweda S, Westermann D, Post H, Edelmann F, Kasner M, Lüers C, Steendijk P, Hasenfuss G, Tschöpe C, Pieske B. Blunted frequency-dependent upregulation of cardiac output is related to impaired relaxation in diastolic heart failure. Eur. J. Heart Fail. 30, 3027–3036 (2009).

Wang P, Zhang W, Feng Z, Zhang J, Sun Y, Zhang W. LDL-induced NLRC3 inflammasome activation in cardiac fibroblasts contributes to cardiomyocytic dysfunction. Mol. Med. Rep. 24, 526–531 (2021).

Wang X, Pan J, Liu D, Zhang M, Li X, Tian J, Liu M, Jin T, An F. Nicorandil alleviates apoptosis in diabetic cardiomyopathy through PI3K/Akt pathway. J. Cell. Mol. Med. 23, 5349–5359 (2019).

Wang, Q., Lin, J. L. C., Erives, A. J., Lin, C. I., Lin, J. J. C. New insights into the roles of xin repeat-containing proteins in cardiac development, function, and disease. Int. Rev. Cell Mol. Biol. 310, 89–128 (2016).

Wei J, Nelson MD, Szczepaniak EW, Smith L, Mehta PK, Thomson LE, Berman DS, Li D, Bairey Merz CN, Szczepaniak LS. Myocardial steatosis as a possible mechanistic link between diastolic dysfunction and coronary microvascular dysfunction in women. Am. J. Physiol. Heart. Circ. Physiol. 310, H14–H19 (2016).

Westermann D, Kasner M, Steendijk P, Spillmann F, Riad A, Weitmann K, Hoffmann W, Poller W, Pauschinger M, Schultheiss HP, Tschöpe C. Role of left ventricular stiffness in heart failure with normal ejection fraction. Circulation 117, 2051–2060 (2008).

Wintrich J, Kindermann I, Ukena C, Selejan S, Werner C, Maack C, Laufs U, Tschöpe C, Anker SD, Lam CSP, Voors AA, Böhm M. Therapeutic approaches in heart failure with preserved ejection fraction: past, present, and future. Clin. Res. Cardiol. 109, 1079–1098 (2020).

Withaar, C., Lam, C. S. P., Schiattarella, G. G., De Boer, R. A., Meems, L. M. G. Heart failure with preserved ejection fraction in humans and mice: Embracing clinical complexity in mouse models. Eur. J. Heart Fail. 42, 4420–4430 (2021).

Woudstra L, Biesbroek PS, Emmens RW, Heymans S, Juffermans LJ, van der Wal AC, van Rossum AC, Niessen HWM, Krijnen PAJ. CD45 is a more sensitive marker than CD3 to diagnose lymphocytic myocarditis in the endomyocardium. Hum. Pathol. 62, 83–90 (2017).

Yamamoto K, Origasa H, Suzuki Y, Takahashi T, Shinozaki T, Watanabe T, Sakata Y, Izumi C, Taira K, Hori M; J-DHF Investigators. Relation of risk factors with response to carvedilol in heart failure with preserved ejection fraction - A report from the Japanese Diastolic Heart Failure Study (J-DHF). J. Cardiol. 63, 424–431 (2014).

Yamashiro Y, Ramirez K, Nagayama K, Hattori N, Liu YY, Matsunaga S, Tomita S, Kubota Y, Yanagisawa H. Partial endothelial-to-mesenchymal transition mediated by HIF-induced CD45 in neointima formation upon carotid artery ligation. Cardiovasc. Res. 119, 1606–1618 (2023).

Yancy, C. W., Lopatin, M., Stevenson, L. W., De Marco, T., Fonarow, G. C. Clinical presentation, management, and in-hospital outcomes of patients admitted with acute decompensated heart failure with preserved systolic function: A report from the Acute Decompensated Heart Failure National Registry (ADHERE) database. J. Am. Coll. Cardiol. 47, 76–84 (2006).

Yang XL, Ma YS, Liu YS, Jiang XH, Ding H, Shi Y, Jia CY, Lu GX, Zhang DD, Wang HM, Wang PY, Lv ZW, Yu F, Liu JB, Fu D. microRNA-873 inhibits self-renewal and proliferation of pancreatic cancer stem cells through pleckstrin-2-dependent PI3K/AKT pathway. Cell Signal. 84, 110025 (2021).

Yoshizumi, M., Perrella, M. A., Burnett, J. C. & Lee, M. E. Tumor necrosis factor downregulates an endothelial nitric oxide synthase mRNA by shortening its half-life. Circ. Res. 73, 205–209 (1993).

Yusuf S, Pfeffer MA, Swedberg K, Granger CB, Held P, McMurray JJ, Michelson EL, Olofsson B, Ostergren J. Effects of candesartan in patients with chronic heart failure and preserved left-ventricular ejection fraction: The CHARM-preserved trial. Lancet 362, 777–781 (2003).

Zhang C, Lu L, Li Y, Wang X, Zhou J, Liu Y, Fu P, Gallicchio MA, Bach LA, Duan C. IGF binding protein-6 expression in vascular endothelial cells is induced by hypoxia and plays a negative role in tumor angiogenesis. Int. J. Cancer 130, 2003–2012 (2012).

Zhang T, Maier LS, Dalton ND, Miyamoto S, Ross J Jr, Bers DM, Brown JH. The δc isoform of CaMKII is activated in cardiac hypertrophy and induces dilated cardiomyopathy and heart failure. Circ. Res. 92, 912–919 (2003).

Zhang, M., Perino, A., Ghigo, A., Hirsch, E., Shah, A. M. NADPH oxidases in heart failure: Poachers or gamekeepers? Antiox. redox. Signal. 18, 1024–1041 (2013).

Zhang, Y., Marmorstein, L. Y. Focus on molecules: fibulin-3 (EFEMP1). Exp. Eye Res. 90, 3 (2009).

Zhao Z, Wang H, Jessup JA, Lindsey SH, Chappell MC, Groban L. Role of estrogen in diastolic dysfunction. Am. J. Physiol. Heart. Circ. Physiol. 306, H628-40 (2014).

Zhou Y, Fu L, Sun J, Zhu Z, Xing Z, Zhou S, Tai S, Wang Y. Association Between Metabolic Syndrome and an Increased Risk of Hospitalization for Heart Failure in Population of HFpEF. Front. Cardiovasc. Med. 8, 117–125 (2021).

Zile MR, Baicu CF, Ikonomidis JS, Stroud RE, Nietert PJ, Bradshaw AD, Slater R, Palmer BM, Van Buren P, Meyer M, Redfield MM, Bull DA, Granzier HL, LeWinter MM. Myocardial stiffness in patients with heart failure and a preserved ejection fraction contributions of collagen and titin. Circulation 131, 1247–1259 (2015).

Zile, M. R., Gaasch, W. H. Abnormal calcium homeostasis: One mechanism in diastolic heart failure. J Am. Coll. Cardiol. 58,155–157 (2011).

Zordoky BN, Sung MM, Ezekowitz J, Mandal R, Han B, Bjorndahl TC, Bouatra S, Anderson T, Oudit GY, Wishart DS, Dyck JR; Alberta HEART. Metabolomic fingerprint of heart failure with preserved ejection fraction. PLoS One 10, 844–850 (2015).

Acknowledgements

Any endeavor in science and research is a collective on and my project was no exception. There are many people to whom I would like to extend my gratitude. I sincerely thank Prof. Dr. Gerd Hasenfuß for giving me the opportunity to work in his department and Prof. Dörthe Katschinski for supervising me along with PD. Dr. med. Dr. Moritz Schnelle. All of you have been a constant source of inspiration and counselling throughout my work. Your guidance will continue to shape my professional as well as personal development. Dr. Manar El-Kenani for training me during my first semester at the department and for being a friend. I would also like to thank Prof. Karl Toischer and Dr. Belal Mohammed for their help.

I would additionally like to thank Prof. Sven Thoms and Prof. Thomas Meyer for always giving me valuable insights and inputs in thesis committee meetings. An extended gratitude is owed to my thesis review board; Prof. Katrin Streckfuß-Bömeke, Prof. Susanne Lutz and PD. Dr. Laura Zelarayan.

A hearty thanks to Dr. Karthika Annamalai for her kind guidance, encouraging words and joyful company in the lab (and for our potluck dinners!). I am also grateful for the members of Hasenfuß-Schnelle-Toischer lab; Daniel, Nikita, Vignesh and Jara for our times together through thick and thin.

A huge shout out for SFB service team members Sabrina, Sarah and Marcel for their indispensable help with mice experiments. Many thanks to Gabriela and Maren from NIG for excellent service and support.

I would like to include my friends here; Sabine (Gö wouldn’t have been the same without you), Ana, Mufassra, Julius, Maithily, Maggie and Alisa for being cheerful companions. A hearty gratitude to IRTG1816 PhD program organizers Dr. Christina Würtz, and Fulya Ören for always being there.

A moment of gratitude specially for all the mice that were instrumental in giving me valuable data and insights, I strive to do my best in making their sacrifice worthwhile. I would also like to appreciate all the animal caretakers, you all are the unsung heroes of medical research.

Finally, Anuruti thank you so much for our lovely time together in Göttingen balancing a PhD and trying to travel the world together, a dream come true indeed! My parents in law, my father and my sister Himanshi for their endless support even from a thousand miles away. In the end, my love Ankit for your unwavering support throughout my journey and for always being there with a kind smile on your face, especially on my hardest days. I am looking forward to whatever adventures life brings for us! In the end, to the loving memory of my mother, I owe everything to you.